ATTENTION: The Singapore Copyright Act applies to the use of this document. Nanyang Technological University Library

DIRECT METAL-TO-METAL THERMOCOMPRESSION BONDING STUDIES

ANG XIAO FANG

School of Materials Science and Engineering

A thesis submitted to the Nanyang Technological University
in fulfillment of the requirement for the degree of
Doctor of Philosophy

2009

ATTENTION: The Singapore Copyright Act applies to the use of this document. Nanyang Technological University Library

Acknowledgement

I would like to take this opportunity to express my heartfelt gratitude to my Ph.D supervisor, Assoc Prof Wong Chee Cheong. Not only has he been an inspirational mentor, Prof Wong has been like a father and a friend to me. From him, I received both valuable research training as well as his attitude towards life. In fact, with his enthusiasm, good teaching and ideas, he has made research fun for me. His constant encouragement and sharing of novel ideas and concepts has always been a source of motivation to me throughout this work. He placed trust on me in making individualistic decisions and remained self-motivated at various stages of this thesis without which I would not have come up to this stage.

I am also indebted to my co-supervisor Dr Wei Jun for providing guidance, support and training at Singapore Institute of Manufacturing Technology (SIMTech). Beside sharing realistic views on research and engineering, his enthusiasm in inculcating values in me beyond being a researcher has made him more than a mentor to me. I am equally grateful to Assoc Prof Chen Zhong for rendering guidance and care, offering brainstorming session, valuable advice and knowledge throughout the candidature.

I would like to thank the many people in SIMTech – Mdm Lu Hai Jing, Mr Cheng Chek Kweng, Mr Mohaime Bin Mohahidin, Mr Steve Lai Foo Khuen, Mr Lok Boon Keng, Mdm Liu Yu Chan for their generous help and assistance in this research. I'm also grateful to Ms. Doreen Lai Mei Ying and Ms Debbie Seng Hwee Leng for

ATTENTION: The Singapore Copyright Act applies to the use of this document. Nanyang Technological University Library

carrying out ToF-SIMS and Mr Zhang Zheng for XPS at Institute of Materials Research and Engineering (IMRE). I am also very thankful to all my technicians from Microelectronics Materials Lab, Polymer Lab and FACTS Lab for the valuable assistance. I wish to thank my mentor – Dr Zhang GuoGe for his patient guidance and my fellow workmates - Chin Li Cheong, June Tan, Ken Li, Li Jia and Lin Aiting for providing assistance in my experiments.

I am indebted to my student colleagues for providing a stimulating and fun environment in which I learn and grow. I am especially grateful to Teh Lay Kuan, Effie Chew Yeong Huey, Lydia Helena Wong, Koh Yaw Koon, Yip Chan Hoe, Lee Kwang Hong, Tan Kwan Wee, Husen Kang, Dr Yan Qing Feng, Cheng Yu Hua, Koh Li Buay, Tay Yee Yan, Yan Hua and I Made Riko.

I wish to thank my best friends in college (Lim Zipin, Liu Ming, Joel Oon and Sim Peishan), as an undergraduate and graduate student (Thelese Foong) and best friends from NTU Taekwondo Club (Jenny Kho, Liza Sem, Wong Lih Yan, Lydia Ho, Edwin Tay and Lee Song Yang), for helping me get through the difficult times, and for all the emotional support, entertainment, and care they provided.

I wish to thank my entire extended family for providing a loving environment. My brother, my twin sister, my grandma, aunts, uncles and cousins are particularly supportive. Lastly, and most importantly, I wish to thank my parents, Richard Ang Kok Beng and Neo Kim Keok. They bore me, raised me, supported me, taught me, and loved me. To them I dedicate this thesis.

ATTENTION: The Singapore Copyright Act applies to the use of this document. Nanyang Technological University Library

TABLE OF CONTENTS

ACKNOWLEDGEMENT I

LIST OF FIGURES VII

LIST OF TABLES XIII

ABSTRACT XIV

CHAPTER 1 THREE-DIMENSIONAL INTEGRATION 1

1.1 2-D VERSUS 3-D INTEGRATION – INTERCONNECTION-LIMITED! 1

1.2 METHODS OF STACKING: 3-D ICS AND 3-D PACKAGING 2

1.3 3-D ICS TECHNOLOGY OPTIONS 3

1.4 THERMAL ISSUES IN 3-D INTEGRATION 6

1.5 PROPOSAL 8

1.5.1 Motivation 8

1.5.2 Objectives and Scope 9

1.6 ORGANIZATION OF REPORT 14

CHAPTER 2 BONDING 17

2.1 INTRODUCTION 17

2.2 WHAT IS BONDING? 17

2.3 ASPERITIES IN BONDING 18

2.4 BARRIER LAYER THEORY 20

2.5 ROLE OF BONDING TEMPERATURE AND PRESSURE – A REVIEW ON BONDING MECHANISM 21

2.6 THERMOCOMPRESSION BONDING 23

2.7 BONDING OPTIONS 24

2.7.1 Metal Bonding 25

2.7.1.1 Direct Metal Bonding 25

ATTENTION: The Singapore Copyright Act applies to the use of this document. Nanyang Technological University Library

2.7.1.2 Eutectic Bonding ... 26

2.7.2 Hybrid Bonding ... 28

2.7.3 Direct Bonding ... 29

2.7.4 Adhesive Bonding ... 30

CHAPTER 3 DIRECT GOLD BONDING ... 33

3.1 INTRODUCTION ... 33

3.2 EXPERIMENTS ... 34

3.2.1 Temperature Dependence ... 34

3.2.2 Effect of substrate: Hardness ... 36

3.2.3 Pressure Dependence ... 36

3.3 RESULTS AND DISCUSSION ... 38

3.3.1 Critical Temperature ... 38

3.3.2 Interfacial Chemical Behaviour ... 42

3.3.3 Influence of interfacial stress distribution ... 45

3.3.4 Pressure Dependence ... 47

3.3.4.1 *Optimum Pressure* ... 47

3.3.4.2 *Critical Shear Stress Criterion* ... 48

3.4 RELATIONSHIP OF BOND STRENGTH TO CONTACT AREA (A_C) AND TRUE CONTACT AREA (A_T) ... 53

3.5 WORK HARDENING EFFECT ... 58

3.6 INWARD BONDING BEHAVIOUR IN GOLD STUDS AND PLATED BUMP ... 59

3.7 FRACTURE MODE ANALYSIS USING INTERFACIAL STRESS DISTRIBUTION AND UNBONDED RADIUS ... 66

3.8 ESTIMATION OF TRUE BONDED AREA ... 68

3.9 CHAPTER SUMMARY ... 69

CHAPTER 4 SURFACE MODIFICATION BY SELF-ASSEMBLED MONOLAYERS ... 71

4.1 INTRODUCTION ... 71

4.1.1 Self-assembly ... 71

4.1.2 Thermal and Mechanical Properties ... 73

4.2 EXPERIMENTS ... 75

4.3 THERMOCOMPRESSION BONDING OF UNCOATED AND SAM-COATED GOLD BUMPS 76

4.3.1 Gold Stud Bump ... 76

ATTENTION: The Singapore Copyright Act applies to the use of this document. Nanyang Technological University Library

4.3.2 Electroplated Gold Bumps *79*
4.4 BONDING HYPOTHESIS 81
4.5 EFFECT OF CHAIN LENGTH 83
4.5.1 Introduction *83*
4.5.2 Experiments *83*
4.5.3 Does Short Chain Alkanethiol Work Better? *84*
4.6 CHAPTER SUMMARY 85

CHAPTER 5 BASIS OF SAMS-ASSISTED BONDING PHENOMENON 86

5.1 INTRODUCTION 86
5.2 SURFACE PASSIVATION 87
5.2.1 Improved Bond Strength in Exposed SAM-coated Gold Joints *87*
5.2.2 Chain Length Dependence *90*
5.3 MECHANICAL DISPLACEMENT 91
5.4 THERMAL DISPLACEMENT 94
5.4.1 In-Situ SPRS Response at a SAMs/Au interface as a function of temperature *94*
5.4.2 Surface analysis using X-ray Photoelectron Spectroscopy (XPS) *98*
5.5 STABILITY AGAINST ENVIRONMENTAL CONDITIONS 102
5.5.1 Introduction *102*
5.5.2 Experimental Procedures *103*
5.5.3 Air Stability *105*
5.5.4 Thermal Stability *108*
5.6 CHAPTER SUMMARY 113

CHAPTER 6 SELF-ASSEMBLED MONOLAYERS FOR LOW TEMPERATURE COPPER BONDING 115

6.1 INTRODUCTION 115
6.2 EXPERIMENTS 116
6.2.1 Sample Preparation *116*
6.2.2 Bonding Experiments *117*
6.2.3 Surface Characterization using X-ray Photoelectron Spectroscopy (XPS) *118*
6.3 EFFECT OF TEMPERATURE ON BOND SHEAR STRENGTH 119
6.4 SELF-LIMITING TEMPERATURE EFFECT 121
6.5 BOND ENHANCEMENT USING SELF-ASSEMBLED MONOLAYERS (SAMS) 122
6.6 SURFACE CHARACTERIZATION 124

ATTENTION: The Singapore Copyright Act applies to the use of this document. Nanyang Technological University Library

6.6.1 Reduction of copper oxide *124*
6.6.2 Thermal Stability *125*
6.7 CHAPTER SUMMARY 127
CHAPTER 7 CONCLUSION AND FUTURE WORK........ 128
7.1 INVESTIGATED THE EFFECTS OF TEMPERATURE AND PRESSURE IN GOLD THERMOCOMPRESSION BONDING 128
7.1.1 Temperature Influence: Barrier Layer /Oxide Theory *128*
7.1.2 Pressure Influence: Optimum Pressure *129*
7.2 DEMONSTRATED LOW TEMPERATURE GOLD THERMOCOMPRESSION BONDING BY SELF-ASSEMBLED MONOLAYERS 130
7.3 ACHIEVED LOW TEMPERATURE DIRECT COPPER THERMOCOMPRESSION BONDING IN AMBIENT 130
REFERENCES 140
APPENDIX A1: LIST OF AUTHOR'S PUBLICATIONS 150
APPENDIX A2: ESTIMATION OF TRUE BONDED AREA AND STRESS-STRAIN CURVES 153

ATTENTION: The Singapore Copyright Act applies to the use of this document. Nanyang Technological University Library

List of Figures

Figure 1-1 Schematics of the long wire connections in 2-D plane 2

Figure 1-2 Schematics of 3-D architectures (a) Face-to-face (b) face-to-back (c) Combination of both... 5

Figure 1-3 Illustration of the 5 key technologies in 3D integration 6

Figure 2-1 Examples of the types of height distributions for surface roughness 19

Figure 2-2 Definition of interfacial area regions in bonding.. 20

Figure 2-3 A comparison of key processes in 3D Integration [MCNC R&D Institute - Semiconductor International (2005)] 24

Figure 2-4 (a) Metal wire bonding to stack the chips using gold or copper (b) 8 stacked layers of IC using copper-plated through-silicon vias- Samsung 16GBit NAND Flash prototype. 26

Figure 2-5 Application of a solder material [Cu-Sn] as a bonding intermediate between metal interconnects [IMEC]. 27

Figure 2-6 Copper and dielectric bonding between the stacked layers at IMEC [55] 28

Figure 2-7 DBI™ Bond: Covalent bond formed between the oxide layers at room temperature[57] 30

Figure 2-8 Wafer-level 3D IC fabrication using adhesive bonding and Cu damascence in RPI.. 32

Figure 3-1 Au and Cu interconnects formed at 20 μm pitch.. 34

Figure 3-2 SEM fractographs of test chip and Au stud bump used 34

ATTENTION: The Singapore Copyright Act applies to the use of this document. Nanyang Technological University Library

Figure 3-3 Plan view of the samples setup in a wafer bonder 37

Figure 3-4 A schematic of the cross-section of the sample setup for bonding using a wafer bonder 37

Figure 3-5 A schematic of the tensile tester setup 38

Figure 3-6 The effect of pick up tool temperature on shear strength of joints at bonding pressure of 975MPa 39

Figure 3-7 Cross section SEM images of Au-Au joints on alumina substrate at different bonding temperatures 40

Figure 3-8 The effect of tool temperature at two stage temperatures using gold-gold on alumina 41

Figure 3-9 Surface chemical composition of gold (a) with/without Ar sputtering and (b) at different detection depths 43

Figure 3-10 Typical stress contour (undeformed and deformed) diagram illustrating the shear stress distribution for gold bump-10μm gold model 46

Figure 3-11 Simulated interfacial shear stress versus radial position of the gold joints ... 47

Figure 3-12 Variation of tensile force against the bonding load applied at two bonding temperatures - 150 °C and 200 °C 48

Figure 3-13 (a) Model I: Gold stud on a layer of gold; (b) Model II: Plated gold bump on a layer of gold 50

Figure 3-14 SEM picture of plated bump at about 16μm in height 51

Figure 3-15 Shear stress distribution at bonding interface as a function of radial position. (a) Gold Stud (Model I) at pressure 550MPa and 973MPa per bump (b) Plated Bump (Model II) at 244MPa and 976MPa 52

Figure 3-16 Schematic illustrates a linear relationship between shear stress distribution and unbonded radius, $r_1 > r_2 > r_3$ as $P_1 < P_2 < P_3$ 53

ATTENTION: The Singapore Copyright Act applies to the use of this document. Nanyang Technological University Library

Figure 3-17 3D raster-scanning of the bumps left on the substrate using surface profilometry. 54

Figure 3-18 Contact diameter (D_o) and inner diameter (d_i) of the ring left as a function of bonding pressure 55

Figure 3-19 Relation between strength and amount of bonded area (a) at different bonding load (b) at different temperatures of 150 °C and 200 °C. 55

Figure 3-20 Schematics of the interfacial shear stress across the radial position of the bump with increasing pressure (P). As P increases, the unbonded radius, r tends to a minimum 56

Figure 3-21 Illustration of the effect of applied pressure on the contacting surfaces at atomic scale 57

Figure 3-22 Top view of the schematics at the bonded interface when the applied P tends to P_{opt}., Increase in A_T instead of A_c where $P_1 < P_2 < P_3$ 58

Figure 3-23 Illustration of two types of failure observed in gold joints after fracture 59

Figure 3-24 (a) SEM fractographs of a gold layer left on a silicon substrate (Low Magnification) (b) A Au stud remains on the chip surface (c) A ring of Au left on the substrate bonded at bonding pressure of 500g/bump [979MPa] 61

Figure 3-25 Optical fractographs of Au stud left on an alumina substrate at different tool temperatures: (a) 150°C, (b) 180°C and (c) 250°C 62

Figure 3-26 SEI fractographs taken at a higher magnification. (Left) Surface A at the central region. (Right) Surface B at the bare gold substrate 63

Figure 3-27 Schematic of failure path of the bonded Au-Au joint during tensile test 63

Figure 3-28 Au stud joint after tensile pull test (a) SEM observation of gold layer left on substrate. Sample is bonded at 216g per bump [550MPa] (b) Sample is bonded at 310g per bump [790MPa] (c) SEM observation of a cylindrical gold material left on the chip side 64

ATTENTION: The Singapore Copyright Act applies to the use of this document. Nanyang Technological University Library

Figure 3-29 Plated bump joint after tensile pull test. a) SEM observation of gold layer left on substrate. Sample is bonded at 125g per bump [244MPa] (b) Sample is bonded at 500g per bump [976MPa] (c) SEM observation of a cylindrical gold material left on the chip side 65

Figure 3-30 Very weak or no bonding at the center of the bump (left). The drawing on the right showed that failure occurs at the weakest bonding region – central region and proceeds cohesively through the bulk material. 66

Figure 3-31 Dependence of interfacial and cohesive bond strength on unbonded radius, r........ 68

Figure 4-1 Schematics of molecular response of SAMs to various amount of compressive loads (10MPa – 1.2GPa) 74

Figure 4-2 Schematics of process flow in SAMs deposition 76

Figure 4-3 Tensile strength of bonded joints bonded at 310 MPa and 516MPa in variation with bonding temperature 77

Figure 4-4 Comparison between gold-gold joints formed with and without the help of SAMs........ 78

Figure 4-5 SEM fractographs of substrate surface at different chip temperatures and bonding loads: (a) 120°C and 200MPa/bump (b) 150°C and 510 MPa/bump........ 79

Figure 4-6 Comparison of the tensile strength of coated electroplated samples and uncoated gold samples at constant bonding pressure at 500MPa 80

Figure 4-7 Illustration of SAMs acting as: (a) a passivation layer (b) a lubricant........ 82

Figure 4-8 A plot of tensile strength of SAM-coated samples - C_6, C_{12}, and C_{18} as compared to an uncoated gold as a function of bonding temperature applied. 85

Figure 5-1 XPS peak area ratio of O1s (top) and C1s (bottom) of both coated and uncoated gold samples with reference to Au 4f peak........ 89

ATTENTION: The Singapore Copyright Act applies to the use of this document. Nanyang Technological University Library

Figure 5-2 Relative percentage improvement in tensile strength of C_{12} -coated to uncoated gold samples as a function of exposure time prior to bonding 89

Figure 5-3 Comparisons of XPS peak area ratios of: (a) O1s, (b) C 1s at different chain length 91

Figure 5-4 Comparison of thiolate and carbon species on all SAMs before and after deformation 94

Figure 5-5 Schematic of the Kretschmann SPR Setup 96

Figure 5-6 Net shifts in resonant angle of C_6 as a function of temperature 97

Figure 5-7 Net shifts in resonant angle of C_{12} as a function of temperature 97

Figure 5-8 Net shifts in resonant angle of C_{18} as a function of temperature 97

Figure 5-9 Core spectra of: (a) C1s and (b) S2p recorded at different heating temperatures for alkanethiols - C_6 at 298K, 323K & 363K, C_{12} at 298K, 363K & 443K and C_{18} at 298K, 363K & 503K. 101

Figure 5-10 %Net loss in carbon and sulphur calculated from the peak area ratio against gold reference for C_6, C_{12} and C_{18}. 101

Figure 5-11 Wetting of alkanethiols (n = 5, 11, 17) absorbed on gold by water after heating at 90°C, 150°C and exposure in air (left) and nitrogen-purged (right) environment for 2 and 7 days. 106

Figure 5-12 Negative TOF-SIMs spectra of freshly prepared alkanethiols (n = 5, 11, 17) in air (left) and nitrogen-purged environment (right)... 107

Figure 5-13 wetting angle of alkanethiols as a function of days of exposure in both air and nitrogen-purged environment 108

Figure 5-14 Relative intensity ratio of the elements against gold as temperature increases in air (left) and nitrogen-purged environment (right) 109

ATTENTION: The Singapore Copyright Act applies to the use of this document. Nanyang Technological University Library

Figure 5-15 Negative TOF-SIMs spectra of alkanethiols [CH3 (CH2)x-SH] where x = 5, 11, 17 on gold at heating temperatures of 25°C , 90°C and 150°C, respectively in air. ... 110

Figure 5-16 Negative TOF-SIMs spectra of alkanethiols [CH3 (CH2)x-SH] where x = 5, 11, 17 on gold at heating temperatures of 25°C , 90°C and 150°C respectively in nitrogen-purged environment. ... 111

Figure 5-17 Net loss (%) of cluster ions against gold as temperature increases in (left) air and (right) nitrogen-purged environment ... 111

Figure 5-18 Effect of the duration of heating (2, 30 & 60 minutes, respectively) at 150° C on wetting properties of alkanethiols under different environmental conditions 112

Figure 5-19 Net loss (%) of cluster ions in alkanethiols after heated over 2, 30 and 60 minutes in air at 150°C ... 113

Figure 6-1 Pressure dependence of copper joints bonded at 25°C for 30secs ... 118

Figure 6-2 SEM micrographs on (left) Top view of electroplated Cu bump; (right) Cross-sectioned bonded Cu Joints at 25°C, 3.28GPa ... 118

Figure 6-3 Temperature dependence of uncoated copper from 25°C to 300 °C at 3.28GPa for 30 seconds ... 120

Figure 6-4 Comparison of shear strength in coated copper against uncoated copper from 60°C to 140°C ... 123

Figure 6-5 Net gain in bond strength by undecanethiol as a function of bonding temperature ... 124

Figure 6-6 XPS survey spectrum of a coated Cu surface (top) and an uncoated Cu (bottom) ... 125

Figure 6-7 Peak Area Ratio against Cu 2p as a function of temperature for both coated and uncoated samples ... 126

ATTENTION: The Singapore Copyright Act applies to the use of this document. Nanyang Technological University Library

Figure 6-8 Core spectra of O1s of undecanethiol on copper at temperatures (top) 25 °C, 80°C, 140°C and 180°C (bottom). 127

List of Tables

Table 1-1 IC Junction temperature limit for various applications [10] 7

Table 1-2 Comparison of bonding techniques that can be used for 3D wafer to wafer or chip to wafer stacking [10] 8

Table 3-1 Mechanical properties of gold and electroless nickel 46

ATTENTION: The Singapore Copyright Act applies to the use of this document. Nanyang Technological University Library

Abstract

Three-dimensional integration, which involves stacking devices vertically, promises several attractive benefits such as high functionality, performance and low system power consumption due to shorter signal delays with the elimination of long wires. One of the common bonding techniques used is metal thermocompression bonding. The greatest stumbling block for using this technique is the need for high bonding temperature and/or pressure to create strong and reliable bonds. This thesis begins with a study on how temperature and pressure affect bonding characteristics and the mechanical integrity of direct gold joints. One important finding of these experiments is the identification of a critical temperature and pressure below which no bonds can be formed. The criteria for bonding to occur include the removal of surface barrier film between contacting sites through sufficient interfacial mechanical and chemical actions. Freshly exposed surfaces are thus activated thermally, leading to an increase in bond strength. Higher bonding pressure increases bond strength but to a maximum. With further geometrical measurements and fracture analysis, the bonding mechanism is elucidated. This thesis also presents, for the first time, a method to lower the required bonding temperature in gold thermocompression bonded joints with the help of self-assembled monolayers [SAMs]. A comparative study on alkanethiols of various chain lengths in influencing its bondability at several temperatures is evaluated.

ATTENTION: The Singapore Copyright Act applies to the use of this document. Nanyang Technological University Library

Its passivation resistance to harsh environmental conditions such as temperature, mechanical deformation and exposure against ambient contaminants are also investigated. Interestingly, longer chain alkanethiols exhibit poorer bondability with temperature. The role of alkanethiols governing low temperature gold bonding phenomenon is thus inferred to play a dual role: (1) to passivate the metal surface prior to bonding and (2) to behave as a milder barrier layer that can be both thermally and/or mechanically displaced. Finally this thesis highlights a demonstration of forming strong copper joints at a temperature as low as 60°C in ambient. The result suggests that the organic layer replaces a more mechanically stable oxide layer such that less thermal effort is needed to promote copper – copper bonding. In summary, this thesis describes the exploration of a method to achieve low temperature metal thermocompression bonding. More importantly, the successful demonstration of reduced bonding temperature will have a significant impact on the efforts in reducing thermal budget for 3D integration.

ATTENTION: The Singapore Copyright Act applies to the use of this document. Nanyang Technological University Library

Chapter 1 THREE-DIMENSIONAL INTEGRATION

1.1 2-D versus 3-D integration – Interconnection-limited!

In conventional integrated circuits (ICs), signals transmit through wire interconnects patterned on a 2D planar design space. In the genesis of integrated circuits, designing on a plane was favored because manufacturing and miniaturizing the planar circuits was easier. All these were made possible by photolithography which eventually became the industry standard production method in the 1960s [1]. Even when more industries were driven by Moore's Law to make bigger chips at high yield to meet the demand for higher circuit density on the 2D space, putting more metal lines at finer dimensions for interconnection on the planar substrate can still be achieved by the progress from conventional lithography process to optical projection. Moore's Law predicts a doubling of transistors integrated per microchip every two years. While researchers are still actively developing technologies to squeeze more circuits on the planar substrate, the continued demand for higher circuit density and further miniaturization forces conventional interconnection methods to limits. As ICs become more complex, so does the wiring to connect all the transistors on the planar substrate. Sophisticated design for routing of long wires within a given small planar area is very complex and challenging which further increases the cost. Besides the routing issues, as further scaling in feature size takes place to improve performance, the closely packed

ATTENTION: The Singapore Copyright Act applies to the use of this document. Nanyang Technological University Library

wires with smaller wire cross-sections and pitch degrades signal integrity by increasing unwanted resistance, capacitance and inductance that inhibit propagation of signals [2]. These long interconnects are definitely not the fastest way for the transmission of signal from one end of input to the output circuits as shown in Figure 1-1. Advances in IC technology can no longer accommodate rising R/C delays. The development of ICs becomes interconnection-limited. 2D integration will very soon become the legacy of monolithic IC architecture. Therefore to alleviate the existing interconnection-related problems, one of the possible solutions would be by a three-dimensional integration that connects different functional layers in the vertical dimension.

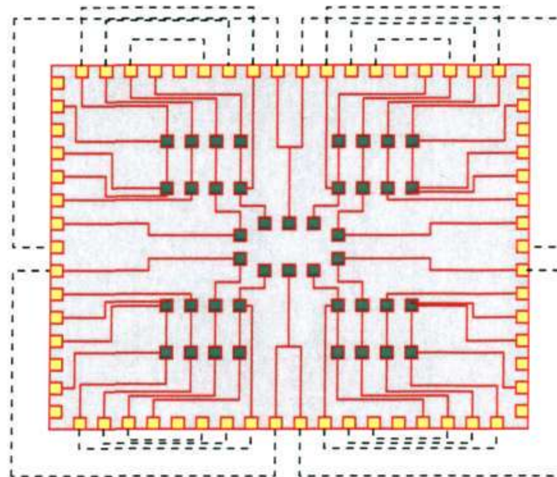

Figure 1-1 Schematics of the long wire connections in 2-D plane

1.2 Methods of Stacking: 3-D ICs and 3-D Packaging

Since 2-D interconnects limit the speed of signal propagation due to the long distances traveled, one possible way to overcome this limitation is to find a shorter distance between the I/O points. As mentioned earlier, the only way is to miniaturize along the z-axis, i.e. making three-dimensional devices by stacking each layer on top of each other. 3-D integration is a system level scheme wherein specific components are fabricated on individual, separate wafer platforms and then integrated onto a single wafer-scaled package; or, wafers diced into single bare dies or multichip modules which are then electrically-interconnected onto chip (chip-to-chip) or wafer (chip-to-

ATTENTION: The Singapore Copyright Act applies to the use of this document. Nanyang Technological University Library

wafer) to form a 3D package or simply by package stacking. One key difference between 3D packaging and 2D ICs is that 3D packaging offers more relaxed interconnect pattern geometry and alignment accuracy requirements as compared to 2D ICs [3]. Nevertheless, driven by greater demands for low cost portable electronic devices that require complex overall systems, the development of three-dimensional integration is the key technology to provide for significant size and weight reductions, higher performance, lower power consumption and higher reliability VLSI integrated circuits. It has been reported that the signal interconnects lines went up to several ten millimeters in a 2-D ICs but this interconnection length was much reduced in a 3-D ICs because the distance between each layers is in the order of 1-2μm [4].

1.3 3-D ICs Technology Options

The assembly of a 3-D IC device is strongly dependent on four key technologies. In the case of 3-D stacked wafers, through-vias are first etched in the device wafers. The wafers undergo chemical-mechanical polishing (CMP) process to planarize the two wafers to provide the surface finish prior bonding. The bonding between the wafers can be based on: (1). Covalent bonding between the wafers achieved by the chemical activation of the CMP-polished surfaces[5]; (2). Buried interconnections with thin metallization layers formed on top of the buried vias and/or bonding between microbumps made of solder or metal such as gold and copper [6]. After bonding, the top wafer/die of the 2-layered stacked device is thinned on the backside to expose the buried vias so that vertical interconnects can be formed on the exposed vias for subsequent stacking of the wafers. Generally, wafer thinning is essential because it helps to facilitate the through-wafer electrical connections and dissipate heat. Finally, a simple 3-D device is fabricated by repeating these steps. It had been reported that companies such as IBM, Intel, Micron, Infineon had demonstrated such stacked products and systems up to four or more stacked functional levels [7].

ATTENTION: The Singapore Copyright Act applies to the use of this document. Nanyang Technological University Library

These 4 key technologies contain their own limitations that can hinder the progress of the development of 3D integration. In the wafer alignment between stacked wafers, double-sided alignment capability is important. Precise positioning of the stacked wafers is necessary to prevent short circuits. Stacking between wafers can be achieved by through-vias technology. Despite being able to form high aspect ratio vias, difficulties in filling up the vias without forming voids due to sidewall profile still exist, especially when the pitch size reduces further [7]. In the wafer thinning step, chemical mechanical polishing (CMP), results in huge thermomechanical damages in the stacked device. While each of these technologies serves as a barrier to be overcome in order to progress further in developing 3-D integration, the true bottleneck arises from the bonding between the stacked layers.

There are a couple of 3-D architectures which are based on different approaches in stacking the device layers of top of each other as shown in Figure 1-2. Stacking devices in the face-to-face, face-to-back or even the combination of both as more layers are stacked dominate the current ways of integrating more circuits with different functions in a single IC. For instance, stacking in the face-to-face configuration with through-silicon vias (TSVs) can be done by simply bonding the two wafers together and later, back-etched to thin the wafer, exposing the TSVs. Without TSVs, the wafers can still be bonded and then back processed to form the TSVs. Again, these options are used to build chip-to-chip, chip-to-wafer and wafer-to-wafer 3-D ICs that are driven by specific applications. It is obvious that all these architectures would not work at all when they are not connected mechanically and electrically.. Hence this highlights the importance of forming suitable bonding between the device layers that not only enable the other key integrating processes in fabricating a 3D chip, but also provides a path for usual signal transmission and mechanical support.

ATTENTION: The Singapore Copyright Act applies to the use of this document. Nanyang Technological University Library

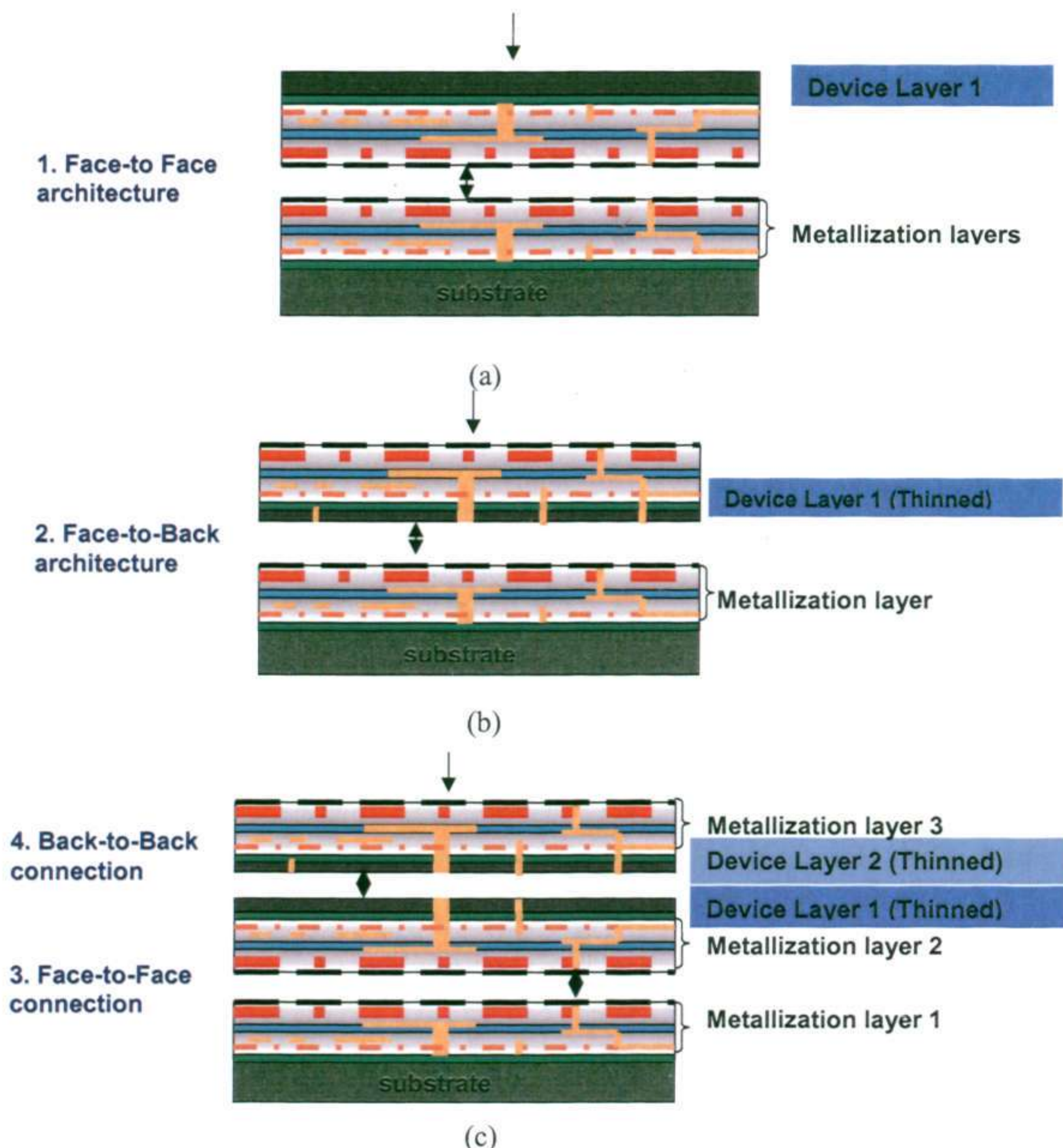

Figure 1-2 Schematics of 3-D architectures (a) Face-to-face (b) face-to-back (c) Combination of both

The crucial step in producing a 3-D integrated circuit involves the formation of bonds between the thinned wafers. With a vision of producing high density 3D integrated devices that contain the highest possible number of functions, highest possible reliability and yield yet at the smallest possible device size and cost, increasing development and research in overcoming the bottleneck caused by interconnects by big companies or research institutes such as IBM, Intel, Ziptronix, Tezzaron, IMEC, MIT etc. are carried out. This vision is briefly illustrated in a schematic shown in Figure 1-3.

ATTENTION: The Singapore Copyright Act applies to the use of this document. Nanyang Technological University Library

It will soon become widely-known that it is more cost effective and efficient to form vertical interconnections such as microbumps than wire interconnects which cause drag [8].

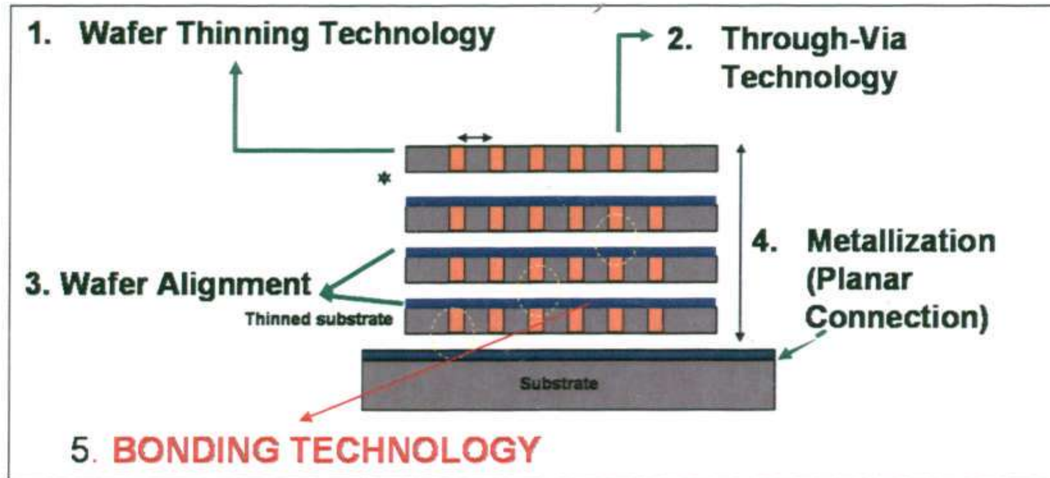

Figure 1-3 Illustration of the 5 key technologies in 3D integration

1.4 Thermal Issues in 3-D integration

Thermal effects are one of the major concerns that determines the performance and cost of a 3D device. As further reduction in chip size and increase in power consumption result from high density circuitry, the thermal effects are exacerbated [2]. This is not unexpected because these effects are already known to have a significant impact on 2D ICs. These thermal effects are due to poor heat dissipation through the stacked layers. With more stacked device layers, each generating a certain amount of heat during full operation, thermal problems have become more pronounced than ever, causing excessive damages in the device. High thermal resistivity materials used in multilayered structures also contribute to the huge thermal stress build-up in the 3D chip. In Table 1-1, a summary of the maximum tolerated IC junction temperature for various device technology or product needs shows a temperature limit below 200°C. It is also noted that for any temperature increase of 20°C, the lifetime of the system is reduced by a factor of two [9].

ATTENTION: The Singapore Copyright Act applies to the use of this document. Nanyang Technological University Library

Table 1-1 IC Junction temperature limit for various applications [10]

Applications	Temperature Limits (°C)
High Performance Logic	75
Low Performance Logic	125
Memory Devices	125
Handheld devices	125
Automotive Devices	175

Besides the self-heating of materials due to the increase in power density, processes during fabrication of 3D device also induce large amount of residual stresses in the device. For example, during chemical mechanical polishing for wafer thinning, the interaction between the wafer carrier, the wafer and the rotating polishing platen might cause residual thermomechanical stresses in the multilayers. In addition, high processing temperature limits the use of polymeric materials and causes huge thermomechanical stresses or mismatch between the dissimilar materials used in the stacked device that eventually leads to the failure of the device. This is valid since the bonding temperature needed for forming metallic interconnects (gold or copper) between the stacked layers in Table 1-2 way exceeds the temperature limits shown in Table 1-1. This situation will worsen since the required temperature and pressure will scale with the number of layers. Besides, bonding pressure used to bond interconnects between the layers might also result in warpage in thinned wafers. While the understanding that thinned wafers help to reduce stress in bump interconnects in stacked wafers remains, the fragile nature of thinned wafers limits the amount of process pressure that is tolerable in the bonding between wafer/chip stacking. These stresses will increasingly grow as technology scaling continues. Current bonding technology will soon be the bottleneck. This prediction is further supported by a report in EE Times [11], saying that according to the International Technology Roadmap in Semiconductors, as power density increases to about 100W/cm^2 by year 2018, there'll

ATTENTION: The Singapore Copyright Act applies to the use of this document. Nanyang Technological University Library

be no manufacturing solutions to manage the thermal flux by conventional packaging techniques. Besides high thermal budget, the reliability issues caused by the excessive thermal and mechanical stresses will lead to an increase in cost inevitably. Developing lower temperature and pressure bonding technology and better understanding of these processes are hence essential as scaling takes place since only low temperature and low contact forces can be tolerated in all key technologies involved in 3-D integration [12].

Table 1-2 Comparison of bonding techniques that can be used for 3D wafer to wafer or chip to wafer stacking [10]

Bonding Technology	Temperature (°C)	Bond Energy (J/m2)	Critical Points
Direct Bonding (SiO2)	200-1100	2	surface cleaning and polishing
Metal surface activated bonding	room temperature	20	in-situ surface cleaning
Au-Au thermocompression	400	strength validated	gold contamination
Polymer	150-400	20	thick glue layer
Sol-gel	400	2	thick glue layer
Soldering	200-300		unusual material formed

1.5 Proposal

1.5.1 Motivation

Large amount of research had been carried out to explore ways to remove heat from the device packages during operation to minimize thermal-induced damages. This includes: (1) using thermal interface materials such thermal greases that consist of metallic or ceramic particles or mixing solder materials to achieve lower eutectic melting temperature, (2) designing complex heat sinks and liquid cold plates to dissipate heat through air and forced convection, (3) implementing thermal vias for heat conduction and finally (4) managing interlayer heat removal through spacers and interlayer fluids. These methods aim at alleviating the thermal heat generated within the device during operation. This renders the system less power efficient as a result of the thermal-related stresses induced. Besides that, thermal stress fatigue or

ATTENTION: The Singapore Copyright Act applies to the use of this document. Nanyang Technological University Library

thermomechanical stresses arising from thermal expansion mismatch of package material combinations can also arise during device fabrication. These stressed regions serve as source sites that could fail catastrophically during operation. Hence the need to explore ways to minimize harsh process conditions and maintain mechanical and thermal stability at the same time aims to create a fundamental approach in relieving the stresses in the device prior to operating conditions. In particular, we highlighted that reducing the rigorous bonding conditions needed for forming the interconnects between multiple stacked layers would be a great challenge and this might limit the progress of 3D integration.

1.5.2 Objectives and Scope

In summary, the proposed research on metal bonding studies is sparked off by a simple yet important understanding that the bonding between the stacked wafers should not only provide electrical connection but must also remain mechanically reliable and stable over the period of its use. Therefore in applications whereby a monolithic 3D IC operates at its high speed and heat generation by each transistor leads to large volume of thermal stresses within the whole device, high temperature bonding is intolerable. The way to improve its bonding technology is by lowering bonding temperature and pressure, which defines the key objective of this PhD study. This thesis aims to achieve low temperature direct metal bonding using thermocompression process. In this work, a novel approach of using a monolayer of organic molecules to alleviate the required bonding temperature has been successfully discovered. Often, the bonding temperature and pressure optimization gives a quantitative indication on the amount of thermal input required for bonding to take place only. True mechanism on how temperature and pressure affect bonding qualitatively is weakly understood despite commonly-known bonding mechanism reported by Jellison [13]. Therefore to enable the realization of

ATTENTION: The Singapore Copyright Act applies to the use of this document. Nanyang Technological University Library

room temperature direct metal bonding, fundamental understanding of the following key areas and exploration of novel approach are essential:

1. Understand Roles of Temperature and Pressure in Thermocompression

In the earlier studies, gold has been the preferred material for thermocompression as it is known to be oxidation-free. It offers the conductive bonds using relatively low temperatures and pressures but it is limited by the organic contaminants present on the surface during bonding that will affect the mechanical strength of the bonds formed [14]. Although direct metal bonding has been explored as early as a few decades ago [15, 16], the roles of temperature and pressure in initiating bonding over a wide range of bonding temperature are not well-understood. In this study, bonding gold under the influence of different temperature below 200 ºC and pressure is investigated to gain insights on how bonding between two surfaces begins. Since copper is a more promising candidate as an interconnect material for 3D IC due to its high electromigration resistance, low electrical resistivity and low cost, it is equally important to understand how bonding temperature affects copper joint integrity since copper surfaces are much more reactive compared to gold. Mechanical behaviour of the bonded metal joints using mechanical tests such as tensile and shear test will then be deduced and analyzed. Prior understanding on the mechanical behaviors of the chosen material system for bonding is often necessary to have better control during actual process development.

2. Investigate surface modification by Self-assembled Monolayers

In the quest of achieving room temperature direct metal bonding, much of this research is focused on obtaining successful Thermocompression bonding at a relatively lower temperature using nanostructured organic monolayer on bare metal surfaces prior to bonding. Surface cleanliness is one of the key factors that determine bonding

ATTENTION: The Singapore Copyright Act applies to the use of this document. Nanyang Technological University Library

parameters required. In order to facilitate low temperature and pressure bonding, aggressive wet and dry cleaning prior to bonding of metal surfaces such as copper were used to remove oxides and organic contaminants, respectively. Such methods are damaging especially on active layers with miniaturized features patterned on the wafers. As a result, it is a great incentive to explore new ways to replace such time-consuming and costly processes. Investigation of surface modification using self-assembled monolayers such as alkanethiols on non-oxidative metal – gold is explored first. Through a sequence of systematic bonding experiments, the impact of coating the metal surface with a single layer of organic molecules is evaluated by assessing the bond strength of the chemically modified - surface with that of the uncoated gold surfaces at various bonding temperature. In this thesis, it is postulated that such coating serves as a passivating layer which inhibits surface contamination on the gold surfaces prior to and during bonding. Besides thermal-activated bonding which involves the interatomic diffusion of the lattice atoms across the two contacting surfaces, it is known that bonding begins only when two fresh metal surfaces are in close contact with each other. Hence simultaneous removal of any barrier layer [surface contaminants, oxide or the organic coating, etc] is assumed to be equally important. Since this work involves the stability of alkanethiols on the metal surfaces against contamination and its behaviour under mechanical wear or deformation during bonding, it is imperative to assess the structural characteristics of alkanethiols with different chain lengths under different environmental conditions, which will consequently determine its efficacy in passivating its underlying substrate as well as its response to mechanical deformation. This will help gain some insights into the mechanism of alkanethiols in enhancing direct metal bonding.

ATTENTION: The Singapore Copyright Act applies to the use of this document. Nanyang Technological University Library

3. Demonstration of Ambient Copper Bonding with Self-Assembled Monolayers

Due to its lower electrical resistivity and higher melting point, copper, instead of aluminum, has become the mainstream material for today's interconnect technology, yielding benefits such as a reduction in interconnect-related RC propagation delay and improved electromigration resistance [2, 17, 18]. However forming good quality Cu bonds is not as easy as compared to other interconnect materials such as gold. The ease of oxidation of copper often entails a need for high bonding temperature (> 300°C) and/or ultrahigh vacuum conditions. A post-annealing process at temperature equivalent to or higher to the bonding temperature under inert atmosphere over an adequate amount of time is also reported to help in enhancing bond integrity [19, 20]. Bond quality of the copper joints is governed by bonding parameters such as temperature, pressure and time [21]. As mentioned above, the highly reactive copper surface thus requires extreme caution in the process of both wet and dry cleaning to remove copper oxide prior to bonding. A typical copper-copper thermocompression bonding process is carried out in an ultrahigh vacuum (UHV) or inert environment at a bonding temperature >300°C. The ultraclean environment serves a single purpose – to maintain oxide-free copper surfaces, allowing intimate physical contact between copper atoms. Yet often, a time lag between sample preparation and bonding leads to an inevitable formation of surface oxide which necessitates more stressful bonding conditions for successful bonding. Due to the high oxidation rate of copper surface, a protective coating such as a cap of tin or gold is plated onto the copper surface. Alternatively a cluster equipment [22] is used to achieve efficient copper-copper bonding. In cluster equipment, in-situ cleaning is carried out under a controlled environment such as ultrahigh vacuum by bombarding low energy Ar ion beam to remove the oxide layer. The wafers were then transferred under high vacuum to avoid any oxidation and subsequently bonded under pressure. This allows room temperature bonding but incurs

ATTENTION: The Singapore Copyright Act applies to the use of this document. Nanyang Technological University Library

huge costs for such complex equipment. Several studies [23-26] have been carried out to evaluate the composition of these oxides that formed naturally when the surfaces are in contact with the environment. A general consensus was derived that dual oxide phases containing CuO and Cu_2O constitute the major components of the oxide layer while intermediate phases such as Cu_3O_2 was also observed especially at low temperature oxidation. To our knowledge, a correct identification of these oxides as well as its properties is still unavailable today. For oxide-covered metal layers, metal-metal bonds are formed through fragments of oxide layers[27]. Further increase in temperature is reported to promote more copper diffusion and grain growth across the original bonding interface, thus improving the bond strength [28].

The use of SAMs for copper bonding applications was first demonstrated in copper wire bonding where the monolayer was coated onto copper bonding pad to improve wire bonding of gold or copper by reduction/removal of copper oxide from the copper bond pad. The enhancement by such technique was observed when the percentage of non-stick bonds formed by coated copper was higher than that of bare copper bond pads, while maintaining comparable bond strength [29-33]. It was believed that the ultrasonic energy applied during bonding resulted in, first, the removal of the SAM layer and then the weld formation between the metallic surfaces, yielding shear strength of 0.06MPa. Subsequently, Liu and Hutt [34] reported the use of self-assembled monolayers in replacement of flux which is commonly used in soldering on copper PCB substrates and foils. They demonstrated high solderability of SAMs-coated copper surfaces even after several months of storage under room temperature, attributing this observation to the superior passivation ability of SAMs. Besides its application in direct copper bonding, the versatility of SAMs enables its application in improving adhesion strength between dissimilar materials such as copper and silicon dioxide. In this work by Rensselaer Polytechnic Institute (RPI) [35], effect of

ATTENTION: The Singapore Copyright Act applies to the use of this document. Nanyang Technological University Library

annealing strengthens the copper-silicon joints through tougher siloxane bridging between the two surfaces. It reports the novelty of using self-assembled monolayers to improve adhesion between two dissimilar materials- copper and silicon oxide. Due to the strong cross-linked structure of the siloxane structure formed between the surfaces, it improves the adhesion between copper and silicon oxide. Since the focus in our report discuss SAMs in simplifying the means to achieve cohesion between two metallic surfaces, no comparison would be made with the work by RPI since their novelty lies in promoting better adhesion between dissimilar materials.

Having known that alkanethiols also serve as effective corrosion protective coatings for highly oxidative copper surfaces, the feasibility of circumventing the need of high vacuum conditions and high bonding temperature for the formation of strong copper bonded joints is investigated by performing bonding studies of coated copper surfaces over a range of temperature in ambient. The impact of the findings is examined by comparing the strength of the uncoated joints with the joints formed under the assistance of a prior organic coating. This insight will elucidate a simple and low cost method in enabling copper bonding under ambient conditions.

1.6 Organization of Report

To summarize the previous sections on project objective and scope, this PhD research topic covers two key areas, namely the mechanical and chemical aspects of bonding studies. The work is divided into six major chapters in which it is hoped that the report will offer a clearer understanding on the importance of bonding temperature and pressure in creating metallurgical joints. The defining idea of this report is to demonstrate the possibility of a novel and simple idea of modifying metal surfaces through a monolayer of molecules in facilitating low temperature bonding. Chapter 1 gives brief background information related to this research and presents the motivation and objective.

ATTENTION: The Singapore Copyright Act applies to the use of this document. Nanyang Technological University Library

A literature review covering various bonding schemes in thermocompression bonding process such as direct metal bonding, eutectic and polymeric bonding, that are related to three dimensional integration is presented. The original work accomplished in this research is presented in Chapters 3 to 6. The addition of a chemical element into a mature material system [metals] used for forming electrical and mechanical interconnects for ICs over almost five decades to date, can be carried out by coating a nanostructured organic monolayer on a microscale metal surface.

Chapter 3 serves to establish the bonding model in the formation of the gold joints under thermocompression. The bonding conditions involved in creating bonding between the two surfaces and approaches employed to assess the mechanical strength to identify the critical factors influencing the bonding model are discussed. In Chapter 4, the first attempt in abating the required bonding temperature for forming relatively high strength gold joints using dodecanethiol is reported. A model on how such a monolayer could have aided the formation of strong bonds at low bonding temperature is briefly discussed. A study on the chain length dependence of the bondability of coated gold surfaces is also provided. This is important since we are able to make use of the intimate relationship between the chain length and its structural response to thermal and mechanical input to reinforce our understanding of what constitutes bond creation between two atomically clean metal surfaces. A more detailed explanation on the role of alkanethiols on direct gold Thermocompression bonding is described. The issues involved and the approaches to verify the key functions of alkanethiols are discussed.

After demonstrating the success of room temperature gold bonding using alkanethiols, it is natural to extend this idea to a more robust material system such as copper. Chapter 6 reports the first demonstration of ambient copper bonding at low temperatures using the same type of coating. Similar experiments with slight modifications to accommodate the highly oxidative nature of copper are carried out.

ATTENTION: The Singapore Copyright Act applies to the use of this document. Nanyang Technological University Library

Based on the characteristics of alkanethiols demonstrated in gold system, similar analysis to validate the role of self-assembled monolayers in bonding are demonstrated. Finally, a summary of the major conclusion of this research will be given in the last chapter and some suggestions are also presented for future research areas.

ATTENTION: The Singapore Copyright Act applies to the use of this document. Nanyang Technological University Library

Chapter 2 BONDING

2.1 Introduction

In this chapter, the current understanding on the bonding mechanism governing thermocompression bonding is reviewed. This involves the following: (1) defining what bonding means at the atomic scale, up to macroscopic scale; (2) looking at what constitutes a real surface (asperity model) and specifying terminology to define the geometrical changes when two real surfaces are bonded (area model) and finally reviewing the current comprehension of thermocompression bonding as a function of bonding temperature and pressure respectively. Various bonding techniques available for forming interconnects were also reviewed.

2.2 What is bonding?

At the smallest scale, bonding can be defined as the binding between atoms or molecules by a strong atomic attraction. The forces responsible for this arise from the coulombic forces based on the separation distance between the two isolated atoms. Basically these atoms bind when there is no net force between them at a specific separation distance – the equilibrium separation. Such binding process is energetically favored since the net potential energy between them reveals a minimum at the equilibrium separation. Consequentially, this minimum energy and equilibrium distance

ATTENTION: The Singapore Copyright Act applies to the use of this document. Nanyang Technological University Library

represent the bond energy and bond length for a single pair of bonded atoms. Hence to bring these two atoms apart to an infinite separation, the energy required must be equal or more than the bond energy. These values vary with material as well as the type of atomic bonding. From these observations, it is understood that when two atoms bind strongly, a discrete amount of bond energy is acquired. In the case of metallic bonds, these primary bonds are formed when an atom shares its valence electrons with its neighbouring atoms, forming an electron cloud around the nuclei of the surrounding metal atoms. Similarly, at that instant, a defined amount of bond energy is also registered based on the collective nature of metallic bonds.

What happens when two surfaces of metallic atoms bond to form a joint? Bond strength, rather than bond energy, is assigned to depict the minimum amount of energy per unit area needed to break the surfaces apart. The bond strength for a particular material type is found to vary as a function of its process parameters during bonding such as bonding time, temperature and pressure. In contrast, bond energy is fixed. That is because bond strength is just the summation of the total number of bonds, all with the same bond energy, over a unit area. In the case of metallic bonds where a "single" metallic bond does not exist, bond strength of metallic joints is the summation of a number of "collective" metallic bonds. The number of bonds created during bonding of two surfaces becomes the real variable – that's the meaning implied in what we call true contact area, a term to be defined later.

2.3 Asperities in Bonding

There is no absolute smoothness in true surfaces. Even at microscopic level, the smoothest surface may be characterized by distribution of asperities as shown in Figure 2-1. These asperities vary in curvature radii, heights as well as densities. In bonding, the surface asperities serve as initial contacting sites when two surfaces are brought intimately close to each other. So when two real surfaces come into contact under

ATTENTION: The Singapore Copyright Act applies to the use of this document. Nanyang Technological University Library

applied pressure, bulk metal experiences a dilation laterally, leaving a projected area on the bottom layer, termed as nominal area (A_n). However not the entire nominal area is bonded. The regions left on the substrate after mechanical shearing or tensile pulling are the nominally bonded area which we defined as the contact area between the two bonding surfaces (A_C). Microscopically, not all contact area is bonded either. As mentioned above, due to surface roughness, the asperity summits touch first before the rest of the discrete spots within the contact area. These asperities undergo extensive deformation due to stress concentration at sharp tips. When they undergo plastic deformation, bonding occurs. Henceforth, the total area of these microscopic discrete bond sites will be called the true contact area (A_T). Naturally, true contact area (A_T) is the quantity that determines the bond strength. It is always a fraction of the contact area A_C, which is itself a fraction of the nominal area A_n after compressive deformation Figure 2-2 illustrates the description above.

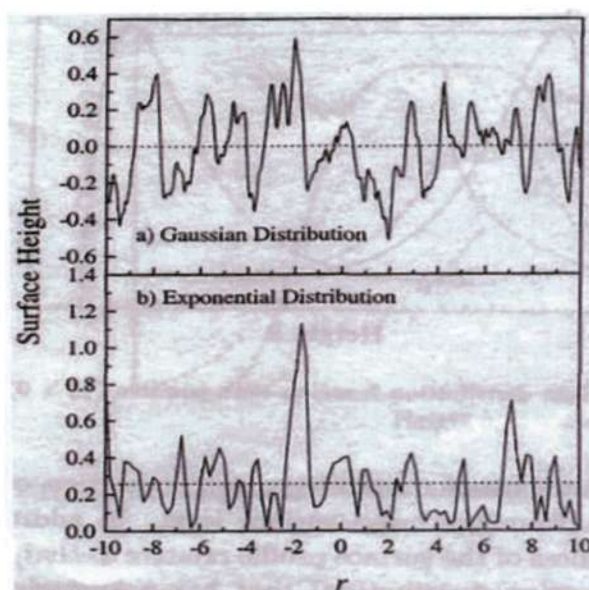

Figure 2-1 Examples of the types of height distributions for surface roughness

ATTENTION: The Singapore Copyright Act applies to the use of this document. Nanyang Technological University Library

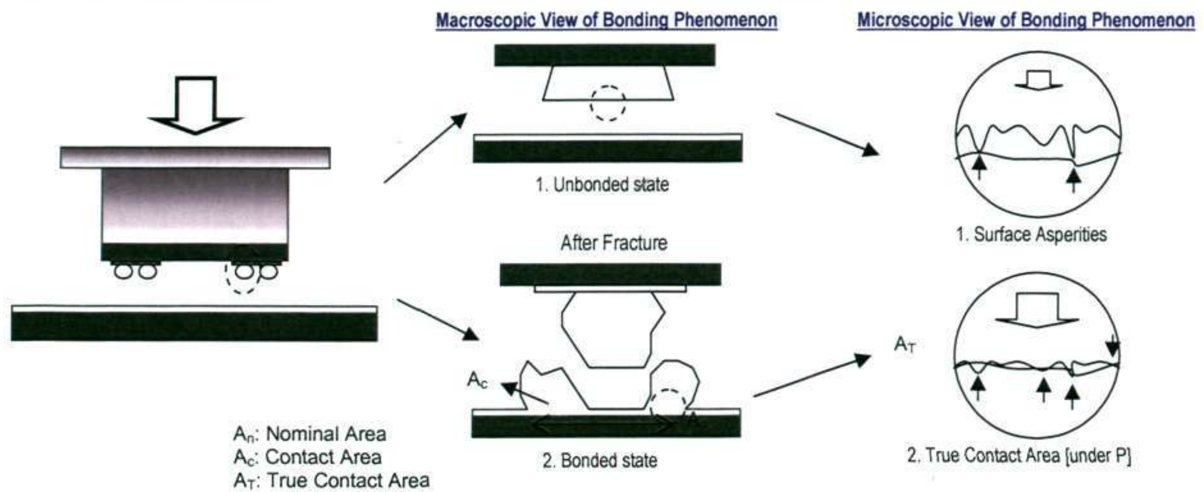

Figure 2-2 Definition of interfacial area regions in bonding.

2.4 Barrier Layer Theory

Thermocompression bonding is a form of solid phase welding (SPW) first demonstrated using electrical metal lead attachments to semiconductor devices [36, 37]. This process requires the application of pressure (usually about 10 - 30% material deformation) and heat (much lower than the melting point of the material) simultaneously in order to form bonds between two otherwise separate surfaces. In the 1960s, Tylecote [16] developed two key prerequisites for solid phase bonding. The surfaces must be kept in intimate contact for short range cohesive forces to act. Besides the conformity between the rough surfaces, surface removal of any contaminants and impurities are equally necessary prior to successful SPW. Following that, several studies [13, 27, 36-38] later supported the argument that surface contaminants indeed act as a barrier to bonding. It is widely known that adsorbed layers of atmospheric gas (especially wet air – water vapour) and other surface contaminants and films such as photoresist residues, oxides, etc on bonding surfaces or even surface irregularities can impair the formation of a metallurgical bond [27, 39]. In the case of noble metals such as gold, the barrier layer is a highly "mobile" layer which resists dispersal. It was suggested that oxygen in wet air was the key culprit preventing bonding. Attempts were

ATTENTION: The Singapore Copyright Act applies to the use of this document. Nanyang Technological University Library

made to analyse the chemistry of these contaminants, namely carbon, oxygen and sulphur. Controversial results were reported. It had been suggested that carbon and oxygen constitute the major components, forming a thin layer of adsorbed gases or hydrocarbon[14]. Others postulated that carbon from atmosphere exists as molecules of hydrocarbons but do not exist as an oxide. The thickness of this carbonaceous layer formed in air was also approximated to be about 2Å which increases with exposure time [40]. To our knowledge, the kinetics of its growth remains unknown and its true chemistry remains a contention.

2.5 Role of Bonding Temperature and Pressure – A Review on Bonding Mechanism

Studies on thermocompression of gold were explored in various aspects such as the influence of bonding parameters, process optimization and modeling [12, 13, 18, 19, 22-28]. Two key parameters - temperature and pressure were most widely studied, varying in its configuration. For example, gold-plated leads were bonded to gold metallization at temperatures between 270 °C and 620 °C to evaluate the corresponding bonding time needed for bond completion. On the other hand, gold ball bonding [41] was investigated at a heated capillary temperature ranging from 150-200 °C and substrate temperature above 300 °C. It is understood that an increase in bonding temperature, pressure or time would increase the shear strength of gold-gold joint [13, 42]. While the prerequisites to bonding are explained in the previous section, it is apparent both temperature and pressure play a major role, respectively. The current understanding on the role of bonding temperature and pressure can be summarized in the following:

(1) The bonding temperature helps to disperse the surface contaminants by thermochemical mechanism. It had been proposed that heating promotes the agglomeration of contaminants, diffusion of these phases into the base metal and then

ATTENTION: The Singapore Copyright Act applies to the use of this document. Nanyang Technological University Library

desorbing adsorbed gases[27]. Jellison [13], on the other hand, reported that the desorption phenomena becomes important only when heating is above 300°C ;

(2) Applied bonding pressure is necessary to produce interfacial conformity between two surfaces as well as shearing displacements at the interface to create appreciable plastic deformation. It was found that under low initial normal load, very low or no bonding between the two surfaces takes place even if the surfaces are very clean [15]. However, if the sites are subjected to adequate amount of normal load which induces plastic deformation at the interface, the bonded sites may be able to retain its joint strength. For contaminated surfaces, plastic deformation under normal loads is ineffective in contaminant disruption [43]. This is evident in N. Ahmed's study which found that the high normal stresses were not sufficient for bond formation. Rather, it is the tangential component of shear stress that could influence bond formation by aiding deformation of asperities and bringing about plastic deformation [38, 44]. It is generally agreed that the applied force is needed to facilitate material flow to achieve full interfacial contact by lateral deformation or interfacial shear. Through surface dilation, barrier films are broken down for formation of metallic bonds [45]. This understanding is further supported by Bay [46] who showed theoretically that the bond interface exposed is governed by the interfacial deformation behaviour. Overall, all these highlight an important point – with or without a contamination layer, plastic deformation at the interface is necessary for solid state bonding.

(3) An inverse relationship between bonding temperature and pressure was first documented when process optimization was carried out to develop a better understanding of thermocompression process at Bell Laboratories [38]. This relation is strongly dependent on the extent of contributing to contaminant removal and amount of interfacial shear stress by each parameter. With higher bonding temperature, an equivalent amount of bonding strength can be achieved using lower bond pressure and

ATTENTION: The Singapore Copyright Act applies to the use of this document. Nanyang Technological University Library

vice versa [13]. However, at very low bonding temperature, little or no bonding occurs despite some compensation of load increase. Alternatively, using very low bonding pressure with sufficiently high bonding temperature also does not seem to form bonds [38]. Such observations strongly imply the existence of a critical temperature as well as a critical interfacial shear stress. Indeed earlier work by Bowden and Rowe[15] reported an existence of a critical temperature beyond which the adhesion strength between clean platinum metals increases rapidly. While other studies on the deformation properties of gold [47] and the kinetics of thermocompression bonding [42] were also reported, a unified theory of the bonding mechanism is still lacking, thus leading to this proposed research in understanding the challenge in achieving bonding at temperature as low as room temperature and its bonding behaviour.

2.6 Thermocompression Bonding

In Figure 2-3, a comparison between bonding schemes undertaken by major 3D ICs manufacturers is shown. Various bonding techniques utilized in stacking the layers include direct fusion, anodic, thermocompression and/or thermosonic bonding. Thermocompression bonding is used in various microelectronics applications because it offers the ability for low temperature bonding and the elimination of complicated pre-cleaning procedure. Unlike thermosonic bonding, thermocompression process does not involve ultrasonic energy which can lead to problems such as silicon cratering or excessive vibration damages. In the earlier studies, gold has been the preferred material for thermcompression as it is known to be oxidation-free. It offers the conductive bonds using relatively low temperatures and pressures only but it is limited by the organic contaminants present on the surface during bonding that will affect the mechanical strength of the bonds formed [14].

The different bonding schemes adapted to wafer or die stacking can be categorized by two different ways: intermediate and non-intermediate layer bonding.

ATTENTION: The Singapore Copyright Act applies to the use of this document. Nanyang Technological University Library

These can then be further subdivided into three main processes, namely- (1) metal bonding which can be direct metal (copper, gold etc.), eutectic (copper-tin) and hybrid (metal with SiO_2) bonding, (2) pure direct bonding (glass, silicon oxide etc) and finally (3) intermediate bonding using conductive adhesives (polymer). Besides wafer-wafer bonding, microbumps formed on the chips are commonly used to connect the stacked layers when they are bonded upon the application of temperature and pressure. Metallic microbumps formed using copper, gold, indium and eutectic solders are often favoured due to the strong metallurgical bonds formed and their excellent electrical and thermal properties.

	3-D Processes								
	RPI	Fraunhofer Munich	ASET Japan	Tohoku University Japan	IBM	Infineon	MCNC-RDI	Toshiba	Tezzaron
Wafer to wafer	X			X				X	
Chip to wafer		X				X	X		
Chip to chip			X				X		
SOI or bulk wafer	SOI		Bulk		SOI		Bulk	Bulk	
Via size (μ m)	2*2	2.5	10	2.5			4	30	
Via etch process	SF_6		SF_6	SF_6			SF_6	SF_6	SF_6
Peripheral vias			X					X	
Area array vias	X	X				X	X		X
Via dielectric	SiO_2	SiO_2	SiO_2	SiO_2		SiO_2	Polymer	SiO_2	SiO_2
Barrier layer	TiN	TiN	TiN			TiN	TiN	TiN	TiN
Metal plug	Cu	W or Cu	Cu	Poly-Si or W	Cu	Cu	Cu	Cu	Cu
Handle wafer	No	Yes	Yes	Yes	Yes	No			No
Bonding scheme	Polymer	Cu-Sn eutectic	Cu-Sn eutectic	In/Au bumps	Si Fusion	Cu-Sn-Cu	Polymer or bumps	Bumps	Cu-Cu

Figure 2-3 A comparison of key processes in 3D Integration [MCNC R&D Institute - Semiconductor International (2005)]

2.7 Bonding Options

There are various bonding options which include direct bonding between silicon dioxide layers (non-metal) and metal surface activated bonding without melting, adhesive bonding using dielectrics or polymer glues and hybrid bonding between both metals and polymeric materials.

ATTENTION: The Singapore Copyright Act applies to the use of this document. Nanyang Technological University Library

2.7.1 Metal Bonding

2.7.1.1 Direct Metal Bonding

Direct metal bonding is a method of joining two flat, clean and smooth surfaces under ambient condition without an intermediate layer or glue between them. This is possible using surface activated bonding and thermocompression bonding [22, 48]. Many studies on direct copper-copper Thermocompression bonding have been evaluated by the Microsystems Technology Laboratories (MTL) at MIT [31-43]. Bonding of blanket copper as well as copper lines does not occur instantaneously at room temperature. Relatively high bonding temperature ranging from 300°C to 400°C is required. Therefore, when the bonded pair is cooled, large amount of stresses will be induced in the bonding layer due to thermal mismatch, resulting in the formation of voids [49]. The presence of voids is highly undesirable since they lead to serious reliability issues such as copper corrosion by the moisture trapped in the air gap. This may degrade the mechanical support between the layers. Milder bonding conditions are essential for reliable integration of copper-copper Thermocompression joints into the stacked devices.

In the case of noble metals such as gold, it is inert to oxidation but highly reactive to organic molecules. It has been reported that due to a higher ionization probability with greater reactivity towards carbon vapour species, adventitious carbon grows faster on gold as compared to other metal such as aluminium [50]. To bond such surfaces, relatively high pressure is also required to deform the surface asperities as well as the organic contaminants on the surface. Then with application of temperature, the contamination layer will be removed thus exposing fresh metal for bonding. Figure 2-4 shows successful stacking between IC layers using direct copper metal bonding.

ATTENTION: The Singapore Copyright Act applies to the use of this document. Nanyang Technological University Library

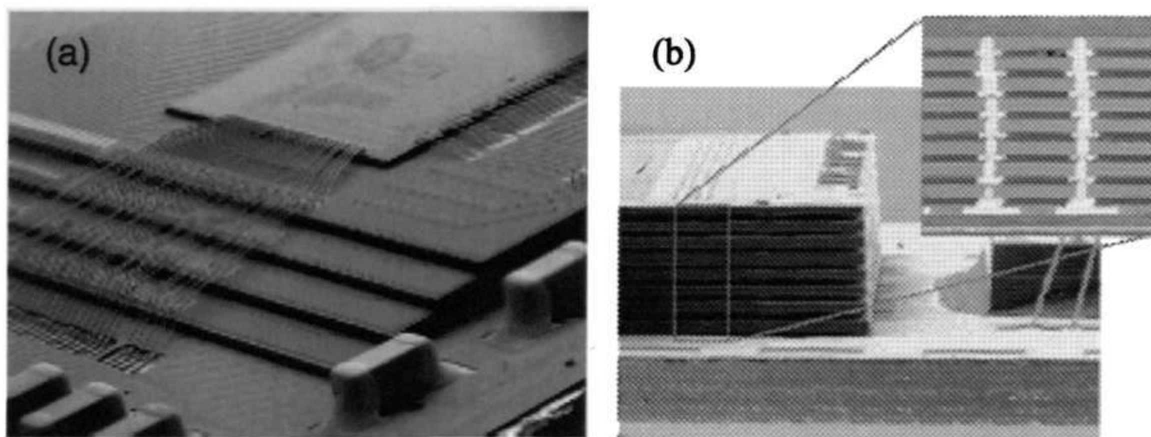

Figure 2-4 (a) Metal wire bonding to stack the chips using gold or copper (b) 8 stacked layers of IC using copper-plated through-silicon vias- Samsung 16GBit NAND Flash prototype.

2.7.1.2 Eutectic Bonding

Soldering is known to be the most suitable method of joining when a packaged chip is attached to another substrate such as an organic laminate [42]. The commonly used solder for bonding in electronic packages are formed by low melting metals such as tin, lead, bismuth, silver and indium, with binary alloy SnPb as the most important solder. The key advantage in solder bonding is the feasibility of mixing two dissimilar metals to tailor the melting temperature of the alloy. In the case of a Sn/Pb solder system, the melting point of pure lead and pure tin is 323°C and 233°C, respectively. At a composition of 63%Sn/37%Pb, the melting point is brought down to 183°C. With such lower bonding temperature, the device will suffer less thermal damages. Besides this, low cost is one of the major advantages in using solder. On the other hand, the key disadvantage of using a Sn/Pb solder is its high solubility for precious metals such as gold, forming intermetallic compounds. Despite the fact that the interdiffusion between two metallic surfaces form strong metallurgical bonds due to intermetallic layer, too much growth will result in detrimental effect in product performance [51].

ATTENTION: The Singapore Copyright Act applies to the use of this document. Nanyang Technological University Library

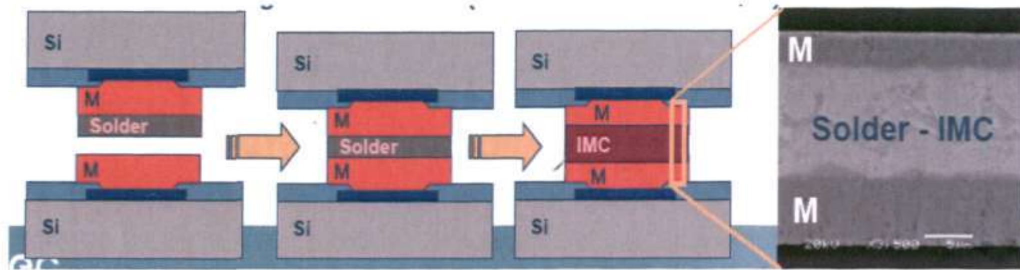

Figure 2-5 Application of a solder material [Cu-Sn] as a bonding intermediate between metal interconnects [IMEC].

Most soldering processes require the use of flux to remove the oxides from the metal surfaces prior to bonding as the oxides prevent effective bonding between the solder and the substrate. The flux contains organic acids that help to etch away the oxides. Even though soldering provides good electrical interconnection, large amount of flux used in soldering often leaves residues that are corrosive in nature and thus reduce the long-term reliability of the packages. Recently fluxless soldering is vigorously researched to prevent the negative effects of flux used in soldering. In the recent report by Choe et al.[52], low temperature fluxless bonding for photonic and fiber optics devices is demonstrated using indium-tin composite material at 140°C. This is especially valuable for emerging devices that cannot tolerate flux.

With greater concern in the Pb contamination in environment, legislation and market trends force every electronic device assembler to replace Pb-containing solder with Pb-free solder. With the removal of Pb from solder, it necessitates the replacement with a suitable material, such as copper and silver. Other Pb-free solders such as tin-bismuth, indium-tin, indium-bismuth or indium/tin-copper are also suitable for IC manufacturing. While such solders offer low melting temperature for bonding, other consideration such as bonding quality cannot be neglected [53]. Extensive studies have been carried out to study the reliability of Pb-free solders and their intermetallics in conventional 2D integration. So far, copper-tin eutectic bonding is the most commonly used bi-material system for 3D integration. Higher melting metal such as copper

ATTENTION: The Singapore Copyright Act applies to the use of this document. Nanyang Technological University Library

diffuses into the low melting metal [eg. tin] forming an intermetallic compound (Cu_3Sn) which is very stable and melts only at temperature higher than 600 °C, as shown in Figure 2-5. This is necessary since any shifting of the underlying device layers while remelting the metallic interconnects during stacking of the next layers can result in electrical shorts of the metallic contacts in very fine pitch applications [54].

2.7.2 Hybrid Bonding

Hybrid bonding refers to bonding between similar surfaces across a heterogeneous surface i.e. between two metal surfaces and two dielectric (glue or silicon oxide) surfaces respectively. In the case of direct thermocompression bonding between copper line interconnects, empty gaps between the bonded copper interconnects serve as potential regions for corrosion which might reduce the mechanical and thermal stability of the stacked structure. One of the possible solutions is to perform hybrid bonding of copper to copper and dielectric-dielectric layer such as benzocyclobutene (BCB) simultaneously which is actively explored by Rensselaer Polytechnic Institute and IMEC [52-54]. Figure 2-6 illustrates one of the 3D stacked chip architecture at IMEC.

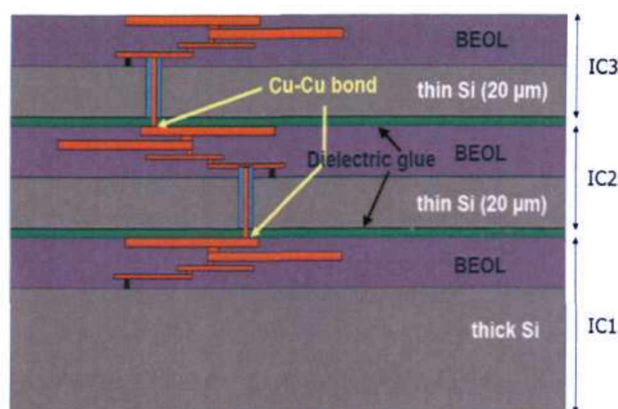

Figure 2-6 Copper and dielectric bonding between the stacked layers at IMEC [55]

ATTENTION: The Singapore Copyright Act applies to the use of this document. Nanyang Technological University Library

2.7.3 Direct Bonding

One of the wafer bonding techniques used for 3D integration includes fusing silicon wafers directly. These bonds are formed when the two highly polished wafers are brought into contact under temperature and pressure. In most cases of direct bonds, some surface treatment is conducted prior to contact to promote the surface attraction and bonding process. One key disadvantage of silicon fusion (SiO_2 - SiO_2) bonding is the high annealing temperatures with peak temperatures at 1100°C. Surface activation methods using oxygen plasma/argon atom etching/chemical solutions [55-57] were found to reduce such temperature to room temperature by altering the surface chemistry. In general, it is required that bonding surfaces be extremely smooth (RMS roughness < 1nm), flat (wafer bow of < 4μm for a 4 inch wafer) and clean, because protrusions or particles can create bonding voids [10]. This method offers the advantage of forming bonds that are high temperature stable and producing structures that have less thermal expansion mismatch compared to other methods. The process steps used in this approach can also be applied to other non-silicon materials such as GaAs to Si [56]. One good example of this has been demonstrated by Ziptronix Inc [57] using Direct Bond Interconnect [DBI™] , as shown in Figure 2-7 or ZiBond that has just been patented recently [58]. The vertical connections formed using this technique involves the hetereogenous integration of both oxide and conductive materials on the bonding surface. Because of the nature of the bonding technique, defect-free surfaces and extreme cleanliness are keys to achieving room temperature SiO_2-SiO_2 bonding. This includes proper CMP polishing, efficient cleaning technologies and cleanroom environment for keeping defect density and contamination under control. It is very important to ensure excellent surface smoothness to avoid any particles/contaminants that would delineate the bond integrity at both the oxide and the metal surfaces. Highly accurate placement and alignment between the die and wafer or wafer to wafer such

ATTENTION: The Singapore Copyright Act applies to the use of this document. Nanyang Technological University Library

that only metal-metal and oxide-oxide contacts are achieved is also critical in ensuring bond formation. Hence bonding occurs between the contacting oxide layers at room temperature through a prior ammonia-based surface treatment which initiates the covalent bonds between oxide layers. The metal surfaces, preferably non-oxidative, will be fabricated slightly higher than its neighbouring oxide layers so that metallic bonds will be formed by the compressive forces induced by the oxide bond energy. This is reported to increase the bond strength further without any increase in bonding temperature and pressure. While bonding is demonstrated at room temperature, an annealing process at relatively high temperature of up to 800°C is usually needed for excellent bond strength and vertical electrical connections. Such high annealing temperature is undesirable for 3D Integration where the temperature limit for standard CMOS process should not exceed 300°C - 400°C [59].

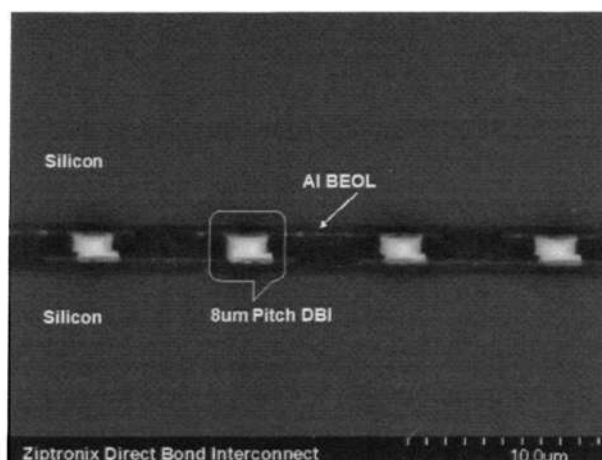

Figure 2-7 DBI™ Bond: Covalent bond formed between the oxide layers at room temperature[57]

2.7.4 Adhesive Bonding

Generally, this method is often used in the fabrication of various microsystems such as infrared focal plane arrays, spatial light modulators, micro-optical systems, laser systems, MEMS such as microfluidics systems, RF-MEMS, stacking of active electronic films for three-dimensional high-density electronic circuits and many

ATTENTION: The Singapore Copyright Act applies to the use of this document. Nanyang Technological University Library

industrial applications such as automotive, air plane and aerospace manufacturing [60, 61]. In adhesive bonding, two surfaces are bonded by placing a liquid phase such as a solution, a gel or a suspension in between and then solidifying through polymerization, crystallization or firing [59]. The use of the liquid phase enables intimate contact between solid surfaces as long as they have good wettabilities, thus eliminating the need for tedious surface preparation which involves the removal of unwanted particles and reduction of surface roughness. In general, the key advantages of this bonding technique consist of its compliance with any surface topography, ease of integration into standard integrated circuit wafer processing, ease of bonding heterogeneous materials and relatively low bonding temperature. In 3D integration, using polymeric adhesive as a bonding intermediate layer between wafers is most commonly used [56-59]. One of the examples is depicted in Figure 2-8. The polymer is applied to one or both wafer surfaces and pressure is applied to bring the two surfaces into intimate contact. Soft baking or curing is conducted to remove some moisture before wafer alignment is done. Finally, the bonded joints are fabricated after ramping up to the desired bonding temperature under constant pressure. While this method is simple and low cost, several concerns including the long term stability of many polymers under harsh environmental conditions, limited properties [thermal, mechanical and reliability] of the adhesive materials need to be considered for its utilization in 3D integration. Recently, new adhesive materials that is only molecularly thick has been reported to yield higher toughness values in joining copper and silicon dioxide as compared to the conventional micrometer thick adhesive layers[35]. Despite so, high annealing temperature of about 400°C – 700°C could potentially induce thermal stresses-related problems in electronic devices as mentioned in the previous chapters.

ATTENTION: The Singapore Copyright Act applies to the use of this document. Nanyang Technological University Library

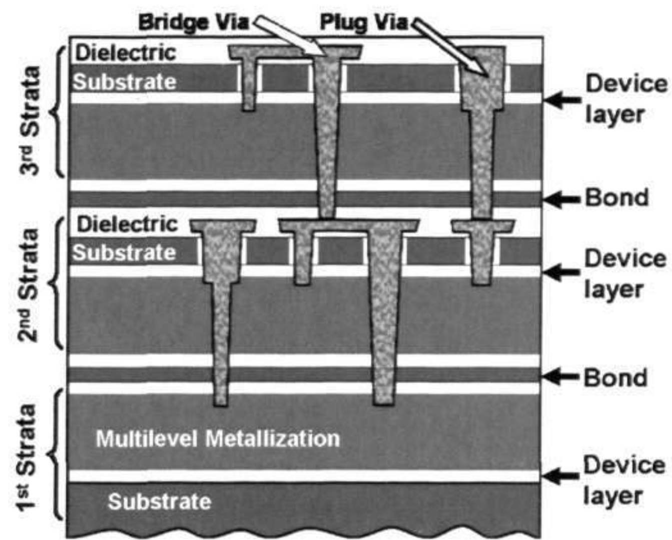

Figure 2-8 Wafer-level 3D IC fabrication using adhesive bonding and Cu damascence in RPI

ATTENTION: The Singapore Copyright Act applies to the use of this document. Nanyang Technological University Library

Chapter 3 DIRECT GOLD BONDING

3.1 Introduction

Advanced 3D stacking technologies include the bonding of high precision and highly reliable microbumps made of metal. For example, in the studies of stacked large-scale integrated chips (LSI), metal joints formed using gold or copper microbumps on the through-hole electrodes at 20μm pitch were demonstrated by thermocompression bonding [6]. As mentioned earlier, this method offers very strong and reliable bonds for scaling compared to solder bumps and requires relatively lower temperature and pressure. While ultrasonic metal bonding offers lower bonding temperature due to the ultrasonic power applied, the bonding strength of the bumps at 20 μm pitch was very weak and worsened as bonding force increased, shown in Figure 3-1 [60, 61]. As the interconnect pitch and thickness of wafers/chips decreases, it is important that the temperature profile and the stress applied is sufficient for bonding of interconnects to take place while no short circuit or damages are introduced. This chapter presents a study on the effects of temperature and pressure on the bond strength of direct gold joints. A correlation between the need for temperature and pressure with surface cleanliness and bonded area respectively is also provided. The understanding of the bonding mechanism should contribute to the ability to explore alternatives to enhance

ATTENTION: The Singapore Copyright Act applies to the use of this document. Nanyang Technological University Library

conventional bonding methods which often requires high temperature and pressure loading.

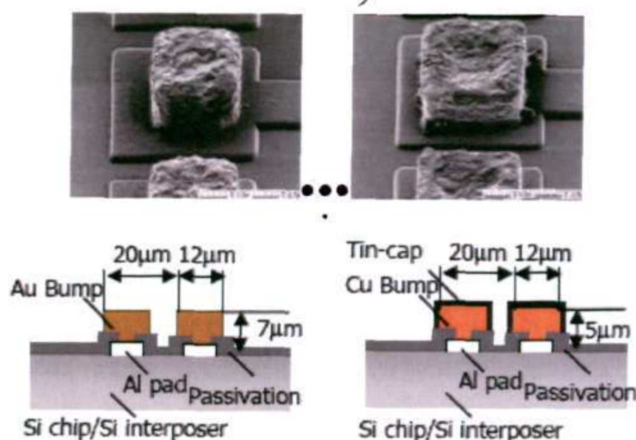

Figure 3-1 Au and Cu interconnects formed at 20 μm pitch

3.2 Experiments

3.2.1 Temperature Dependence

Pure gold (99.999%) studs formed on aluminium pads of 250 μm pitch were fabricated using a Panasonic wire-bonding machine with a 25 μm gold wire, resulting in bump sizes that range from 75 to 80 μm in diameter and 47 to 50 μm in height, as shown in Figure 3-2. Substrates used consisted of 0.5mm thick silicon wafers with metals deposited sequentially as follows: 80 nm TiW adhesion layer, 100 nm sputtered Cu and 5 μm electroless plated Ni and finally 50 nm immersion gold.

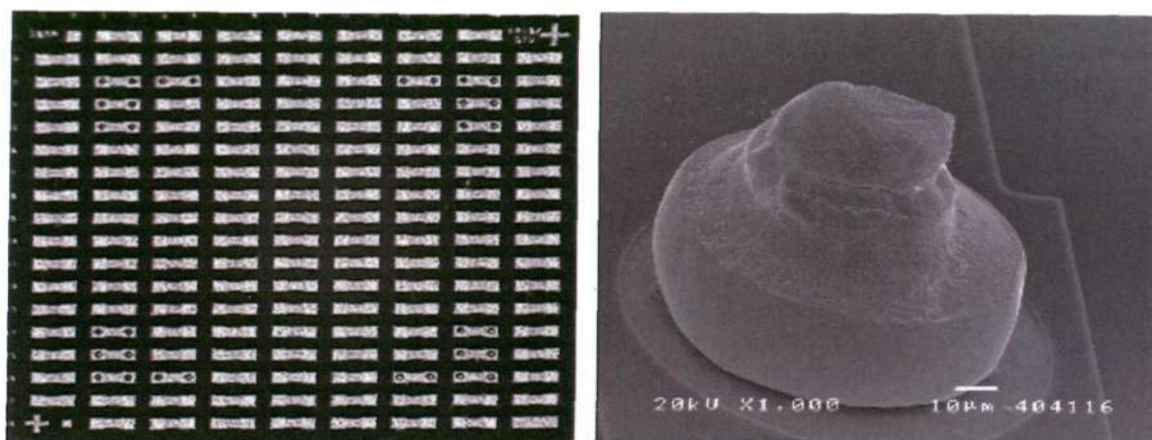

Figure 3-2 SEM fractographs of test chip and Au stud bump used

ATTENTION: The Singapore Copyright Act applies to the use of this document. Nanyang Technological University Library

The thermocompression bonding process was done using Panasert FCB-M Flip Chip Bonder. The bonding procedure begins with the substrate sitting on a heated stage. When the stage is heated to a specified temperature, the chip is picked by the bonding tool with vacuum and is brought into contact with the substrate. After the bonding force has reached a certain level, the pick up tool is heated to predetermined temperature and maintained for 10 seconds to complete the process. The stage temperature is fixed at 150 °C and a bonding pressure of 500g per bump [~975MPa] is applied. The chip temperature is varied from 100 °C to 300 °C. The samples are left on the heated stage long enough to eliminate any effects of temperature transients. Bonding quality was evaluated by die shear test, which was performed at a rate of 0.2 mm/s. The joint strength was expressed as the average shear force per bump. It is necessary to state here that nominal stress of the joints formed will be used throughout the entire thesis to describe the strength obtained when bonds were forged. Nominal stress is computed based on the pressure applied over the initial bump area while the determination of true stress require measurements of actual load and instantaneous cross-sectional area at the bonding interface which is in micron scale. Since the dimensions of the gold bumps used are relatively similar and a comparison was made between bumps that are coated and non-coated, it is imperative and fair that nominal stress can be used to represent the strength of the joints formed adequately. While it is understood that true stress depicts more accurately the continual strengthening of the metals when they undergo considerable deformation, it is beyond the scope of thesis to track the amount of deformation present at the bonding interface to achieve a certain amount of joint strength. The fracture surfaces were examined by scanning electron microscopy (SEM) and optical microcopy.

ATTENTION: The Singapore Copyright Act applies to the use of this document. Nanyang Technological University Library

3.2.2 Effect of substrate: Hardness

Two kinds of substrates were used for the bonding: one was 1 mm thick 96.5% alumina with 10 μm thick gold layer produced by paste printing and co-firing (sintering) in a furnace at about 900°C to form multilayer ceramic structure. Organic residues present after firing were removed after cleaning. The other was 0.5 mm thick silicon with metal films deposited sequentially: first a 80 nm TiW adhesion layer, then 100 nm sputtered Cu and 5 μm electroless- plated Ni (16 at% phosphorous (P) in NiP), and followed by 50 nm immersion gold. The hardness, yield strength and young's modulus of electroless plated nickel differ from that of gold. The two materials were used so that the results would be far apart enough to study the effect of the substrate. Similar bonding process, as described in the previous section, was used. Even though two different substrates are being used, their small thermal masses ensure that the actual substrate temperature can be approximated by the stage temperature in both cases, with an estimated difference of only about 0.05 °C between the two substrates. The bond strength of the joints formed was evaluated using shear test.

3.2.3 Pressure Dependence

In this study, the bonding process was carried out using a wafer bonder since the maximum allowable pressure of the flip chip bonder is capped at about 1GPa. In preparation of the bonding process, a 4" silicon wafer was first placed on the wafer chuck followed by the gold substrates. The stud-bumped chips were flipped down manually and placed onto the substrates. The next wafer was placed on top of the samples and clamped tightly onto the wafer chuck using a piece of glass plate. Finally the graphite plate was placed on top of the wafers. The whole setup is illustrated in Figure 3-3 and 3-4. The whole chuck was then carefully loaded into the wafer bonder chamber.

ATTENTION: The Singapore Copyright Act applies to the use of this document. Nanyang Technological University Library

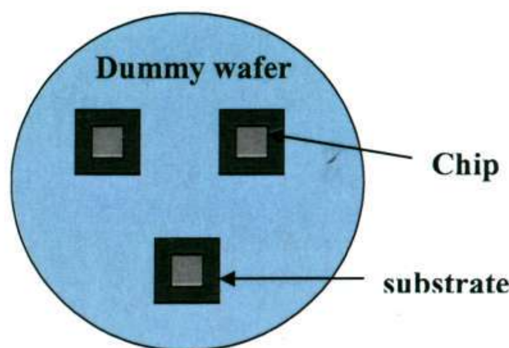

Figure 3-3 Plan view of the samples setup in a wafer bonder

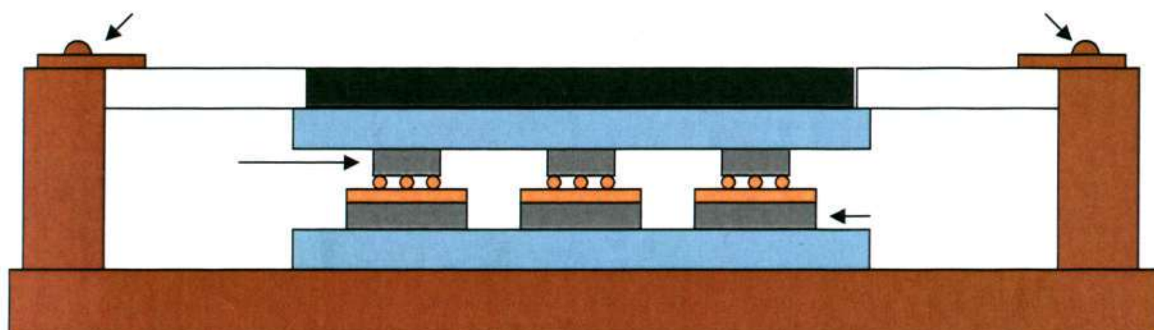

Figure 3-4 A schematic of the cross-section of the sample setup for bonding using a wafer bonder

Bonding took place in vacuum where the chamber was first purged with N_2 gas and pumped down to a vacuum level of 10^{-3} mbar. At the same time, the two temperatures involved, namely the top and bottom chuck temperature, were gradually increased to set temperature. In our case, the pressure dependence was studied at two bonding temperatures - 150 °C and 200 °C. To study the pressure dependence, the bonding load was varied from 216 to 700 grams per bump [~421.5MPa – 1.36GPa], keeping the other parameters such as temperature and bonding time fixed at 150°C and 10 seconds respectively. Once the set temperature was reached, the piston was placed down. After bonding for 10 seconds, the piston was removed and the whole chamber cooled to about 60 °C. To assess the bond quality, the tensile strength of the joints was measured using the stud pull test on an Instron microtester and observed under a scanning electron microscope. A tensile pull test offers several advantages over another

ATTENTION: The Singapore Copyright Act applies to the use of this document. Nanyang Technological University Library

commonly used technique – shear, because it enables (1) minimization of material deformation above the bonded interface, (2) less influence from mechanical bonding between surface irregularities that may manifest during a shear test and (3) simple test load as compared to the complex load from shear test which consists a triplet of shear, compressive and tensile forces. The bonded samples were adhered to a screw at the chip using two-system epoxy glue and left overnight. The screw was then inserted into the pulling tool. Figure 3-5 shows the schematic of the test setup.

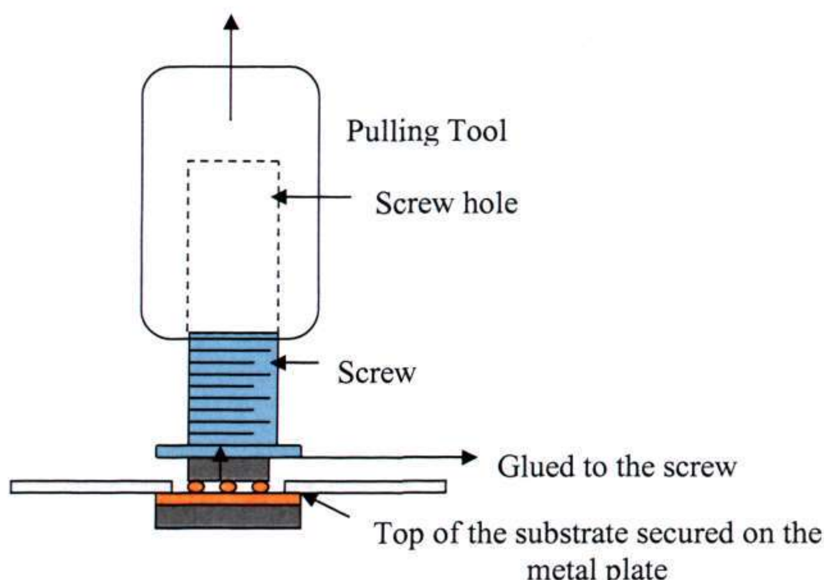

Figure 3-5 A schematic of the tensile tester setup

3.3 Results and Discussion

3.3.1 Critical Temperature

In this section, a lower range of bonding temperature was explored to evaluate the minimum temperature required to form a gold-gold bond, followed by a postulation of the role of temperature in bonding. In the thermocompression bonding of gold stud to 10 μm gold layer on alumina (Au-printed Au) and on immersion-gold on electroless plated nickel (Au-immersion Au/Ni) the influence of pickup tool temperature (T_{tool}) was studied from 100°C to 300°C, while keeping the stage temperature (T_{stage}) fixed at 150°C. The result is shown in Figure 3-6, which indicates the existence of a threshold

ATTENTION: The Singapore Copyright Act applies to the use of this document. Nanyang Technological University Library

T_{tool} for both substrates. Below this critical value (150°C in the case for Au-printed Au joint and 120 °C for Au-immersion Au/Ni joint), there is nearly no joining as the joint strength is near zero. Above this critical point, small increase of temperature produces large improvement in joint strength. In other words, critical T_{tool} is the transition from "no bonding" condition to "bonding" condition. With the further increase in temperature, the joint strength increases steadily. Evidence that bonding does not take place below the critical T_{tool} can also be seen in the cross sectional SEM images of Au-printed Au joints, as shown in Figure 3-7. At the T_{tool} of 100 °C, an obvious bonding interface was observed between the gold stud and gold layer. Such interface depicts the presence of unbonded region. However this interface disappeared at a higher temperature of 180°C.

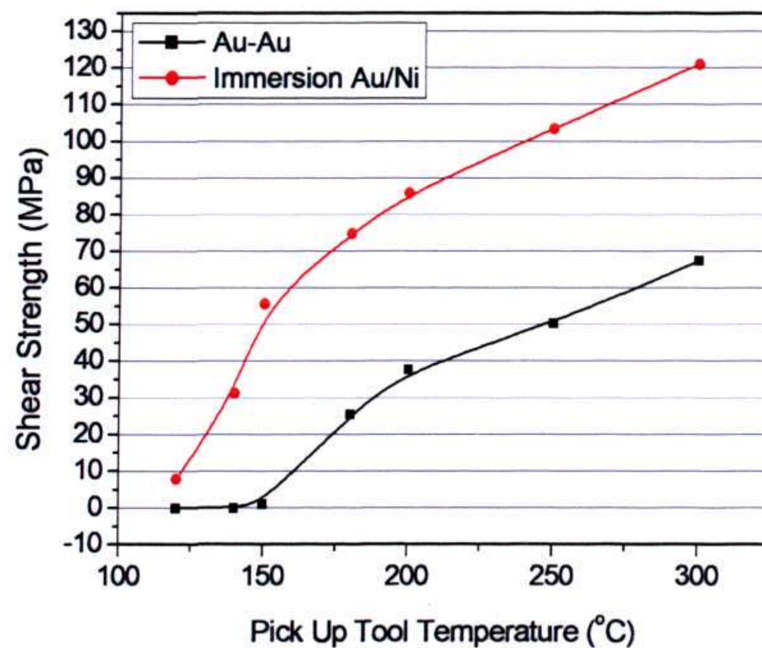

Figure 3-6 The effect of pick up tool temperature on shear strength of joints at bonding pressure of 975MPa

ATTENTION: The Singapore Copyright Act applies to the use of this document. Nanyang Technological University Library

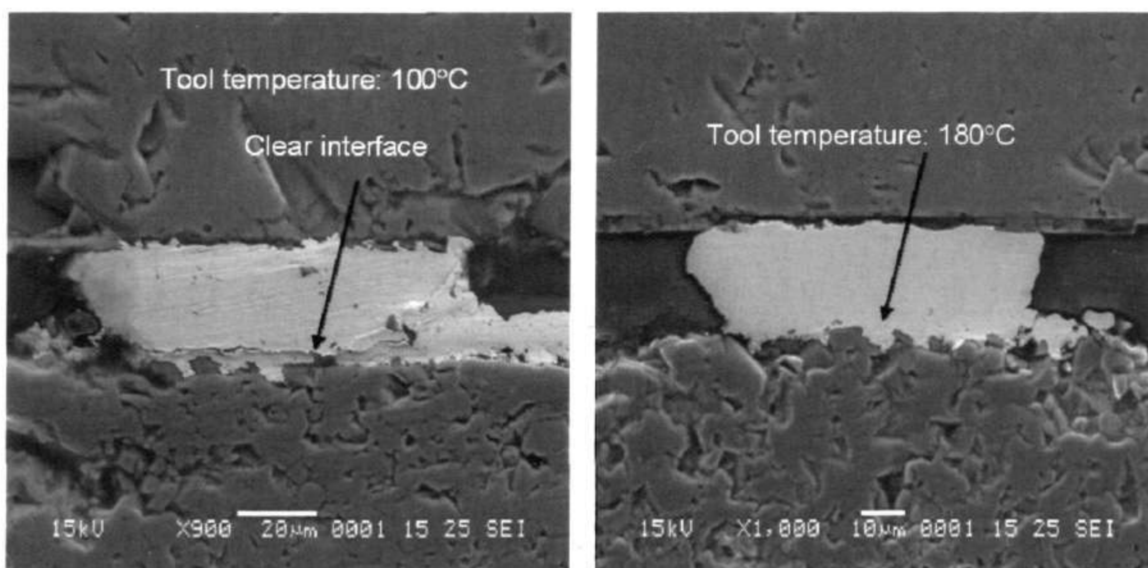

Figure 3-7 Cross section SEM images of Au-Au joints on alumina substrate at different bonding temperatures

In such thermocompression bonding process, it is the interfacial temperature (T_{inter}) that controls bonding quality. The existence of critical T_{inter} is exhibited through threshold T_{tool} in the above investigation. T_{inter} depends on both T_{tool} and T_{stage}. Thus with higher T_{stage}, lower critical T_{tool} is needed to produce certain critical T_{inter} for the bonding and vice versa. This indicates that the change of T_{stage} would result in the shift of threshold T_{tool}. To study the effect of T_{stage} on critical T_{tool}, bonding was carried out with lower T_{stage} of 100°C. The result of this is shown in Figure 3-8, together with that of 150°C for comparison. When T_{stage} is decreased to 100°C, the critical T_{tool} shifted to higher value (180°C). At T_{tool} above threshold, the joints are always weaker when bonded with lower T_{stage} because the net T_{inter} is lower. This indicates that higher T_{stage} can be used to lower critical T_{tool}, so as to achieve satisfactory bonding.

ATTENTION: The Singapore Copyright Act applies to the use of this document. Nanyang Technological University Library

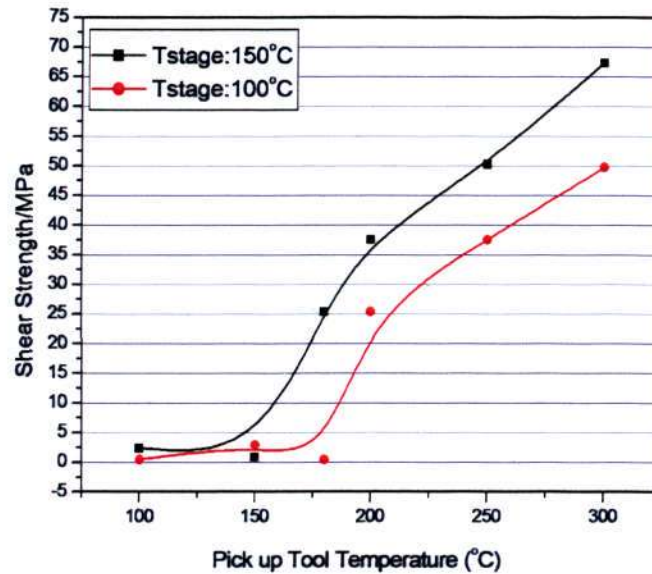

Figure 3-8 The effect of tool temperature at two stage temperatures using gold-gold on alumina

While bonding time is also known as a contributing factor in influencing the bondability of metal joints, it is believed that the critical temperature will vary significantly with bonding time only if the bonding is expected to occur in a very short time since critical temperature depicts the onset of bonding. Similarly, the effect of the obvious differences in surface morphology between Au-printed Au and Au-immersion Au/Ni substrates is not expected to exert much influence in the critical temperature observed. While a thick printed gold layer (R_a: 1 - 2μm) is spatially rougher than a 50nm immersion gold layer, the true contact surface between the stud surface and the substrate layer at submicron scale does not differ much for both types of surfaces.

Due to the unknown gold composition [it is only understood that 5N gold wires were used to form the stud bumps] and difficulty in measuring engineering stress-strain curve of a stud bump, the stress-strain behaviour during bonding is equivalated to reports obtained for gold wires. Qualitative discussion on the temperature effect on the mechanical properties of gold can only be made since different composition will affect the mechanical properties significantly. It is reported that for gold wires doped with

ATTENTION: The Singapore Copyright Act applies to the use of this document. Nanyang Technological University Library

various dopants such as calcium, lead, tin etc, both the elongation and tensile strength of gold is unaffected when annealing temperature falls below 300°C [62, 63].

3.3.2 Interfacial Chemical Behaviour

As mentioned in the previous chapter, the requirement for producing a joint is that the two metal surfaces must be brought together within the operating range of interatomic attractive forces. If these two metal surfaces are atomically clean, flat and smooth, a very strong bonding would be produced in the whole contact area when they are brought together. No external energy input is needed. One way to flatten the surfaces and break the barrier films is to apply high pressure. Earlier studies on bonding had shown it is impossible for perfect removal of such organic contaminant film or oxide film, thus necessitating the presence of plastic interfacial deformation to break down and disperse the barrier films [13]. The success of such methods depends critically on whether the barrier film could be broken. Even after an extensive deformation shown in our experiments (for the bonding load of 500g per bump, the pressure is about 975 MPa, much larger than the yield strength of gold, which is about 200 MPa), there may still be a monolayer of water vapor or other gases between the two flattened gold surfaces which prevents bonding. This postulation is brought about by the existence of a critical temperature observed which could be explained in terms of the minimum work needed to overcome a barrier film.

A survey spectrum was collected on the Au-immersion Au/Ni silicon substrate using x-ray photoelectron spectroscopy (XPS) to determine the existence of a layer of organic contaminants on gold surface. From Figure 3-9 (a), the presence of the organic contaminant layer on gold surface was demonstrated. A comparison was made between the compositional spectrum for gold surface prior to cleaning and gold surface after some cleaning using argon sputtering for 3 minutes. Results revealed that there is an inherent layer of surface contaminants on gold that consists of carbon and oxygen as the

ATTENTION: The Singapore Copyright Act applies to the use of this document. Nanyang Technological University Library

major constituents. This is not surprising as it has been understood that for a real surface, a layer of surface contaminants exists. However after 3 minutes of argon sputtering, O 1s spectra disappeared and C 1s emission peak showed a significant drop in intensity compared to that without cleaning. With the huge reduction in organic contaminants present, emission peaks from outer core shells - Au 4s and Au 4p gradually emerged.

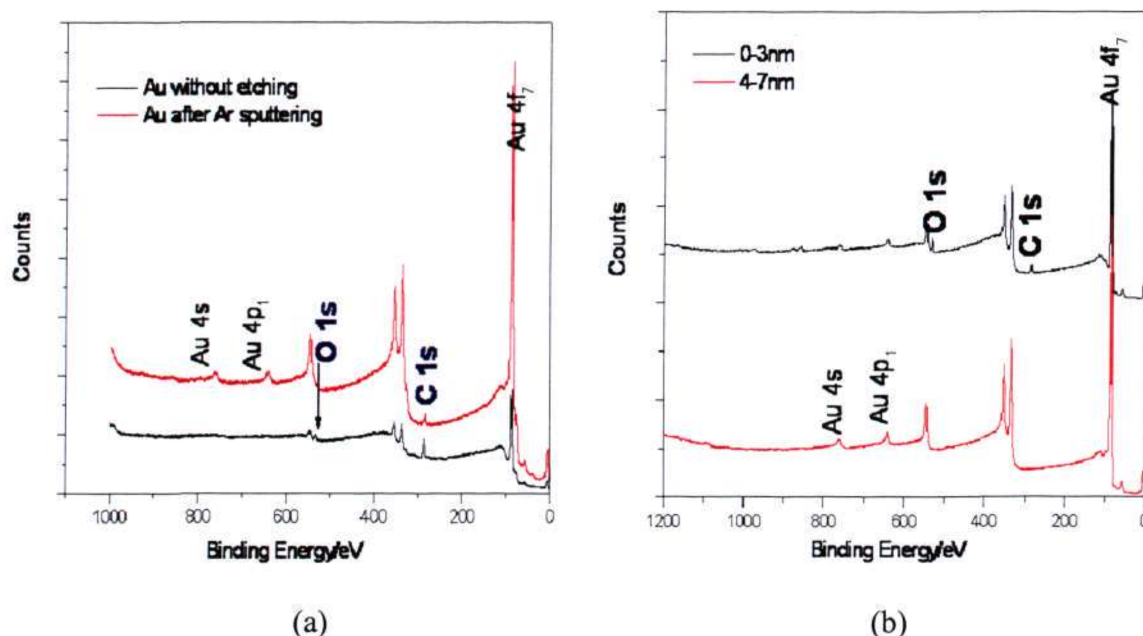

(a) (b)

Figure 3-9 Surface chemical composition of gold (a) with/without Ar sputtering and (b) at different detection depths

Besides that, a surface composition analysis done on the gold surface at different detection depth revealed that the thickness of the contamination layer is most likely to be less than four nm, evidenced by the chemical composition spectra at 0-3nm and 4-7nm detection depth, respectively as shown in Figure 3-9 (b). Beyond 4nm depth, no carbon and oxygen content are present as only sharp peaks due to gold are observed. The XPS spectra at depth below 4nm showed high core level peaks for gold at 87.6eV (Au $4f_7$) as well as for C 1s (285.6eV) and O 1s (532.6eV). These major components of surface contaminants are both absent in the chemical spectrum at above 4nm depth.

ATTENTION: The Singapore Copyright Act applies to the use of this document. Nanyang Technological University Library

Therefore, as explained previously, a certain amount of energy is thus needed to overcome barriers which remain after mechanical deformation. One such mechanism is thermal desorption. Because the barriers are already very thin and could easily diffuse away, the activation energy is relatively low and could be supplied by moderate heating. The critical temperature is thus the point where the supplied thermal energy is sufficient to remove the deformed barrier film. When a sample surface contains a ductile contamination layer, bonding could not be achieved without sufficient thermal energy input, even if a sufficiently high pressure is applied and localized contact produced. Hence critical temperature also exists even when ultrasonic energy is applied [64]. This is not surprising since the ultrasonic input serves similar purpose as the pressure applied in disrupting the barrier film and thermal input is thus necessary to complete the bond formation.

In the case of gold stud bonding to a harder substrate, Au-immersion Au/Ni bonding also exhibits a critical T_{tool} in the bonding as shown in Figure 3-6. However, compared to Au- printed Au bonding, Au-immersion Au/Ni bonding has a lower critical T_{tool}. Under the same bonding condition, Au- printed Au samples did not bond at the temperature of 150°C, while the joint strength of Au-immersion Au/Ni bonding is 55.6MPa. Since the electroless nickel surface was covered by a layer of immersion gold, the bonding itself is still gold to gold bonding, which, in all likelihood, will be contaminated by similar ductile organic surface layers as in the earlier case of Au-Au bonding. The interfacial chemical state could be considered the same as that of Au-printed Au, thus explaining why a critical temperature is also observed. Therefore it is believed that the different critical T_{tool} would be more likely caused by the different interfacial mechanics caused by the harder underlying metal layer which would be explained in the next section.

ATTENTION: The Singapore Copyright Act applies to the use of this document. Nanyang Technological University Library

3.3.3 Influence of interfacial stress distribution

Critical temperature is caused by the existence of ductile contaminant layer and is related to the thermal desorption of the deformed barrier film. With a larger shear deformation, a thinner barrier film is produced and thus a lower threshold temperature is needed. In the case of thermocompression bonding, the interfacial shear is dependent on both pressure and the mechanical property of the material being bonded. To compare the interfacial shear stress between the bonding of gold bump to different hardness substrate, finite element (FE) analysis was carried out. Since the initial contact area between the two real surfaces is too small to be accurately represented by the FE models, the models created aim to capture the later stage where actual bonding occurs as initial disparities were flattened and surface contact area increases with increasing load. The physical properties of gold paste and electroless nickel layer respectively (yield strength and Young's modulus are determined by nanoindentation) are shown in Table 3-1. Such values are comparable to that of bulk gold [yield strength – 205MPa and Young's modulus – 77MPa] [65] and nickel at [yield strength ~ 1962MPa and Young's modulus – 204MPa] [66] since the layers are relatively thick. It was also assumed that there is no relative motion between the bump and the substrate, since any force sufficient to deform the bump will cause "sticking" between the two contacting surfaces [67]. Material properties for printed gold paste are used for both models to investigate the effect of a harder underlying layer on the interfacial stress distribution after compression. Surface load which implies a distributed load over the top surface of the bump were applied in the model. The bonding temperature in actual thermocompression bonding is neglected in this simulation.

While surface irregularities are expected on a real stud surface, random distribution of asperities across the entire surface is assumed such that the stress distribution observed in the finite element model represents bulk deformation behaviour.

ATTENTION: The Singapore Copyright Act applies to the use of this document. Nanyang Technological University Library

Gold bump to thin Au-printed Au/Ni layer and to thick Au- printed Au layer were selected. The simulated results are shown in Figure 3-11. It could be seen that shear stress at the interface is much smaller when gold is bonded to softer substrate, such as gold, shown by the stress contours in Figure 3-10.

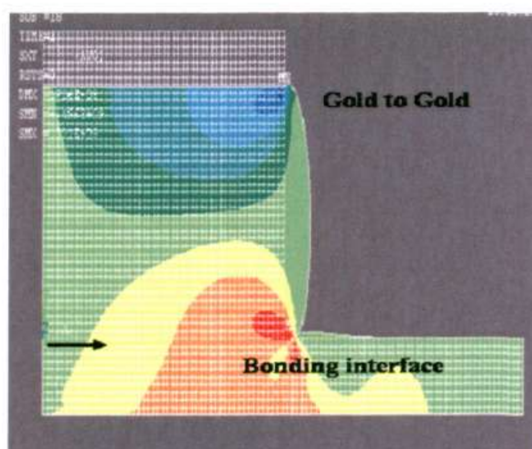

Figure 3-10 Typical stress contour (undeformed and deformed) diagram illustrating the shear stress distribution for gold bump-10μm gold model

Table 3-1 Mechanical properties of gold and electroless nickel

Materials	Young's Modulus (GPa)	Poisson Ratio	Yield Strength (MPa)	Tangent Modulus (GPa)
Gold Paste	70	0.42	200	1.1
Electroless Nickel layer	199	0.312	1500	1.2

ATTENTION: The Singapore Copyright Act applies to the use of this document. Nanyang Technological University Library

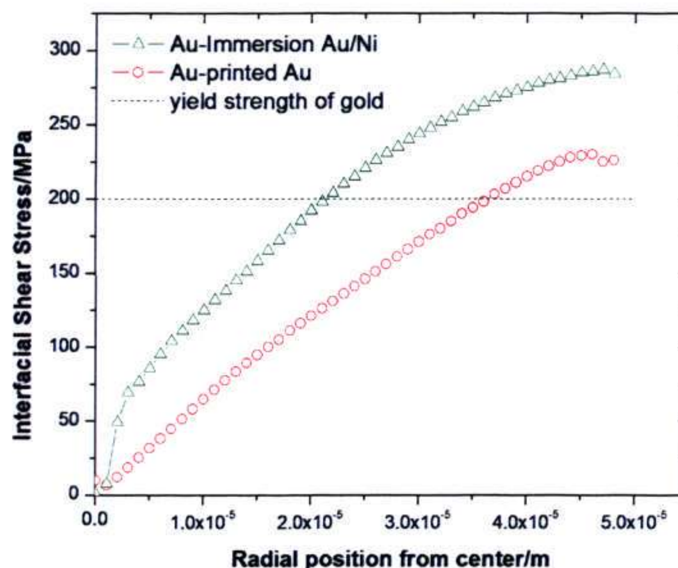

Figure 3-11 Simulated interfacial shear stress versus radial position of the gold joints

As shown above by the simulation, in the point of interface deformation, bonding would be favoured in the harder substrate. Given the yield strength of gold bump, the simulated results extracted at the interface shown in Figure 3-11 reveal that a larger degree of plastic deformation will be expected at the bonded interface for Au-printed Au/Ni model since the amount of stress induced is much larger than that of a softer substrate. There appears to be less plastic flow in Au-printed Au model because the bump is more embedded into gold than into nickel. It is inferred that in Au-printed Au bonding, the residual contamination layer will be thicker than that in Au-immersion Au/Ni bonding under the same load. This reveals the need for more energy to break the layer which results in higher threshold bonding temperature. Such simulation results agree well with the experimental observation on the influence of substrate hardness on critical T_{tool} shown in Figure 3-6.

3.3.4 Pressure Dependence

3.3.4.1 *Optimum Pressure*

Our study on pressure dependence showed a maximum in the tensile strength of the Au stud – Au joint with respect to the pressure variable, as shown in Figure 3-12.

ATTENTION: The Singapore Copyright Act applies to the use of this document. Nanyang Technological University Library

Below an approximated critical amount of bonding pressure of 100 MPa and 300MPa at the respective bonding temperatures of 200°C and 150°C, very weak bond strength can be obtained. This is shown in Figure 3-12 where very weak tensile strength of about 10MPa was measured when bonding pressure falls below critical limits. Further increase in the applied pressure results in an increase in bond strength before reaching a maximum, which we have defined as the optimum bonding pressure. With a higher bonding temperature, a higher maximum strength value is obtained for the bonds formed, as shown in Figure 3-12. Similarly, a shift in the peaks to the left for increasing temperature, or equivalently, a smaller amount of optimum pressure needed, is also observed, clearly identifying the inverse relationship between bonding pressure and temperature.

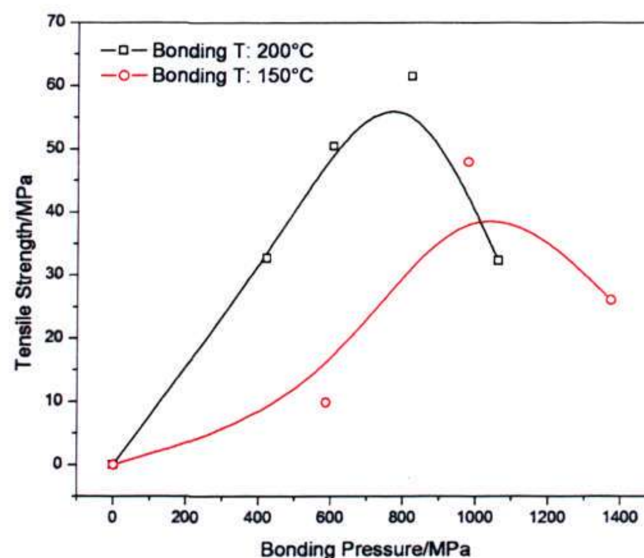

Figure 3-12 Variation of tensile force against the bonding load applied at two bonding temperatures - 150 °C and 200 °C.

3.3.4.2 *Critical Shear Stress Criterion*

A finite element model showing joint bump compression for both gold stud and plated bump was created to study the variation of the interfacial stress distribution along the radial bonding surfaces. The 2-D finite element model (plane82) with

ATTENTION: The Singapore Copyright Act applies to the use of this document. Nanyang Technological University Library

axisymmetrical condition assumed was built using Ansys 8.0. Since there is an axis of symmetry at the center of bump and the substrate, only one half of the cross-section was used for the model. Plane82 element used is a higher order version of a 2D element such as plane42. It gives better accuracy results when the meshing consists of a mixture of quadrilateral-triangular meshes and coarser mesh is used. Physical properties such as elastic Young's Modulus, Poisson ratio and yield strength of gold were used as inputs for material properties of the model. It was also assumed that there is no relative motion between the bump and the substrate, since any force sufficient to deform the bump will cause "sticking" between the two contacting surfaces [67]. These values chosen are approximated to those calculated from the actual experimental pressure found by dividing the load (N) by area of the bump (m^2). Two models were created to represent gold stud and plated bump that would be used in actual bonding experiments, shown in Figure 3-13. The following parameters used as inputs for the two models:

1) Model I: stud radius, height (35μm, 20μm); bump radius, height (40 μm, 50 μm);

2) Model II: bump height (16 μm); bump radius (40μm);

3) Substrate width and thickness: 80 μm and 5 μm respectively;

4) Material Properties: Young's modulus (70GPa); Poisson ratio (0.42); Yield stress (200MPa); Tangent Modulus (1.1GPa)

5) Meshing Element Size: 1μm

6) Normal load: 216 g and 382g per bump [550 MPa and 973MPa - calculated by dividing the applied normal load against the original bump diameter] for Model I; 125g and 500g per bump for Model II [244MPa and 976MPa].

ATTENTION: The Singapore Copyright Act applies to the use of this document. Nanyang Technological University Library

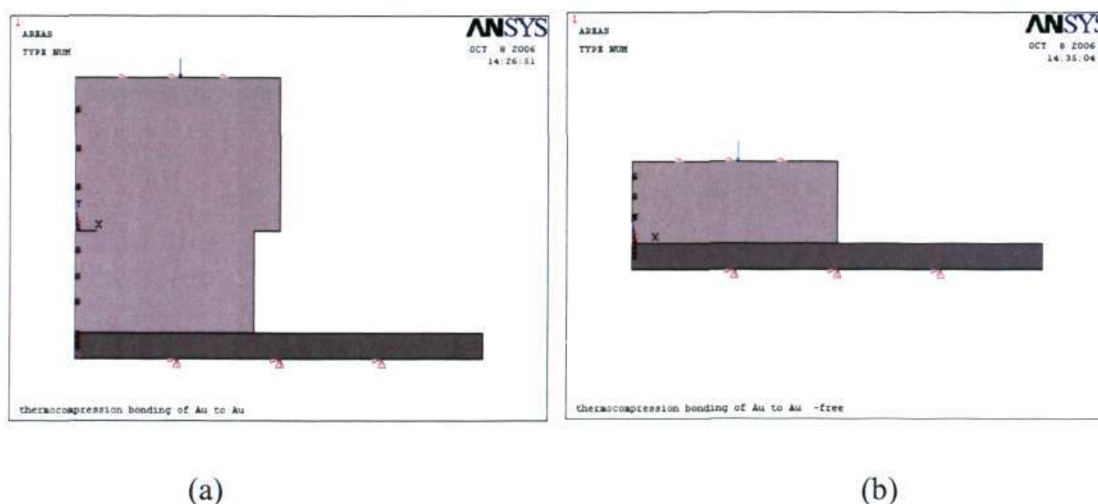

(a) (b)

Figure 3-13 (a) Model I: Gold stud on a layer of gold; (b) Model II: Plated gold bump on a layer of gold

Gold Stud Bonding

The sample fabrication was described in Section 3.2 of this chapter.

Plated Bump Bonding

Dies of 4mm by 4mm in size was used. Bonding was carried out using 8 bumps that are formed on gold pads that are patterned around the peripheral of the square die. Silicon wafers sputtered with 50nm thick Ti, 100nm thick TiW and finally 200nm Au layer were coated with a thick positive resist which were then patterned by UV exposure. These plated bumps shown in Figure 3-14 are fabricated by electrolysis using commercial noncyanide-based gold solution. The bonding procedure was described in the earlier section of this chapter. For the case of gold stud bonding, the load applied is 216g and 382g per bump [550MPa and 973MPa] while load applied on the plated bump are 125g and 500g per bump [244MPa and 976MPa]. The load were chosen to ensure that the joints formed are of sufficient strength so that they do not fail before mechanical test.

ATTENTION: The Singapore Copyright Act applies to the use of this document. Nanyang Technological University Library

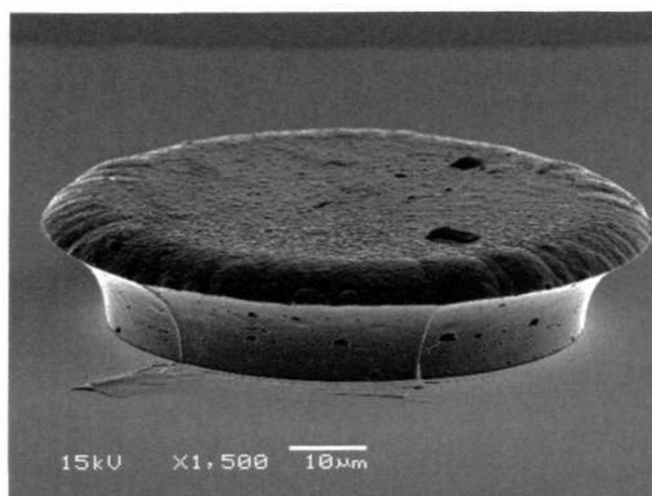

Figure 3-14 SEM picture of plated bump at about 16μm in height

The shear stress distribution along the interface between the bump and the gold substrate was extracted and plotted against the radial position, as shown in Figure 3-15. Similarly, it was observed that in both models, the shear stress distribution at the interface increases progressively along the radial position, exhibiting highest shear stress at the outermost region of the bump. Given that a critical shear stress level is necessary to fulfill the minimum amount of deformation required for bonding to take place, the region containing bonding sites where the amount of shear stress are below the critical value were perceived as the unbonded area. From the simulated results, it can be seen that accumulation of these bonding sites [the central ring] predicted lie in the central region of the bumps. This prediction is not unusual since it had also been predicted that the center region in a compression model should not bond based on by McLauren and Chen's strain criterion [67]. Shear stress was also seen to be highly concentrated in the outermost region for both Model I and II, suggesting that bonding initiates from the outer region.

ATTENTION: The Singapore Copyright Act applies to the use of this document. Nanyang Technological University Library

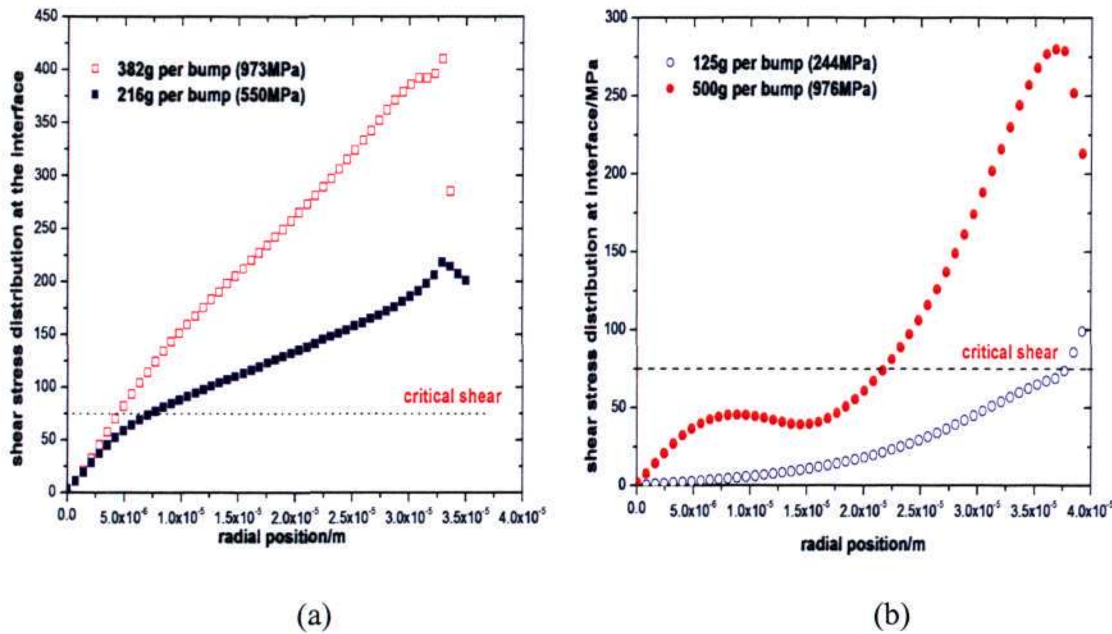

(a) (b)

Figure 3-15 Shear stress distribution at bonding interface as a function of radial position. (a) Gold Stud (Model I) at pressure 550MPa and 973MPa per bump (b) Plated Bump (Model II) at 244MPa and 976MPa.

When pressure applied increases, a steeper slope of the stress distribution is obtained. Using the critical stress criterion, assuming a linear relationship between the shear stress (σ) at the bonding interface and the unbonded radius of the bump (r), a steeper slope seen when pressure applied increases translates into a smaller r, shown in Figure 3-16. In other words, pressure applied can be seen to have an inverse relation with unbonded radius, but only up to a certain point, as we shall discuss later, depicting the progressive inward bonding as a function of pressure. Hence regardless of the differences in the bump geomerty – a stud as compared to a relatively flat plane on the topmost surface of a single plated bump, both models showed that the shear stress would always be the lowest at the center, leading to a prediction that extremely weak or no bonding would take place in the central region of the bump.

ATTENTION: The Singapore Copyright Act applies to the use of this document. Nanyang Technological University Library

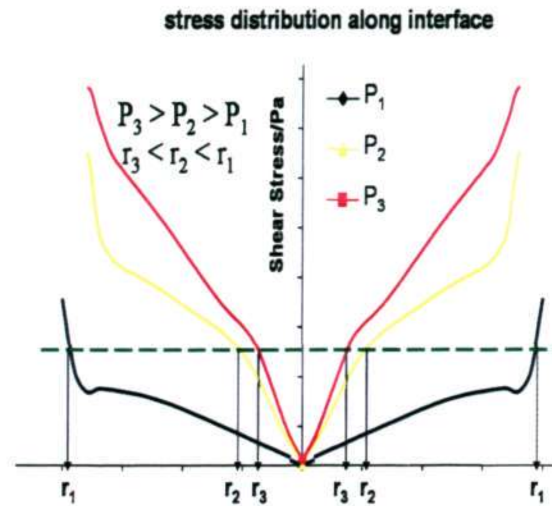

Figure 3-16 Schematic illustrates a linear relationship between shear stress distribution and unbonded radius, $r_1 > r_2 > r_3$ as $P_1 < P_2 < P_3$.

3.4 Relationship of bond strength to contact area (A_c) and true contact area (A_T)

Pressure dependence of Au-Au bonds formed by thermocompression is determined based on the deformation of metal layers at the bonding interface. The previous two sections highlight the significance of interfacial shear stress required for surface deformation to bond surfaces. The surface asperities present at the bonding interface behave as stress concentrated points when brought into contact. Both interfacial and normal loads are necessary for adequate removal of barrier films by mechanical disruption. Because deformation brought about by normal loads is ineffective in the disruption of the contaminants [6], interfacial shear stress is required to reduce the barrier film to a certain thickness. Fresh gold is then exposed upon application of temperature. The shear movement at the interface then helps to extend the exposed surface, thus aiding bonding to take place.

Correlation between the bonding strength with the proportion of bonded area at microscale was evaluated by 3D measurement of the bonded region defined by the ring left on the substrate after tensile test in Figure 3-17. Combined with the strength results shown in Figure 3-12, the contact diameter of the ring [d_{oc}] and the inner diameter of

ATTENTION: The Singapore Copyright Act applies to the use of this document. Nanyang Technological University Library

unbonded region [d_i] were plotted against a range of bonding pressure applied at 150°C and 200°C respectively, as shown in Figure 3-18. The following observations are made.

At zero bonding pressure at both bonding temperatures, no bonding occurs, i.e. $d_i = d_{oc} = d_o$ [initial bump diameter].

At bonding pressure above 100MPa and 300 MPa for both bonding temperatures, bonding occurs; leaving a shape of the gold "doughnut" on the substrate after fracture, or equivalently, a finite value of d_i and d_{oc} can be recorded. In other words, a siginificant/finite amount of bonded region was formed, giving rise to the mechanical integrity of the joints. However, as bonding pressure increases, these values do not increase significantly despite a continual rise in bond strength.

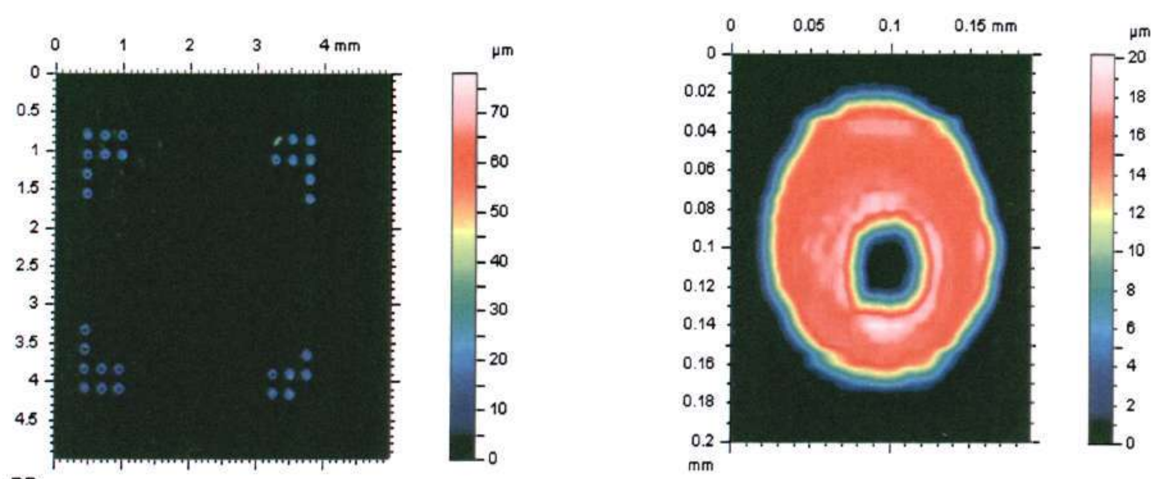

Figure 3-17 3D raster-scanning of the bumps left on the substrate using surface profilometry.

ATTENTION: The Singapore Copyright Act applies to the use of this document. Nanyang Technological University Library

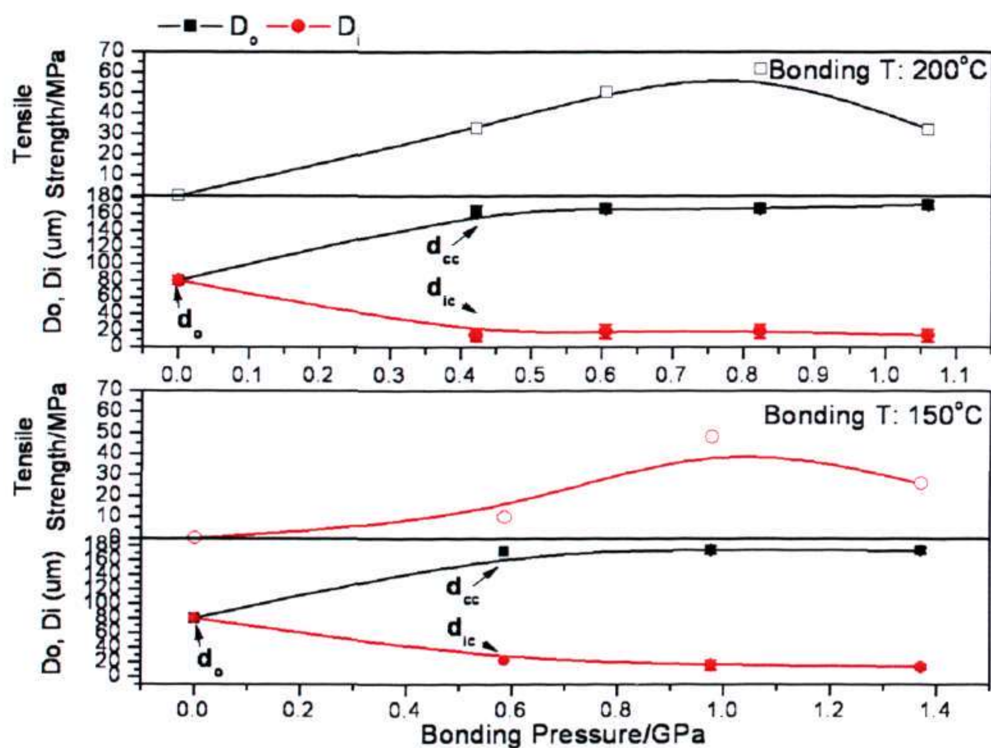

Figure 3-18 Contact diameter (D_o) and inner diameter (d_i) of the ring left as a function of bonding pressure

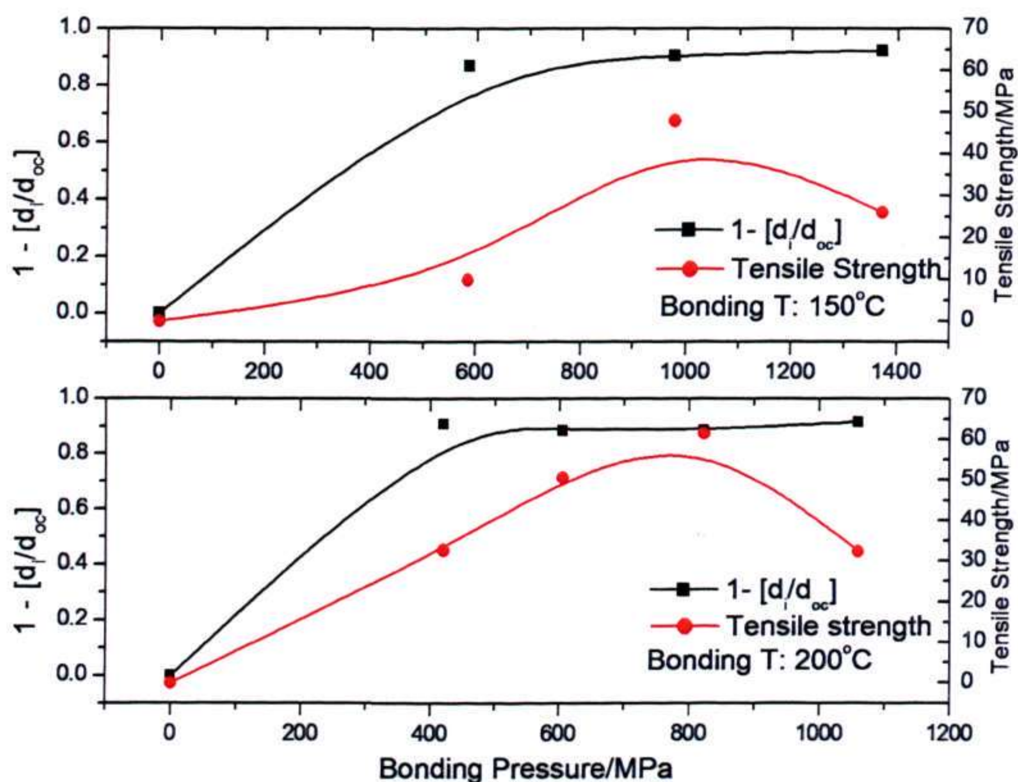

Figure 3-19 Relation between strength and amount of bonded area (a) at different bonding load (b) at different temperatures of 150 °C and 200 °C.

ATTENTION: The Singapore Copyright Act applies to the use of this document. Nanyang Technological University Library

This is supported by the microscopic measurements of the bonded region [$A_C=1-\frac{d_i}{d_{oc}}$] which did not show significant increase in the bonded area with rising pressure. By looking at the schematics of the interfacial shear stress behaviour with pressure predicted by the simulation model in Figure 3-16 and 3-20, the plot suggests, to a first approximation, that when the normal pressure applied increases, the amount of unbonded region [unbonded radius, r] reduces non-linearly. As pressure reaches a sufficiently high value [P_{opt}], changes in r will tend to zero with further increase in applied pressure.

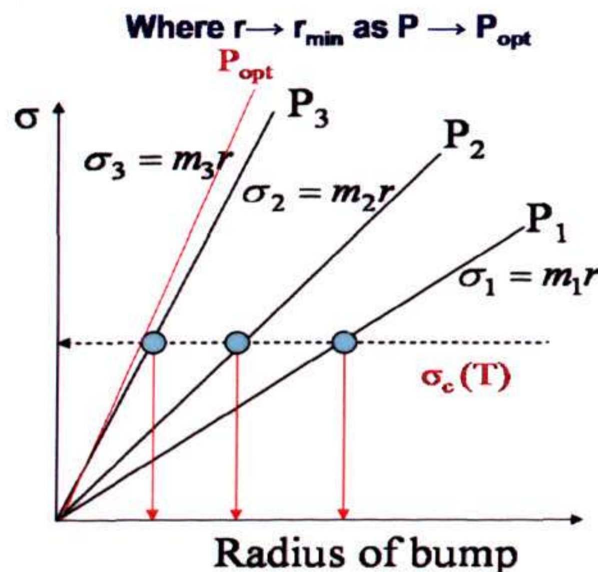

Figure 3-20 Schematics of the interfacial shear stress across the radial position of the bump with increasing pressure (P). As P increases, the unbonded radius, r tends to a minimum.

To explain the minimum seen in the unbonded radius (r), we propose the following. At a particular temperature sufficiently high to induce bonding, if bonding pressure applied is below critical point, bonding may occur only at a few bonding sites (A_T), depending on the amount of asperities in contact and the amount of deformation present at these sites. Beyond the critical limit, A_T would have increased with increasing pressure applied, leading to the rise in the bond strength. While the

ATTENTION: The Singapore Copyright Act applies to the use of this document. Nanyang Technological University Library

relationship between AT and its mechanical strength once bonds are formed remains unclear, it is indicative from the results shown above that the bond strength does not scale linearly with the amount of bonded area (AC). In fact, we believe that as pressure is sufficiently higher than the critical value, the change in AC with rising pressure is minimal. Rather, the rise in strength with pressure beyond Popt depends on the number of locally bonded sites (AT), as illustrated by Figure 3-21 and 3-22. Gold work hardens as it experiences deformation beyond its yield point. When this happens, higher dislocation density hindered movement of dislocations, making deformation more difficult. This also suggests why there is a limit in the rise in strength with pressure since it is more difficult to create new locally bonded sites. A preliminary suggestion to explain the drop in the bond strength with higher applied pressure can be elaborated in the following: we believe that when further rise in pressure does not promote a corresponding increase in AT, external loading actually 'fracture' existing bonded sites when the bonded sites experience deformation beyond its breaking strength. At these bonded sites of micron sizes, there is a possibility that catastrophic material failure-fracture will occur when the sites experience stresses beyond their fracture stress, thus resulting in a drop of bond strength.

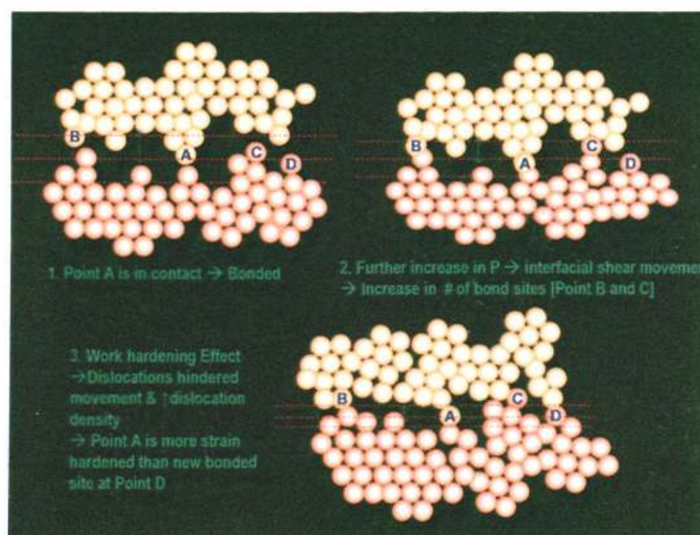

Figure 3-21 Illustration of the effect of applied pressure on the contacting surfaces at atomic scale

ATTENTION: The Singapore Copyright Act applies to the use of this document. Nanyang Technological University Library

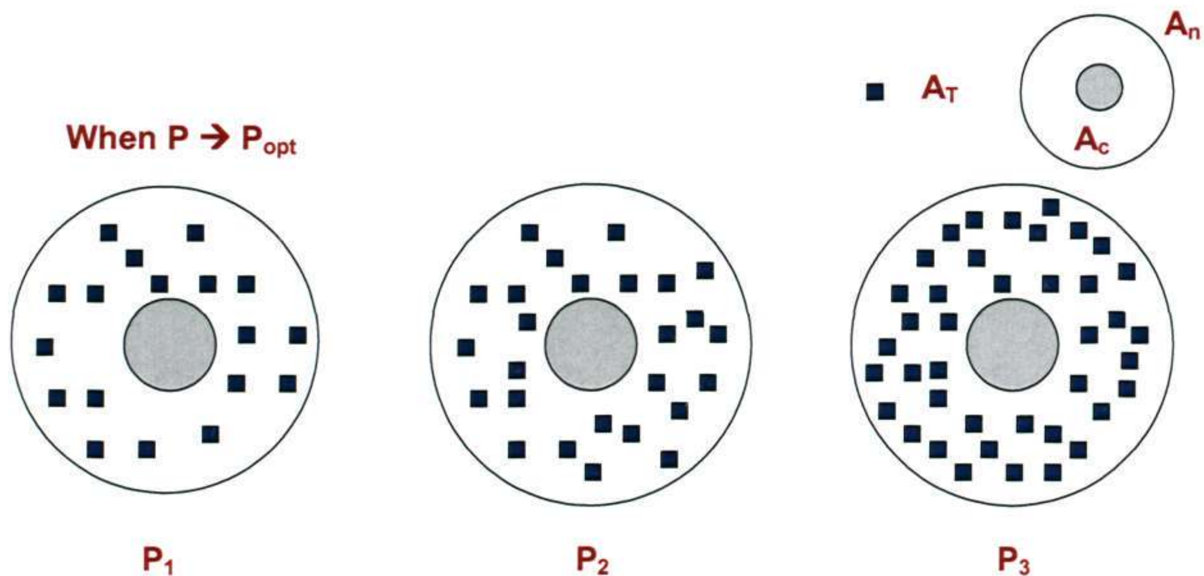

Figure 3-22 Top view of the schematics at the bonded interface when the applied P tends to P_{opt}., Increase in A_T instead of A_c where $P_1 < P_2 < P_3$

3.5 Work hardening Effect

Generally work hardening, also known as strain hardening or cold working, is a phenomenon where ductile metals changes its mechanical properties such as hardness, ductility and yield strength as it deformed plastically [65]. In general, as metals work harden more, the yield and tensile strength will increase, thus resulting in a corresponding drop in ductility. It becomes harder for the metal to deform with further cold working. This can be illustrated by a typical stress-strain curve of ductile metals where further strain beyond yield point makes the metals stronger till a maximum [also called ultimate tensile strength -UTS], refer to Appendix A2. Beyond UTS, material will fracture upon further straining. The applied pressure used in this thesis has already incorporated the work-hardening behaviour of the metals. This can be shown in Figure 3-12 and Figure 6-1 in the later chapter. The optimum pressure evaluated to bond gold and copper respectively well exceeds its yield strength. If work hardening effects are absent, the bonding pressure needed to form the metal joints would be much lower than those plotted.

ATTENTION: The Singapore Copyright Act applies to the use of this document. Nanyang Technological University Library

3.6 Inward Bonding Behaviour in Gold Studs and Plated Bump

a. Gold Stud

Further analysis was carried out by observing the fractured surfaces on both the alumina and silicon substrates using Secondary Electron Imaging (SEM). Two types of failures were observed – adhesive and cohesive failure illustrated in Figure 3-23. Adhesive failure occurs when fractures occur at the interface between the gold bump and the gold layer. When failure occurs within the bulk material at the bump or within the sputtered gold layer, it is considered as a cohesive failure. The SEM fractographs reveal a mixture of cohesive and adhesive failure along the bonded interface as bonding pressure increases, thus leaving a ring of gold stud on the substrate, as shown in Figure 3-23. This ring can be evaluated as the boundary between the bonded and unbonded area.

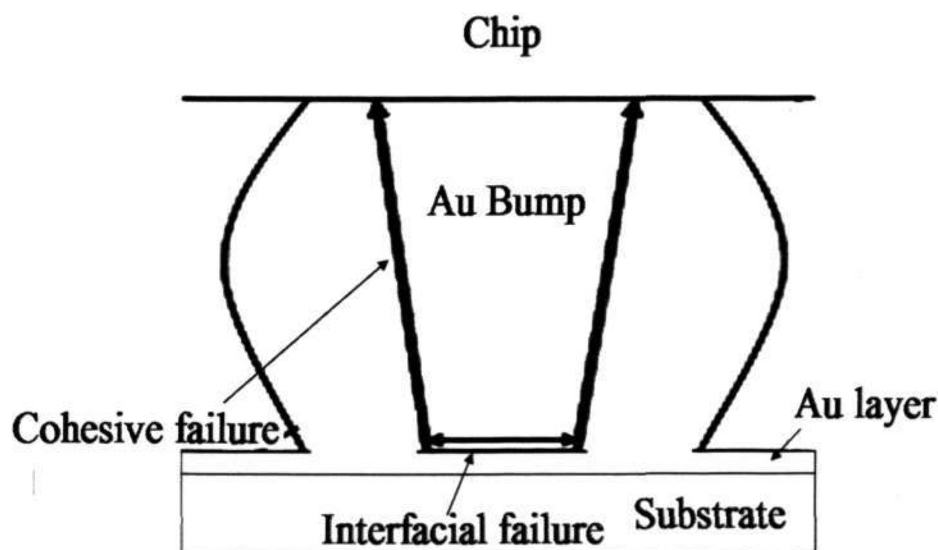

Figure 3-23 Illustration of two types of failure observed in gold joints after fracture

Figure 3-25 shows the optical fractographs of Au-printed Au bonding at different pick up tool temperatures. When bonded at lower tool temperatures, such as 100°C and 150°C, all joints failed at the interface between the gold bump and the gold layer. The shear force was near zero, indicating no bonding. When tool temperature was

ATTENTION: The Singapore Copyright Act applies to the use of this document. Nanyang Technological University Library

raised over 150°C, shear failures began to occur along the interface between gold layer and alumina substrate. In some areas the gold layer was pulled off from substrate and adhered to gold bump. The shift of failure path from Au-printed Au interface to gold - alumina interface represents the improvement of joint strength and also the start of bonding. At that region the bonded interface between Au bump and gold layer is no longer the weakest point. It is at least stronger than the gold – alumina interface, whose adhesive strength is about 20 MPa. Thus for the Au-Au bonding, it is reasonable to assume that there is no bonding if the joint fails along the bonded interface, and some degree of successful bonding if the failure is along gold layer and alumina interface. Similar behaviour was observed for Au-immersion Au/Ni samples. Comparing Figure 3-24 (a), (b) and (c), it could be seen that bonding first initiates at the outer region, and the bonding region grows inward with the increase of tool temperature. We found that the bonding progression corresponds with the simulated interfacial shear stress (Figure 3-11). The shear stress is the largest in the outer region, where the contamination layer is disrupted more and the surface is easier to be activated for bonding. In the case of a cylindrical joint, the unbonded region should be the central region. Such peripheral bonding observed is not unique though. This ring structure was first briefly noted by Bell Laboratories. They observed no bonding at the center region too [38]. Since largest amount of shearing displacement was seen at the periphery of the bond edge as compared to the center, it was believed that the lack of sufficient shear displacements to remove the barrier film at the center leads to no bonding. Such fractographs were also seen in various reports though no further discussion or explanation was given in the work [41, 44, 67, 68]. Wire thermocompression bonds [4, 45] and even ultrasonic welds [69] were found to exhibit bonding at the periphery and no central bonding. In this thesis, gold stud thermocompression bonds revealed similar behaviour.

ATTENTION: The Singapore Copyright Act applies to the use of this document. Nanyang Technological University Library

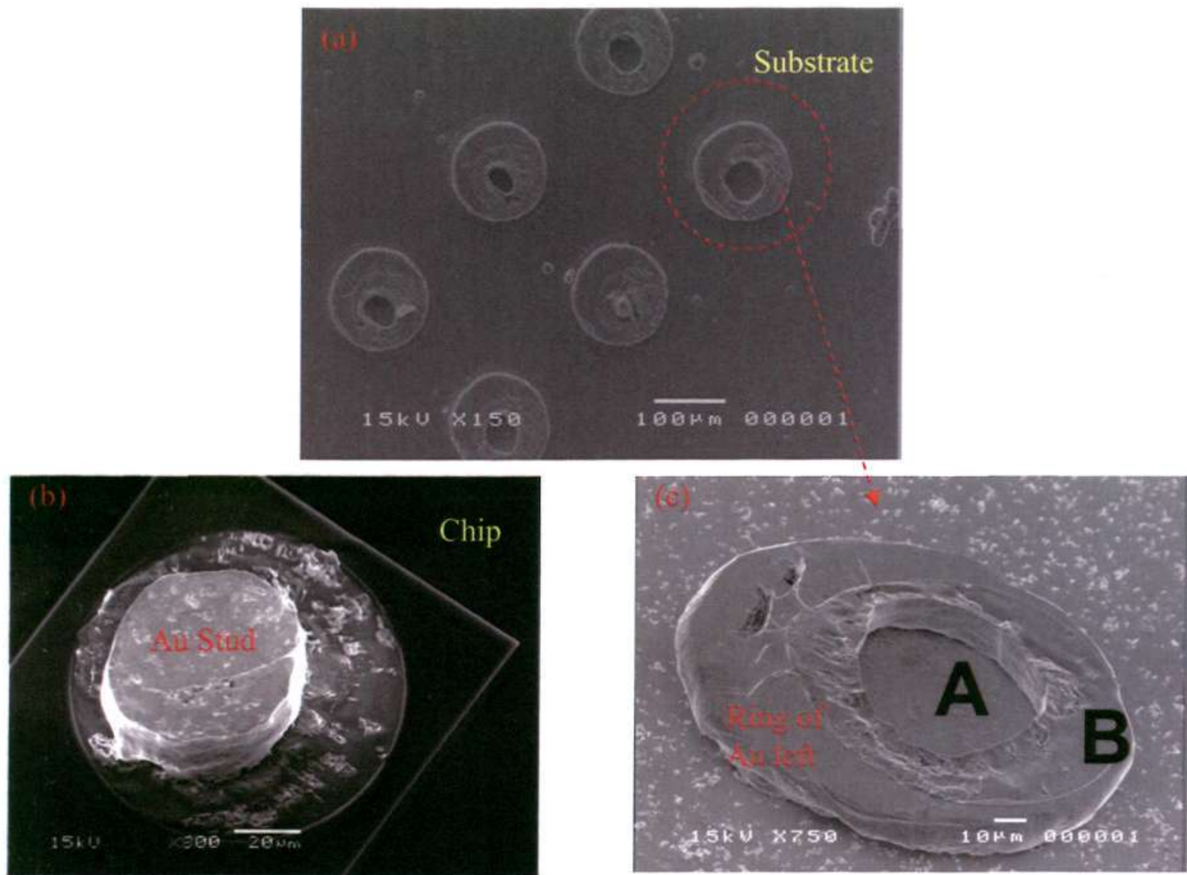

Figure 3-24 (a) SEM fractographs of a gold layer left on a silicon substrate (Low Magnification) (b) A Au stud remains on the chip surface (c) A ring of Au left on the substrate bonded at bonding pressure of 500g/bump [979MPa]

ATTENTION: The Singapore Copyright Act applies to the use of this document. Nanyang Technological University Library

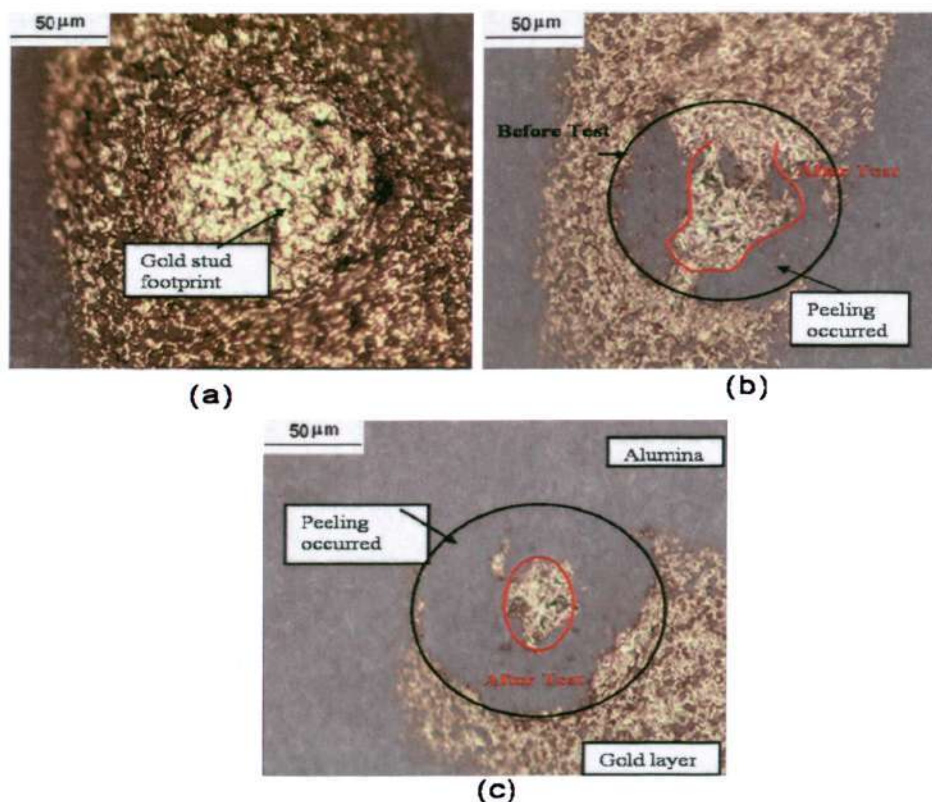

Figure 3-25 Optical fractographs of Au stud left on an alumina substrate at different tool temperatures: (a) 150°C, (b) 180°C and (c) 250°C

SEM observations shown in Figure 3-25 were carried out at higher magnification to determine the unbonded region in a gold-coated silicon substrate. Figure 3-26 shows that failure at the central region A could have happened along the interface between the Au bump and the substrate (B). The grains at the center portion are flattened as compared to that of the Au substrate due to the harder underlying Ni layer. From the SEM fractographs, we hypothesize the failure path by the schematic illustrated in Figure 3-27. Interfacial failure takes place at the central region and proceeds cohesively into the bulk Au material. The fracture path in fact agrees with the proposed mechanism reported earlier that bonding takes place from the outer peripheral region of the bump inwards. Hence interfacial fracture occurs at the central region.

ATTENTION: The Singapore Copyright Act applies to the use of this document. Nanyang Technological University Library

Figure 3-26 SEI fractographs taken at a higher magnification. (Left) Surface A at the central region. (Right) Surface B at the bare gold substrate

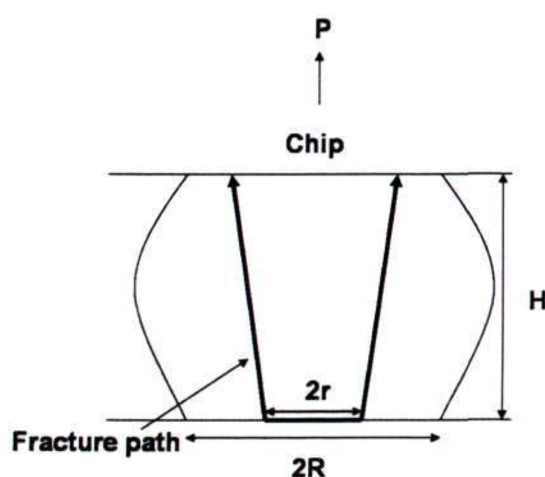

Figure 3-27 Schematic of failure path of the bonded Au-Au joint during tensile test

b. Plated Bump

Bonding experiments using plated bumps were also carried out. The details of the bonding procedure were described in the experimental section of this chapter. After bonding, the bonded joints were subjected to a tensile pull test and the lift-off pattern of the bonded area were observed under the scanning electron microscope. The fractographs of gold stud-bonded joints were compared to that of a plated gold joint. In both Figure 3-28(a),(b) and 3-29(a), (b), a ring of gold material were found left on the substrate after tensile pull test. The central region of the bonded joint were pulled off at

ATTENTION: The Singapore Copyright Act applies to the use of this document. Nanyang Technological University Library

the interface which is evident in Figure 3-28(c) and 3-29(c). A cylinder of gold material left on at the central of the bump imprint at the chip side was observed. Figure 3-30 showed the schematics of the failure path of joints after tensile pull test.

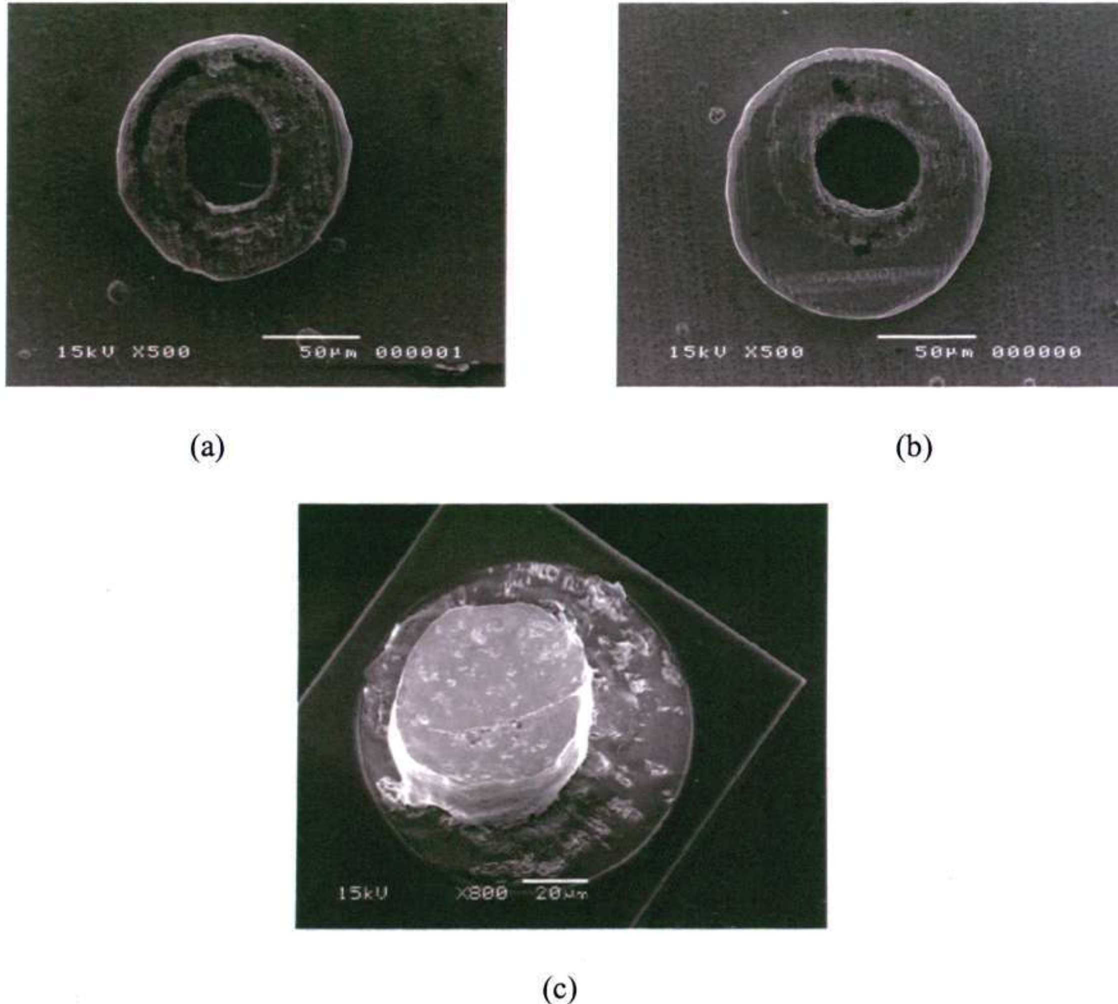

(a) (b)

(c)

Figure 3-28 Au stud joint after tensile pull test (a) SEM observation of gold layer left on substrate. Sample is bonded at 216g per bump [550MPa] (b) Sample is bonded at 310g per bump [790MPa] (c) SEM observation of a cylindrical gold material left on the chip side

ATTENTION: The Singapore Copyright Act applies to the use of this document. Nanyang Technological University Library

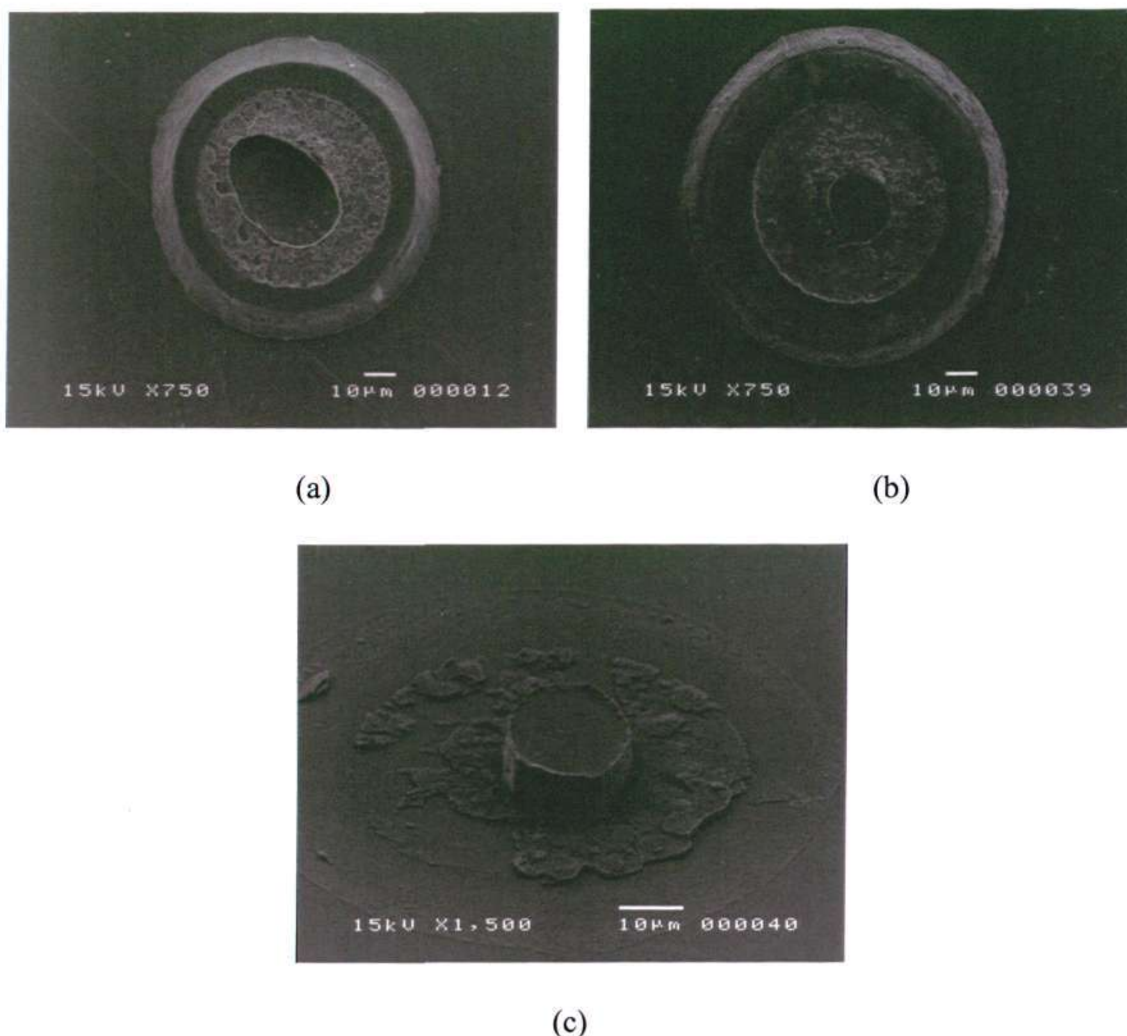

(a) (b)

(c)

Figure 3-29 Plated bump joint after tensile pull test. a) SEM observation of gold layer left on substrate. Sample is bonded at 125g per bump [244MPa] (b) Sample is bonded at 500g per bump [976MPa] (c) SEM observation of a cylindrical gold material left on the chip side

It is known that failure occurs at the weakest region of a bonded joint. The experimental data showing that the central region of the joint is the weakest region despite geometrical differences, supported the analysis computed in our Figure 3-15 in Section 3.3.4.2. Illustrated in the schematics shown in Figure 3-30, due to low shear stress distribution in the central region, no bonding can take place. Hence the ring seen in the experimental results defines the onset at which interfacial shear stress exceeds the critical shear stress.

ATTENTION: The Singapore Copyright Act applies to the use of this document. Nanyang Technological University Library

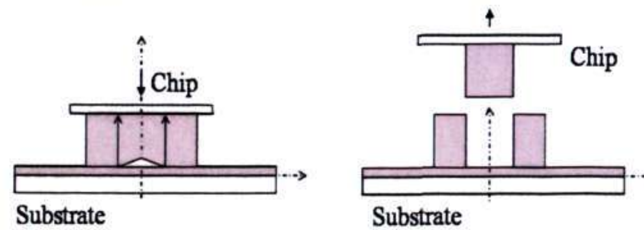

Figure 3-30 Very weak or no bonding at the center of the bump (left). The drawing on the right showed that failure occurs at the weakest bonding region – central region and proceeds cohesively through the bulk material.

The inward bonding behaviour observed in both stud and plated bump can be explained as follows. The interfacial shear stress present at the contacting bond sites is believed to lead to high deformation i.e. complex displacement or relative motion between the bonding surfaces which in turn shear away the surface contaminants, thus exposing more bonding sites for bonding. When pressure increases, a larger number of bonding sites (A_T) in the region from the bump periphery experiences higher shear stress beyond the critical value, leading to a progressive inward movement of the bonding front.

3.7 Fracture mode analysis using interfacial stress distribution and unbonded radius

With increased plastic flow at the interface, true contact area increases and thus improves bonding. From the previous section, fractographs of bonded joints after tensile tests exhibit two failure modes. The first failure mode shows an interfacial failure between the bump and the substrate when bonding pressure is relatively low, indicating a low tensile value. The second type of failure mode involves interfacial and normal cohesive strength where failure occurs at the bonded interface and across the bulk gold, leaving a ring of gold bump on the substrate. From the fractographs, it is clear that the bond strength of a Au-Au joint at higher bonding pressure is determined by both interfacial and normal cohesive strength. Shown in the schematics in Figure 3-

ATTENTION: The Singapore Copyright Act applies to the use of this document. Nanyang Technological University Library

30, interfacial failure occurs at the central region due to the upward pulling force and cohesive failure occurs too when the failure propagates across bulk gold bump by shear movements. Hence, upon a normal pulling force, interfacial and cohesive normal failure is predominantly determined by shear (τ^*) and tensile strength (σ^*) of gold respectively.

Mathematical equations are derived to explain the peak seen in tensile strength with respect to the mixed fracture modes consisting of interfacial and normal cohesive strength. Interfacial failure represented by tensile force (F_t) can be expressed in Equation 1 where R is the contact radius, r is the unbonded radius and σ^* is the tensile strength.

$$F_t = \frac{\pi}{4}\left(R^2 - r^2\right)\sigma^* \qquad \text{Eq. 1}$$

Since the normal cohesive failure is dominated by shear failure of bulk gold, the shear force can be expressed in terms of H (the height of the bump) and τ^* (shear strength) of gold.

$$F_s = 2\pi r H \tau^* \qquad \text{Eq. 2}$$

Both expressions are plotted against the unbonded radius r in Figure 3-24. Expression in equation 2 shows an obvious linear relationship between the normal cohesive (shear) force needed for shear failure and r. Conversely, the tensile force for interfacial failure is inversely related to r. In fact there are two other parameters R and H. As pressure increases, there is no significant change in R and H. For simplicity, they are assumed here to be constants. Since failure occurs at the weakest point of a system, the derivation of the mathematical expressions hypothesizes that the resultant strength of the Au-Au joint will follow the dotted line shown in Figure 3-31.

ATTENTION: The Singapore Copyright Act applies to the use of this document. Nanyang Technological University Library

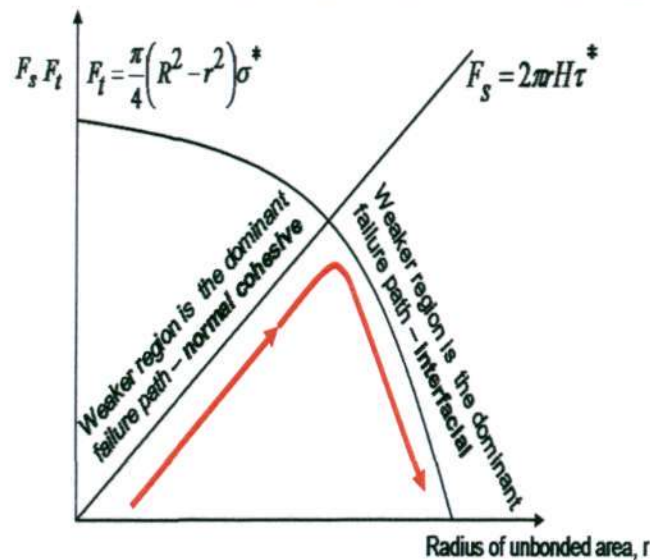

Figure 3-31 Dependence of interfacial and cohesive bond strength on unbonded radius, r

3.8 Estimation of True Bonded Area

When two real surfaces are in contact, the amount of contact area should be as high as possible in order to achieve higher bond strength. This can be achieved by creating perfectly flat surfaces. However surfaces will always be microscopically rough even after vigorous polishing. It has been reported that the true contact area between two contacting surfaces are often much lower than the nominal contact area [70]. In this section, the fraction of true bonded area is estimated based on the ratio of the calculated true shear area of the gold to measured bonded area of the gold ring left. The calculation can be found in Appendix A2. Nanoindentation test using Berkovich pyramidal indenter was used to evaluate the hardness (H) of the gold, giving an average of 0.902GPa. This value is higher than pure gold (cast or hard drawn at 295MPa and 687MPa) [66]. This is expected since the hardness of metals depends on the exact composition and degree of work hardening. The gold ring has undergone excesssive deformation during bonding and mechanical test, thus giving a harder characteristic. The yield strength (Y) of the gold can be estimated from the measured hardness value using the correlation H = 3Y [66]. Since the amount of bonded area - $A_{measured}$

ATTENTION: The Singapore Copyright Act applies to the use of this document. Nanyang Technological University Library

(macroscopic) is defined by the ring of gold left on the substrate, the shear force was measured to evaluate the shear strength of gold. Based on the measured shear force and Y, the true bonded area ($A_{T\text{-}shear}$) is estimated to be 5 x $10^{-10}m^2$. By taking the ratio of $A_{T\text{-}shear}$ over $A_{measured}$, it was found that the fraction of area truly bonded is only 10% over the entire bonded region at macroscopic level.

3.9 Chapter Summary

Studies on both temperature and pressure dependence for gold-gold thermocompression bonding were carried out. The main conclusions can be summarized in the following points:

- For a particular pressure, no bonding can occur when temperature falls below a critical value. This critical limit depicts the onset of bonding where the surface has to be thermally activated before true bonding between two intimately close surfaces occurs.
- Surface analysis showed a layer of barrier film on gold containing mainly of carbon and oxygen at a thickness of less than 4nm. Both temperature and pressure applied provide large deformation at the bonding interface to remove the layer, exposing clean surfaces for bonding, thus translating to a rise in bond strength.
- A ring structure is left on the substrates after mechanical tests, suggesting that bonding is weakest at the central region of the bump. This can be explained by the interfacial shear stress distribution across the radial position with increasing pressure.
- No significant increase in amount of bonding area despite an apparent rise in bond strength was observed when bonding pressure and temperature exceeds well above critical limits. Finite element modeling supported this argument. The increase in bond strength with higher bonding parameters observed here is

ATTENTION: The Singapore Copyright Act applies to the use of this document. Nanyang Technological University Library

attributed to the increase in the number of locally bonded sites when higher pressure (beyond $P_{min.r}$) is applied at a particular temperature.

ATTENTION: The Singapore Copyright Act applies to the use of this document. Nanyang Technological University Library

Chapter 4 SURFACE MODIFICATION BY SELF-ASSEMBLED MONOLAYERS

4.1 Introduction

Following the fundamental study on how bonding occurs between two metallic surfaces under the influence of temperature and normal pressure, this chapter explores surface chemical modification using self-assembled monolayers or SAMs (n-alkyl thiols, $C_nH_{2n+1}SH$) on the gold surfaces prior to bonding. SAMs have been intensely studied for interface engineering applications which are highly influenced by nanometer-scale topographies and composition, such as corrosion inhibition[75-78], lubrication[71, 72], and wetting [73, 74].

4.1.1 Self-assembly

These layers are molecular assemblies that are formed spontaneously by the immersion of an appropriate substrate into a solution of an active surfactant in an organic solvent [75]. They are made up of three main molecular parts – head molecule, alkyl chain and terminal group. The strong molecule-substrate interactions lead to the formation of a chemical bond between the head group and surface sites, yielding a crystalline molecular assembly. Once chemisorption occurs, the alkyl chain which

ATTENTION: The Singapore Copyright Act applies to the use of this document. Nanyang Technological University Library

forms the second molecular part, will assemble to form an ordered (i.e. with translational symmetry) and close-packed (i.e. high density) layer. Finally the terminal functional group determines the surface properties. A methyl terminated (-CH_3) monolayer is considered well ordered, close packed when the advancing water contact angle is more than 100°. It is believed that the unique properties of the well ordered, densely packed structure is due to the interaction between the sulphur atom and the gold surface [75]. Alkanethiols are the most intensively studied system especially with gold. These monolayers are amphiphilic, consisting of 2 parts: lyophilic (polar group; soluble in a specific fluid) and lyophobic (insoluble). The amphiphilic structure is responsible for their tendency to concentrate at interfaces.

The adsorption process of alkanethiols onto metal surfaces was governed by two distinct adsorption kinetics [76]. The first step takes only a few minutes, whereby the contact angles are close to their limiting values with thicknesses about 80-90% of their maximum. This initial step is described by the diffusion controlled Langmuir adsorption and was found to have a rate limiting dependence on the thiol concentration in the solvent. The higher the concentration, the shorter the time needed for adsorption. It is because this chemical reaction is governed by the surface-head group interactions. The second stage involves a slow step, which lasts for several hours before their thicknesses and contact angles reach their final values. In this stage, a surface crystallization process has occurred, where the alkyl chains get out of their disordered states and rearranged themselves into ordered arrays. This step is related to the degree of chain disorder, Van der Waals forces, dipole-dipole interactions and the nature of the chains.

ATTENTION: The Singapore Copyright Act applies to the use of this document. Nanyang Technological University Library

4.1.2 Thermal and Mechanical Properties

The thermal and mechanical properties of alkanethiols are of particular interest in this dissertation since these layers undergo thermal and mechanical deformation during thermocompression bonding. Several parameters govern the thermal stability of the SAM layer namely - bond strength of Cu-S or Au-S bond, packing density of the SAM molecules on the substrate, intermolecular interactions between the chain groups, and electron density distribution within the SAM molecules. Many studies have been done on the thermal desorption of SAMs using different techniques [75-77] where thermal desorption and ion sputtering are the most convenient techniques. The common observations made by these studies revealed that the adsorption of the SAMs are often made up of two components – the physisorbed and chemisorbed, thus giving rise to more than one desorption peaks observed. The use of raman spectroscopy in investigating self-asembled monolayers provides structural information such as molecular chain order of the layer deposited[77]. However due to the weak Raman scattering of the layer, characterization of SAMs are often obtained using surface-enhanced raman effect[78]. This technique requires nano-patterning of underlying substrate after which the layers are deposited onto the nanostructures. This does not lie within the scope of this work. The understanding of the mechanisms of adsorption and desorption of SAMs are important in order to obtain useful and repeatable applications such as in the surface modifications to control surface properties. In the case of oxidative metals such as copper, the type of ambient would also have an effect on the thermal desorption mechanisms of SAMs. In air, desorption is initiated by the sulfonation reaction of the thiolate groups with surface oxygen or O_2 and H_2O in air [79] followed by the desorption of the monolayers. In vacuum, the mechanism is different, as the decomposition is initiated via γ–hydrogen elimination [80].

ATTENTION: The Singapore Copyright Act applies to the use of this document. Nanyang Technological University Library

Due to its molecular structure (head, main chain and tail group) and the versatility in tailoring the properties of self-assembled monolayers, SAMs techniques is one of the most common methods for building model lubricants, adhesion promoters or wear resistant coatings for applications such as microelectromechanical systems (MEMs). Therefore, it is technologically interesting to conduct extensive studies on the unlimited possibilities of designing the layer parameters and correlating its mechanical behaviour during friction, adhesion and wear. The determining parameters include the following: (1) the head group which determines its binding energy to the substrate, (2) the chain length and type of intramolecular bonds which can alter the elastic compliance and finally (3) the tail group which can conveniently tailor the adhesion and friction [81]. Generally when the layers experience compressive forces exerted by sharp asperities or contacts exceeding 1GPa, they can be displaced away, as shown in Figure 4-1 [81].

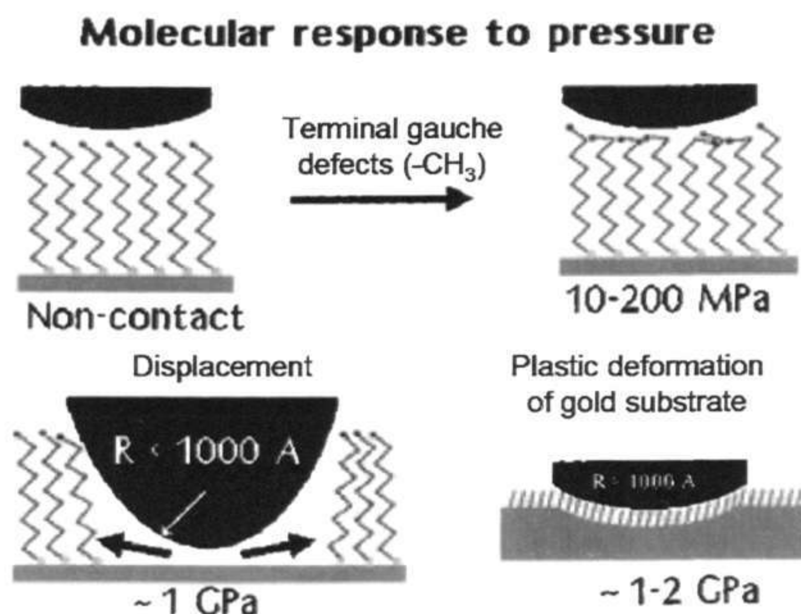

Figure 4-1 Schematics of molecular response of SAMs to various amount of compressive loads (10MPa – 1.2GPa)

Since bonding phenomenon between two bulk materials is based on interfacial interactions, it is believed that surface modification through self-assembled monolayers

ATTENTION: The Singapore Copyright Act applies to the use of this document. Nanyang Technological University Library

can be the one of the feasible approaches in improving conventional bonding methods. Here, we report an enhancement in the tensile bond strength of gold joints that were coated with a layer of dodecanethiol (C_{12}) prior to bonding at a temperature range of 80°C to 180°C. Since it is known that the properties of alkanethiols vary as a function of their chain length [82-84], this chapter also reports the chain length dependence in SAMs-assisted bonding whereby shorter chain alkanethiol, C_6 exhibits better strength improvement at very low temperatures compared to the longer ones. Further discussion to explain the superior strength improvement by C_6 will be reported in the next chapter.

4.2 Experiments

Proper cleaning of the substrates and the glasswares are required for good deposition of the SAMs layer. Sputtered Au wafers consists of these layers: SiO_2 on Si wafer, followed by 50nm Ti layer, 100nm TiW and finally 200nm Au layer in sequence, were used. To remove any hydrocarbon contaminants on the surfaces prior to SAM deposition, the gold bumps and substrates were treated with UV/ozone cleaning for 10mins, followed by sonication in absolute ethanol for about 20mins before immersing into 1-5mM ethanolic solution placed in a N_2-purged glove box. After 24 hours, a layer of dodecanethiol [$CH_3(CH_2)_{11}SH$, DDT] was deposited on the gold surfaces at room temperature. The spontaneous assembly of the molecules is known to form a densely packed and highly oriented structure on the exposed gold surfaces [85]. The schematic of the process flow is illustrated in Figure 4-2. The solution was prepared in the glove box to minimize contamination in the solution. The clean substrates were fully immersed into the SAMs solution for 24hours before they were removed and rinsed with copious amount of absolute ethanol, followed by drying using nitrogen gas.

ATTENTION: The Singapore Copyright Act applies to the use of this document. Nanyang Technological University Library

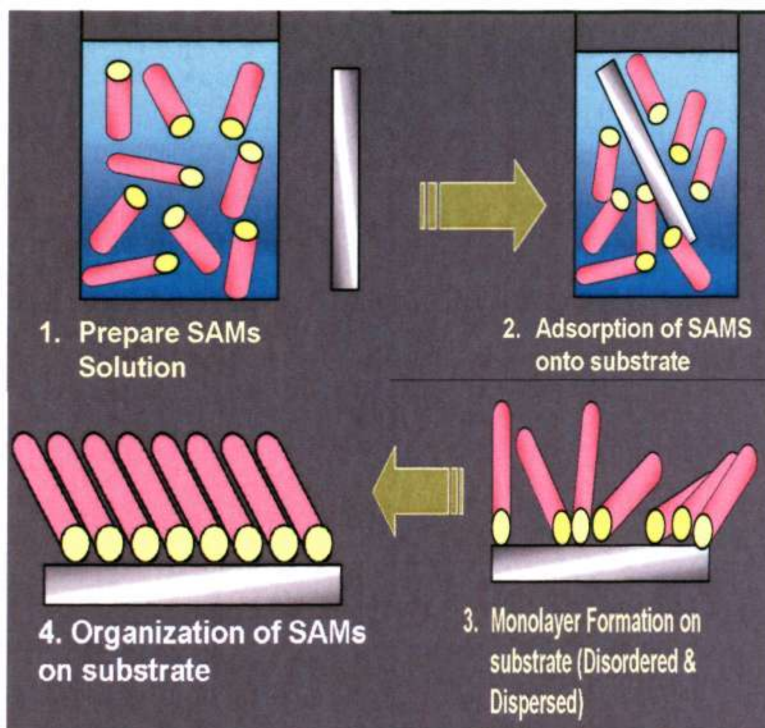

Figure 4-2 Schematics of process flow in SAMs deposition

4.3 Thermocompression Bonding of uncoated and SAM-coated gold bumps

4.3.1 Gold Stud Bump

During the bonding process, the chip temperatures were varied from 80°C to 180°C, while keeping the substrate temperature at 80°C. The bonding load varied from 310 MPa to 516MPa. Results shown in Figure 4-3 indicate that the bond strength increases with chip temperature, with higher strength obtained at higher bonding pressures. This temperature dependence of the bond strength is in agreement with the behavior reported by Zhang [86], interpreted to be due to the necessity to rupture barrier films prior to bonding.

ATTENTION: The Singapore Copyright Act applies to the use of this document. Nanyang Technological University Library

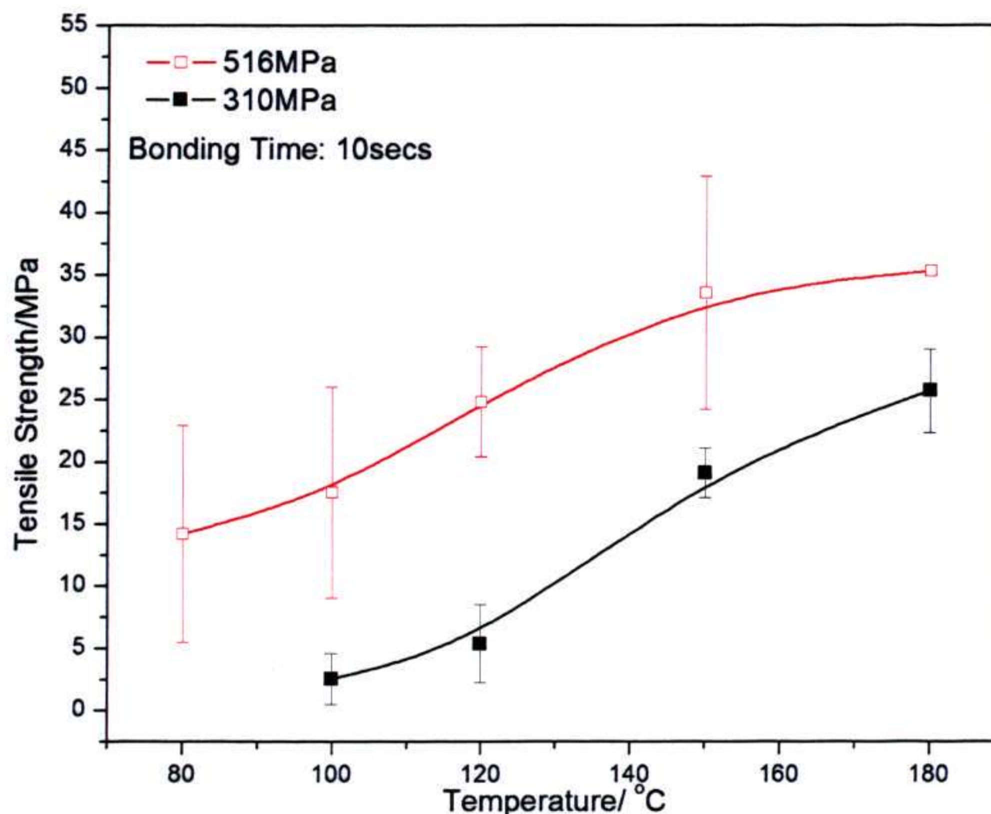

Figure 4-3 Tensile strength of bonded joints bonded at 310 MPa and 516MPa in variation with bonding temperature

A comparison between the bond strength of traditional direct gold stud-gold and SAMs-assisted gold-gold bond was carried out. The bonding temperature was plotted against normalized tensile strength of two types of joints to evaluate the role of SAMs in bonding. Normalization is carried out to take into account of the difference in measurement techniques and the measurement mode. Figure 4-4 shows that equivalent strengths can always be obtained at a lower temperature with SAMs compared to without SAMs.

ATTENTION: The Singapore Copyright Act applies to the use of this document. Nanyang Technological University Library

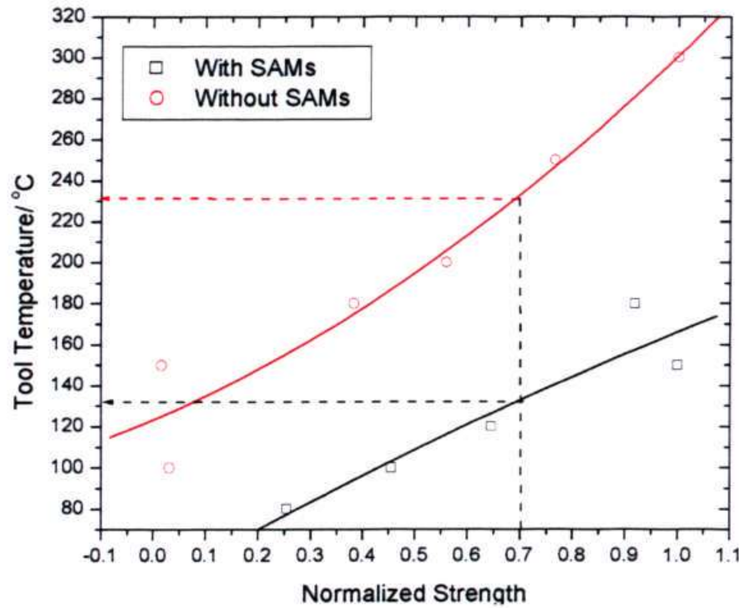

Figure 4-4 Comparison between gold-gold joints formed with and without the help of SAMs

Further analysis on the fracture surfaces after mechanical test were carried out. Figure 4-4 shows the SEM fractographs of Au-Au bonding at different chip temperatures and bonding load. In general, the modes of failure observed can be classified into two groups: adhesive failure–Au footprint on Au substrate in Figure 4-5a and adhesive and cohesive failure–Au bumps attached to substrates in Figure 4-5b. Mode 1 is observed when the failure strength is <10 MPa /bump, while mode 2 is observed when the tensile values exceed ~20MPa/bump. In the latter, from the SEM images, it can be observed that fracture occurs at the interface between bulk Au bump and Al bond pad. In other words, the bonding strengths of bumps-Au substrate interface are stronger than that of the bump-pad adhesion strength. Hence it is obvious that strong bonding is achieved between the bumps and substrate. On the other hand, for failure mode 1, fracture occurs at the bump-Au substrate interface, suggesting that a weak boundary layer is formed around the interface between the two media. The energy

ATTENTION: The Singapore Copyright Act applies to the use of this document. Nanyang Technological University Library

supplied is insufficient to bring about effective bonding at the interfaces. Obviously, mode 1 will result in lower fracture strength than mode 2.

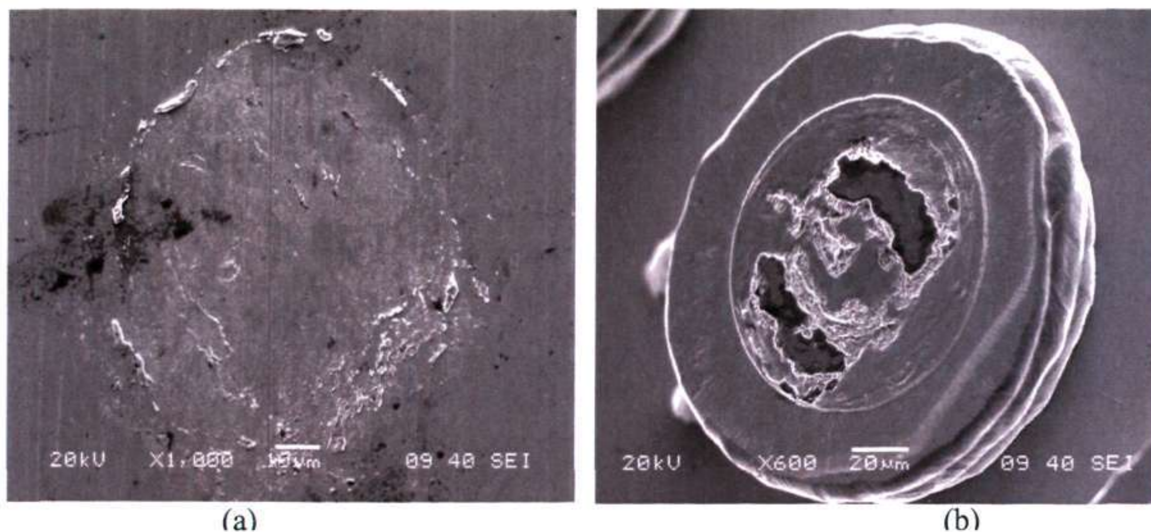

(a) (b)

Figure 4-5 SEM fractographs of substrate surface at different chip temperatures and bonding loads: (a) 120°C and 200MPa/bump (b) 150°C and 510 MPa/bump

4.3.2 Electroplated Gold Bumps

Since the drive towards finer pitch and thinner packages and integrated chips, likewise the interconnects used for such packages, electroplated gold bumps offer both finer pitch and shorter bump height as compared to the stud bumps. Similar bond strength enhancement was observed where the coated gold samples exhibited superior tensile strength at all temperatures above 140°C.

ATTENTION: The Singapore Copyright Act applies to the use of this document. Nanyang Technological University Library

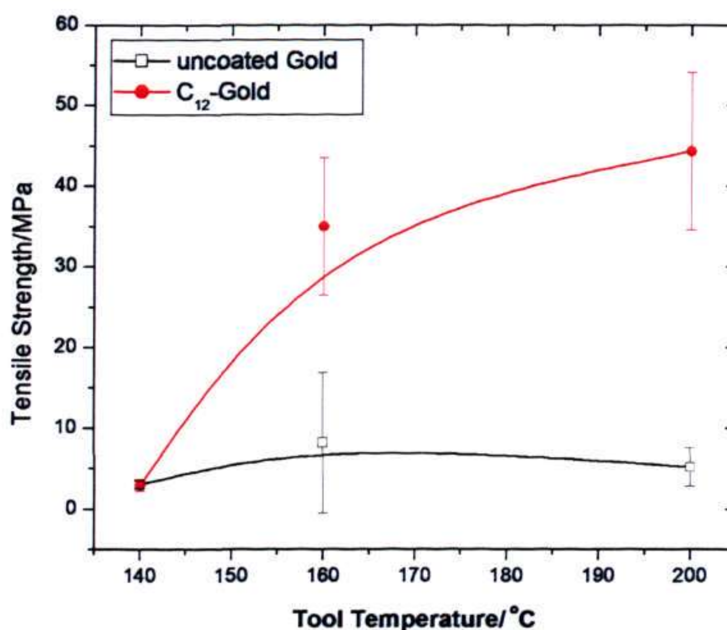

Figure 4-6 Comparison of the tensile strength of coated electroplated samples and uncoated gold samples at constant bonding pressure at 500MPa

Electroplated gold bumps at bump heights of 26μm – 29μm were fabricated using non-cyanide based gold electrolyte. The coated electroplated bumps and gold substrates were prepared as described in the earlier paragraph. These freshly-deposited samples were then bonded in ambient at 140°C, 160°C and 200°C (tool temperature), respectively under a constant bonding load of 744MPa per bump for 20 seconds. Several minutes were necessary for the bonder to heat and cool to the set temperature respectively. No additional cleaning steps besides solvent rinsing were employed for the blank gold samples. Similar bonding parameters were then used to bond the samples, after which the bonded samples were subjected to a tensile pull test using a dynamic mechanical analyzer (DMA).

Enhanced bond strength was observed for the gold joints coated with DDT (C_{12}) prior to bonding. Figure 4-6 compares the tensile strength of both types of bonded samples as a function of tool temperature. Bond strength increases with bonding temperature, as expected. All capped joints are stronger than uncapped joints at all

ATTENTION: The Singapore Copyright Act applies to the use of this document. Nanyang Technological University Library

temperatures tested, or equivalently, to achieve a specific joint strength, capped joints require a lower bonding temperature. For example, our data suggests that a joint strength of 20MPa per bump can be obtained at 150°C through SAMs-capping.

4.4 Bonding Hypothesis

In chapter three of this dissertation, one of the key conclusions drawn to metal-metal bonding is the necessity of a clean metal surface prior to bonding. Despite gold's inertness to oxidation, it is highly reactive towards adsorbed layers of molecules that are present in the environment such as gaseous or organic molecules. The ease of forming such layer on gold is the main reason for the need of high temperature in thermocompression bonding. Hence the alleviation of such contamination as well as the displacement of this layer from the surfaces prior to bonding is critical in allowing bonding between fresh gold atoms. In our approach, an organic monolayer (SAM) was deposited intentionally on 'clean' gold surfaces prior to bonding.

With the preliminary results obtained, a working hypothesis is created to explain the role of SAMs, illustrated in Figure 4-7. The preliminary cleaning prior to SAMs deposition using UV /ozone and subsequent sonication in ethanol will remove organic contaminants and the gold oxide [87]. SAMs modify the surface during deposition process. Contact angle goniometry measurement results show a significant increase in the contact angle from 79° for blank Au substrate to 97° for SAMs-coated substrate. This is typical and has been widely reported in literature [73, 76, 85, 88].

ATTENTION: The Singapore Copyright Act applies to the use of this document. Nanyang Technological University Library

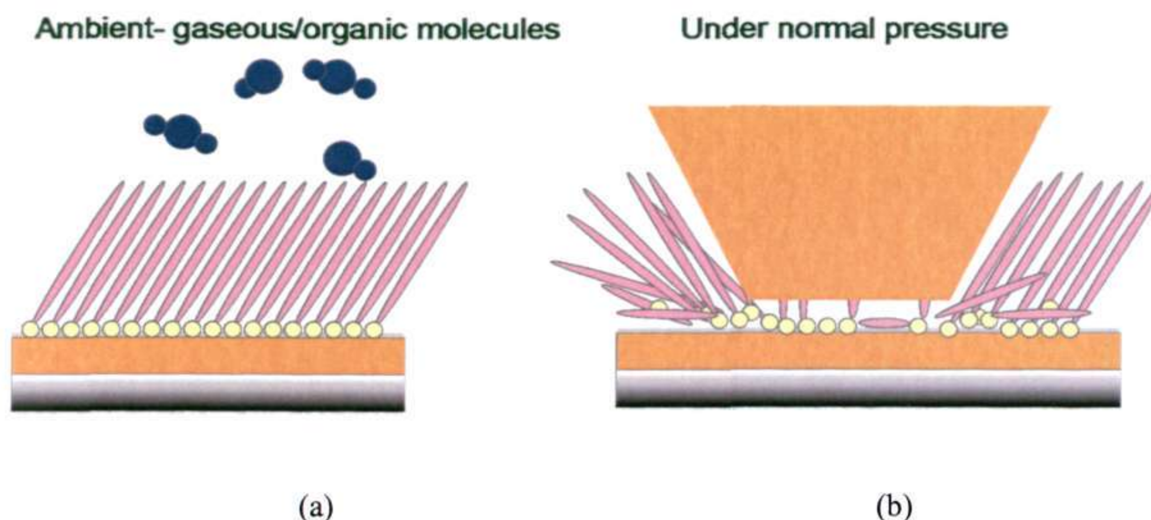

(a) (b)

Figure 4-7 Illustration of SAMs acting as: (a) a passivation layer (b) a lubricant

It is believed that SAMs serve as a passivation and lubricant layer on the gold surface, preventing further adsorption of organic contaminants from the air onto the gold surface and facilitating the whole contact area bonding. The absence of the organic contaminant films will contribute to a lower barrier encountered in creating conventional Au-Au bonds by simultaneous application of temperature and pressure in thermocompression. As reported, bonding is highly temperature-dependent. Application of adequate amount of temperature provides necessary activation energy to overcome the minimum work to disrupt the organic films, thus exposing gold for bonding[86]. SAMs reduces the required energy i.e. the bonding temperature to do work by the proposed mechanism.

Besides the passivation function, SAMs is believed to serve as a lubricant. During bonding process of Au-Au under pressure, Au was pressed in Z direction and elongated along X and Y directions. With a lubricant SAM layer between Au bump and Au pad, the friction between Au bump and Au pad was significantly reduced. The shear movement by the lubricant at the interface is believed to improve sliding at the bonding interface which helps in activating more area for bonding. Therefore, the whole contact area between Au bump and Au pad was facilitated to be bonded together. Accordingly,

ATTENTION: The Singapore Copyright Act applies to the use of this document. Nanyang Technological University Library

the bond strength was increased. Even at low bonding temperatures, the friction and micro-welding can still happen at Au-Au joint interface. This description of the bonding mechanism is consistent with the fractographic observations made by SEM, whereby the fracture occurs at the bump-substrate interface and bump-chip interface at low and high chip temperatures respectively. However, lubrication properties of SAMs is chain-length dependent. In the following chapter, it was found that the lubricating characteristic of SAMs has little or no influence in promoting bonding. Longer chain length alkanethiols which exhibit lower friction [72] does not help to enhance bond integrity.

4.5 Effect of Chain Length

4.5.1 Introduction

Our previous section had shown that by coating a gold surface with a self-assembled monolayer [SAM, $C_nH_{2n+1}SH$], lowered bonding temperature can be achieved [89]. In this section, we evaluated the influence of different SAM chain length on the bondability between gold surfaces and found that bond strength improvement is most significant with shorter chains (n = 6 as compared to n = 12). SAMs with longer chain lengths, (n = 18) lead to joint strengths slightly lower than those formed with uncoated gold, for all bonding temperatures investigated. The reason for this behaviour, to be discussed later, helps clarify how SAMs function as a moderation layer in thermocompression bonding of noble metal surfaces.

4.5.2 Experiments

The bonding samples were fabricated by electroplating gold bumps at heights of 24μm – 26μm on silicon wafer before dicing to yield individual bonding chips. Substrates were prepared by sputtering 50nm Ti, followed by 100nm TiW and finally 100nm Au on 0.65mm Si wafer. The bonding chips were then immersed into 1mM

ATTENTION: The Singapore Copyright Act applies to the use of this document. Nanyang Technological University Library

ethanolic solution of 1-hexanethiol (C_6), 1-dodecanethiol (C_{12}) and 1-octadecanethiol (C_{18}) respectively. Kept over 24 hours in a N_2-purged glove box, a relatively good quality layer of ordered and densely packed organic molecules self-assembled onto the gold surfaces. These freshly-deposited samples were then bonded in ambient at temperatures of 25°C, 40°C, 50°C, 65°C and 80°C under a constant bonding pressure of 487 MPa based on initial bump area for 20 seconds. Uncoated gold surfaces underwent 10 minutes of UV/ozone cleaning before bonding. It is necessary to note that the bonder takes some time to heat and cool to the set temperature respectively. Finally the bonded samples were subjected to a tensile pull test using a dynamic mechanical analyzer (DMA).

4.5.3 Does Short Chain Alkanethiol Work Better?

Figure 4-8 displays the tensile strength obtained from all 3 types of SAMs-coated samples as compared to uncoated gold joints as a function of bonding temperature. These results confirm again that bond strength increases with bonding temperature [86]. It is apparent that among all the samples, C_6-coated gold joints exhibit the highest joint strength at all temperatures, achieving usable bond strength of about 49 MPa at a temperature as low as 25°C. As demonstrated earlier, C_{12} improves bonding by lowering bonding temperature [89]. Using this as a reference, C_6 showed even greater bond improvement. In contrast, it is evident that over this range of bonding temperatures, C_{18}-coated gold joints are much weaker, even when compared to bare gold.

ATTENTION: The Singapore Copyright Act applies to the use of this document. Nanyang Technological University Library

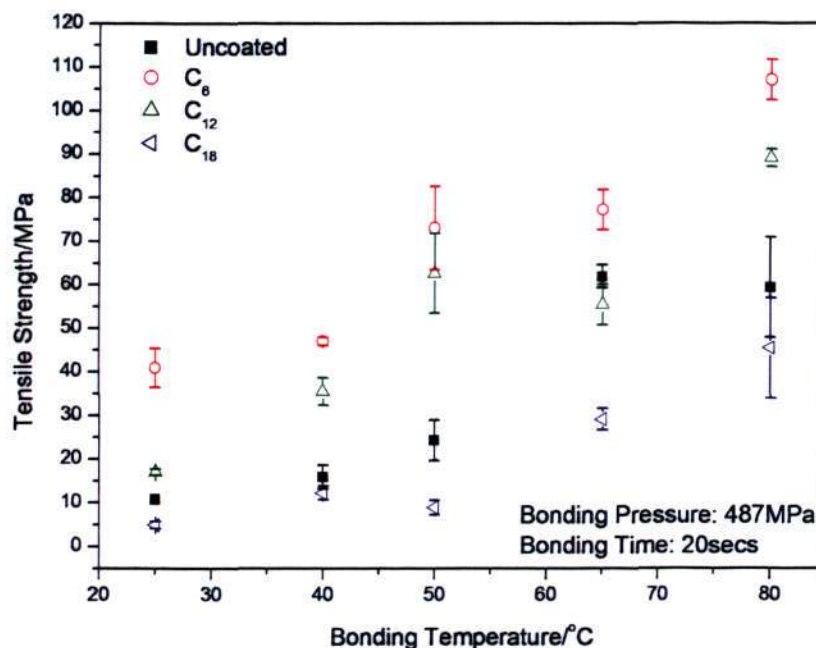

Figure 4-8 A plot of tensile strength of SAM-coated samples - C_6, C_{12}, and C_{18} as compared to an uncoated gold as a function of bonding temperature applied.

4.6 Chapter Summary

In summary, we have demonstrated enhancement in low temperature gold-gold thermocompression bonding for both C_6 and C_{12}-coated gold surfaces. The ability of SAMs in aiding low temperature gold bonding decreases as its chain length gets longer. At n = 18, no strength improvement is observed while at n = 6, highest joint strength is obtained. We deduce that the consideration behind the applicability of SAMs at different chain length for bonding application depends on three primary actions at the bonding interface: (1) surface passivation to alleviate surface contamination; (2) thermal activation to "weaken" or desorb the monolayer through structural disorientation and (3) mechanical displacement to expose virgin gold surfaces for bonding to take place, which will be discussed in greater details in the next chapter.

ATTENTION: The Singapore Copyright Act applies to the use of this document. Nanyang Technological University Library

Chapter 5 BASIS OF SAMS-ASSISTED BONDING PHENOMENON

5.1 Introduction

This chapter explains how bond enhancement varies according to the structural integrity (thermal and mechanical) of the monolayer coating which is a function of the thickness of the monolayer. Gathered with the findings, we have evaluated on the bonding mechanism between two metallic surfaces and coated surfaces in Chapters 3 and 4, a working hypothesis is derived which highlights three key factors enabling low temperature direct metal thermocompression bonding, namely: (1) surface passivation, (2) thermal activation through bond-weakening or desorption of SAMs and (3) mechanical displacement of the weakened SAMs layer.

Self-assembled monolayers on planar substrates such as thin metallic films on silicon wafers, mica or glass are most commonly characterized due to the ease of preparation as well as its compatibility with several surface analytical techniques such as X-ray photoelectron spectroscopy (XPS)[76, 90, 91] , contact angle measurements[76, 92], surface plasmon resonance spectroscopy (SPRS)[93], time-of-flight secondary ions mass spectroscopy (TOF-SIMS)[84, 94, 95]and many more. This chapter presents several surface studies to evaluate the passivating properties of alkanethiols at various chain length on gold metal by comparing the amount of carbon

ATTENTION: The Singapore Copyright Act applies to the use of this document. Nanyang Technological University Library

and oxygen present on the coated and uncoated surface exposed over a period of time. We further simulate the mechanical behaviour of the alkanethiols on the gold surfaces after they were subjected to a normal bonding pressure, revealing the disappearance of the molecular species at the bonding interface. A novel method of predicting the thermal behaviour of alkanethiols using an in-situ SPRS monitoring is also carried out. Besides understanding issues related to the use of novel materials for improving conventional bonding method, the understanding of their storage life is also important for easier integration into the semiconductor processing.

5.2 Surface Passivation

5.2.1 Improved Bond Strength in Exposed SAM-coated Gold Joints

To substantiate the role of SAMs as a passivation layer, we measured the surface composition of two types of surfaces (uncoated gold and freshly coated C_{12}-gold) over a period of time as described below. X-ray photoelectron spectroscopy (XPS) measurements were performed using a Perkin-Elmer PHI 5600 spectrometer with a non-monochromatized Mg $K\alpha$ radiation (2.5 x 10^{-9} Torr). All XPS data were acquired using analyzer pass energy of 23.5 eV for narrow scan spectra. The electron take-off angle was 45°. To monitor the relative changes to the amount of contaminants on their surfaces with time, both samples were exposed in a desiccator for a period of 0, 1, 11 and 31 days before loading into the vacuum chamber. The corresponding changes in the quantities of C1s and O1s elements with time are further quantified by comparing the respective peak area ratios of these elements with Au 4f. These peak areas were taken from fitted curves under the raw spectra.

Figure 5-1 shows the peak area ratios of O1s/Au 4f and C1s/ Au 4f for C_{12}-coated gold and uncoated gold respectively. The ability of thiols in removing the oxygen contaminants during solution deposition explains why the C_{12}-coated surface is

ATTENTION: The Singapore Copyright Act applies to the use of this document. Nanyang Technological University Library

much lower in O content prior to ambient exposure [96]. As the exposure time increases, there is a concurrent rise in O as well as C content on the uncoated Au surface. In contrast, the C_{12}-coated surface exhibits very low O uptake and even a slightly negative C uptake. It has been pointed out that the primary surface contaminants on surfaces consist of mainly carbon and oxygen [97, 98] and several reports have documented the formation of chemisorbed CO-metal bonds on metal surfaces [99]. The simultaneous increase in the oxygen and carbon found on uncoated gold surface can thus be attributed to CO adsorption. Therefore, the low uptake of C and O found on C_{12}-coated gold must be due to an effective passivation of the surface against further surface contamination. The decrease in C content on C_{12}-coated surface with prolonged exposure is probably due to the desorption of carbon from the alkyl chains [100] .

Further bonding experiments were carried out to evaluate the hypothesis. We exposed UV-cleaned gold bumps and substrates as well as freshly-coated C_{12} samples to ambient over 1 and 3 days before they were each bonded. All C_{12} – coated samples displayed enhanced tensile strength (equivalent to lower bonding temperature needed) over UV-cleaned samples as a function of exposure time. This, again, supports our hypothesis that C_{12} layer blocks off contaminants from gold surface. All bonding steps in this work were carried out in ambient conditions, and there was a finite time lag (a few seconds) in temperature stabilization, as mentioned in the experimental section, which means that all samples, regardless of capping conditions, will experience inevitable environmental exposure prior to bonding. This non-zero net exposure explains why there is a net improvement in strength of capped Au surfaces over uncapped surfaces even at time zero, as shown in Figure 5-2. This underlines the extreme difficulty of maintaining a pristine clean gold surface at the moment of bonding. Interestingly, it was noted that the gain in strength relative to UV clean

ATTENTION: The Singapore Copyright Act applies to the use of this document. Nanyang Technological University Library

samples was found to be more apparent for samples exposed over a longer period of time before they were subjected to bonding, shown in Figure 5-2. The efficacy of SAMs in protecting gold surfaces for bonding is accentuated as unprotected gold surface gets dirtier, consistent with the exposure results.

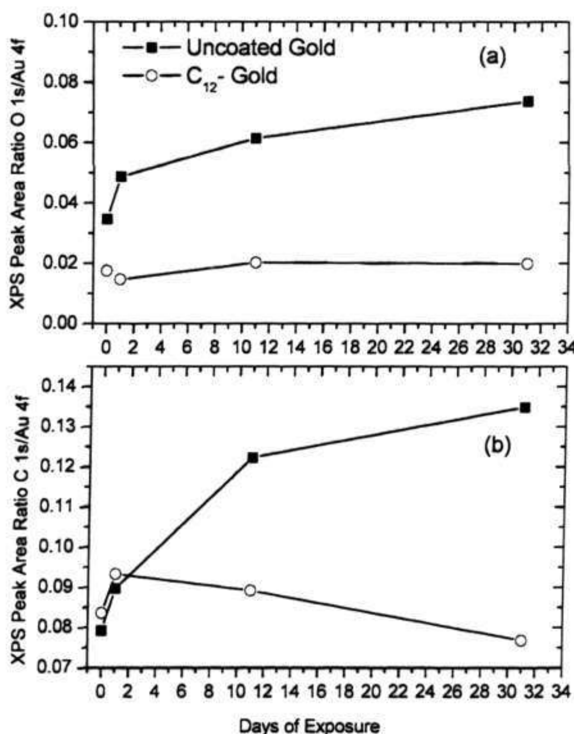

Figure 5-1 XPS peak area ratio of O1s (top) and C1s (bottom) of both coated and uncoated gold samples with reference to Au 4f peak

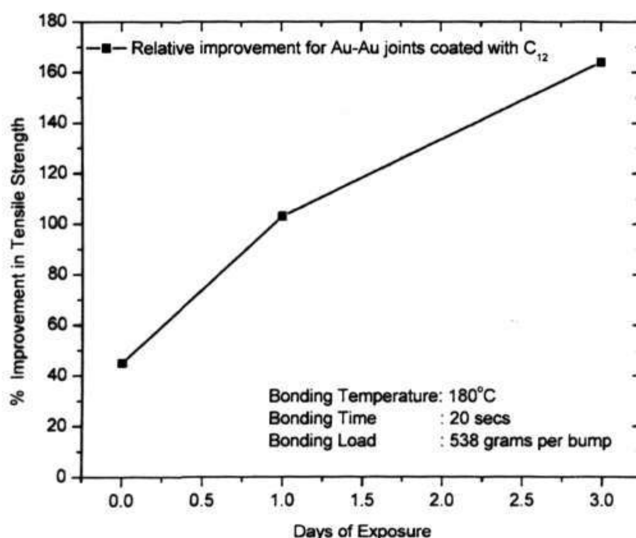

Figure 5-2 Relative percentage improvement in tensile strength of C_{12} -coated to uncoated gold samples as a function of exposure time prior to bonding

ATTENTION: The Singapore Copyright Act applies to the use of this document. Nanyang Technological University Library

5.2.2 Chain Length Dependence

To compare the total amount of C and O present on both coated and uncoated gold surfaces at different chain length, higher resolution peak acquisition using a monochromatic Al Kα radiation (1486.7 eV photons, 10^{-10} mbar background pressure) by VG ESCALAB 220i-XL instrument that is equipped with a concentric hemispherical analyzer and a magnetic immersion lens was used. Since SAMs of thiolates were found to be susceptible to X-ray induced damage where dialkyl sulfides or disulfides could form within the layer [101, 102], short scan time of the coatings was employed to avoid such effects. High resolution spectra of C1s and O1s for elemental quantification were recorded with pass energy of 20 eV at 0.1 eV step width. As a reference, the Au 4f peak is used for computing the peak area ratios of all elements for all samples. We observed an absence of oxygen in all SAM-coated gold samples even though the freshly coated samples were inevitably exposed in ambient for a few minutes just before loading, as shown in Figure 5-3. Carbon content was also detected on cleaned gold surface despite cautious effort to minimize ambient contamination prior to chamber loading. The higher carbon content was apparent as the monolayer chain of SAM gets longer. One important point to note is that the carbon content in C_6 that was deposited "intentionally" on the gold surface is less than the adventitious contamination on the uncoated Au, suggesting that the ambient contaminant layer has been replaced by a milder or thinner barrier. In addition, we found that this delicate monolayer is capable of preventing further contamination during the short time span of exposure just before bonding. A smaller amount of surface contamination leads to greater ease of removal, thus metallic bonding between the two clean surfaces can be more readily achieved [13].

ATTENTION: The Singapore Copyright Act applies to the use of this document. Nanyang Technological University Library

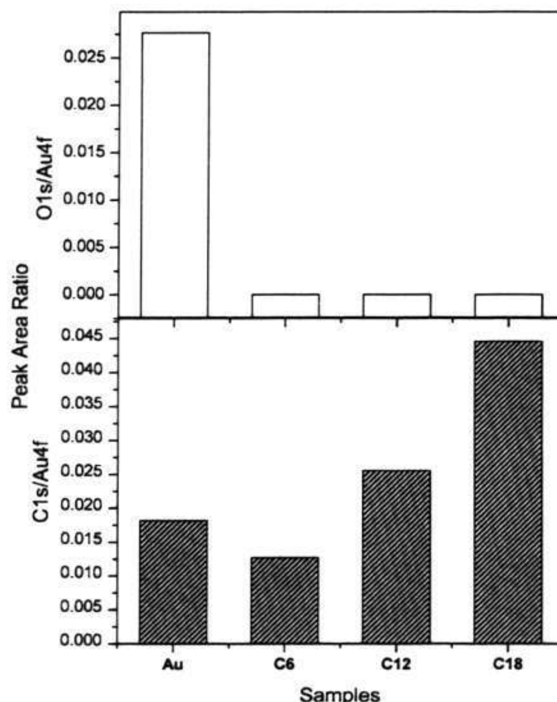

Figure 5-3 Comparisons of XPS peak area ratios of: (a) O1s, (b) C 1s at different chain length

5.3 Mechanical Displacement

Octadecanethiol (C_{18}), having a longer chain length, is known to be more corrosion-resistant and air-stable, and is therefore expected to be a stronger passivation layer [101, 103]. If surface passivation is the sole factor responsible for bonding enhancement, then SAMs with longer chain lengths should be more effective than shorter SAMs. However, its poor behavior in the current bonding study [In section 4.5] clearly indicates that surface passivation is not the only determining factor influencing the effectiveness of SAMs-enhanced bonding. Here, we postulate that the ease of displacement of SAMs should play an important role as well. In our experimental context, this displacement could come from the combined means of thermal desorption and mechanical deformation. During the bonding process, both the chip and substrate were heated before the two surfaces were brought into contact. Alkanethiols on gold desorb thermally in a wide temperature range, from 117°C – 227°C [103, 104]. In the

ATTENTION: The Singapore Copyright Act applies to the use of this document. Nanyang Technological University Library

lower temperature range (25-80°C) used in the study shown in Section 4.5 of the dissertation, complete thermal desorption of SAMs is not expected, thus the displacement of SAMs by mechanical deformation becomes more important. Despite the fact that SAMs were not thermally displaced completely, heating does disrupt the orderness of the layer and introduces defects that can be associated with mechanical instability within the structure. This could render the monolayer more susceptible to mechanical displacement during bonding. Longer chain SAMs, such as C_{18}, are known for their higher thermal stability as a result of denser molecular arrangement, less gauche defects and stronger interchain molecular forces [105] . Thus the poor bonding results of C_{18} can be interpreted as a failure of SAM displacement prior to bonding.

We then evaluated the ease of mechanical displacement of SAMs with different chain lengths in elucidating its role in bonding. In thermocompression bonding the normal load applied is commonly considered to induce a shear displacement at the bonding interface, thus deforming surface asperities and barrier layers to ensure intimate contact between the two surfaces. The bonding results imply that C_6-coated gold samples have the least shear resistance, resulting in the greatest ease of displacement from the gold surfaces during bonding. To investigate SAM removal by mechanical action, the loading action during actual bonding process was simulated by pressing a SAMs-coated gold surface onto a gold substrate at a sufficiently low pressure (~72.6 MPa) to avoid bonding and at room temperature (23°C) to eliminate the thermal contribution. The reason why non-bonding conditions are used is that the loaded surfaces can be subjected easily to surface analysis.

The extent of mechanical degradation on the alkyl chains of different chain length was examined by measuring the combined area of the thiolate before and after deformation. The loss of thiolate can be taken as a qualitative indicator of SAMs coverage on gold since the thiol group is known to attach strongly to gold. Peak area

ATTENTION: The Singapore Copyright Act applies to the use of this document. Nanyang Technological University Library

ratios of thiolate and carbon with respect to Au 4f core peak defined from the raw core spectra at binding energies of 161.9 ± 0.1 eV, 284.8 eV and 83.8 eV, respectively were utilized to eliminate effects from sample variations. Figure 4 shows the amount of thiolate and carbon left on the gold surface prior to and after deformation for three different SAMs. Upon deformation, the greatest loss of thiolate and carbon occurs in C_6. The surface coverage after non-bonded loading is higher for C_{18} layer, suggesting that the more structurally robust C_{18} layer is more capable of withstanding the mechanical loading. The disappearance of thiolate species implies the removal of S-Au bond, thus freeing available pristine Au – Au bonding sites which again, support our bonding results. The lack of atomic sulfur (at BE = 161 eV) [106] after deformation also indicates that C-S cleavage did not occur, further supporting our deduction that fresh gold atoms will be available for bonding between two gold surfaces. Our findings are consistent with extensive studies in the tribological properties of alkanethiols with various chain lengths for boundary lubricant applications [71, 72]. For longer chain alkanethiols where n >15, strong Van der Waals forces of attraction between the neighbouring alkyl chains allows the layer to disperse the normal forces effectively, exhibiting low friction and high wear resistance. In contrast, the shorter chain monolayers studied here [n = 2 - 7] could not retain molecular order during shear, and thus can be efficiently worn away [72].

ATTENTION: The Singapore Copyright Act applies to the use of this document. Nanyang Technological University Library

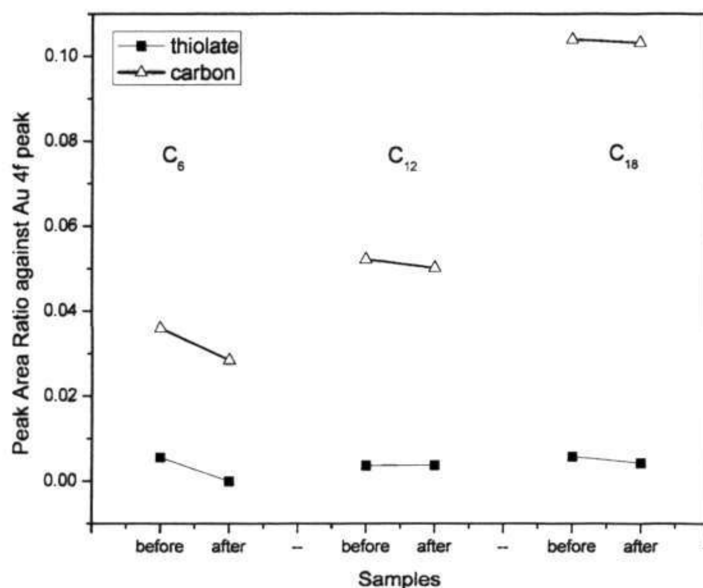

Figure 5-4 Comparison of thiolate and carbon species on all SAMs before and after deformation

5.4 Thermal Displacement

5.4.1 In-Situ SPRS Response at a SAMs/Au interface as a function of temperature

It is also worth mentioning that while the SAM layer behaves as an adequate coating to inhibit further surface contamination, it is imperative that this layer be sufficiently and easily displaced prior to bonding, either by thermal or mechanical action. To evaluate this, we made use of a surface-sensitive technique - surface plasmon resonance spectroscopy (SPRS) to predict the degradation temperature of SAMs. Often such studies were carried out using techniques such as thermal desorption spectroscopy (TDS), scanning tunneling microscopy (STM) and X-ray photo-electron spectroscopy (XPS). Other tests such as thermogravimetric analysis (TGA) could help to measure the weight changes in the layer as a function of temperature. The accuracy of such analysis depends very much on the control of the environment and requires very small samples. It is more suitably used to characterize the thermal stability of SAM-coated gold

ATTENTION: The Singapore Copyright Act applies to the use of this document. Nanyang Technological University Library

nanoparticles [107]. Recently, SPRS has been used to characterize SAMs [8]. SPRS has the advantage of high surface sensitivity, and the possibility of an in-situ monitoring of chemical and physical processes at metal interfaces. SPRS based on Kretschmann configuration, called the attenuated total reflection (ATR) technique, employs a monochromatic 632.8nm beam from a 75W Xe lamp p-polarized parallel to the plane of the sample interface [93]. All measurements were acquired using a J.A. Woollam Co. VASE instrument and analyzed using WVASE software. BK 7 right-angled prisms were chosen as a prism coupler. A less than 2 nanometers thick chromium adhesion layer, followed by 45nm thick gold layer were coated directly on the hypotenuse surface of all coupling prisms. The gold coated prism was placed on motorized stages such that the rotation of the incidence plane of the gold surface with respect to the incident laser beam produces attenuation (Figure 5-5). The SPRS signals were collected as a function of the actual incidence angle at prism/metal interface instead of the incidence angle at air/prism interface. Heat was applied by convection through a heating rod placed about 1 mm from the SAMs surface. SPRS measurements of bare gold coated prisms during heating serve as reference points for future measurements of alkanethiol coated gold.

SPRS is very sensitive to changes in the vicinity of the metal surface due to the rapid decay of the evanescent wave generated at the prism/metal layer interface. At a pre-given wavelength of 632.8nm, the propagation constant of the evanescent wave propagating along the interface can be adjusted to match the surface plasmon wave by adjusting the incident angle on the prism to a specific resonant angle [108]. Near this resonant angle, excitation of surface plasmons at the gold/air or gold/SAMs interface results in a sharp decrease in the reflectance. The resonant condition of the SPRS signal will vary when any physical or chemical changes occur including refractive index and thickness variations of the dielectric medium [108].

ATTENTION: The Singapore Copyright Act applies to the use of this document. Nanyang Technological University Library

Here, we need to ascribe this angular shift only to the change in thickness of the SAMs, to a first approximation, for simplicity. Since the resonance angle shifts linearly with the refractive index and/or the thickness and the reflectance minimum does not change as the resonance angle shifts for a non-absorbing dielectric medium [108], the resonant angular shift from 43.2 degrees for bare gold film to a larger value indicating an increase in thickness confirms the presence of a layer of alkanethiol on the gold surface. The influence of temperature on the resonant angle of alkanethiol-coated gold film is shown in Figures 5-6 to 5-8. Generally, resonance angles decrease linearly as temperature increases for all three SAMs samples. Therefore, all three types of SAMs were dissociating from the gold surface, albeit to different extent, during the heating process. Extrapolation of the linear behavior of the resonant angle of Au/C_6, Au/C_{12} and Au/C_{18} with temperature intersects the bare Au/Air reference horizontal line at 110 °C, 168 °C and 225 °C, respectively. Since the intersection point represents total desorption of SAMs at that particular temperature, the results indicate that octadecanethiol is the most thermally stable while hexanethiol is the least. It is surprising to note that for C_6, the first intersecting experimental point exists at 90°C, suggesting that the layer should desorb completely at this temperature. This contradicts surface analysis data which will be discussed in a later section.

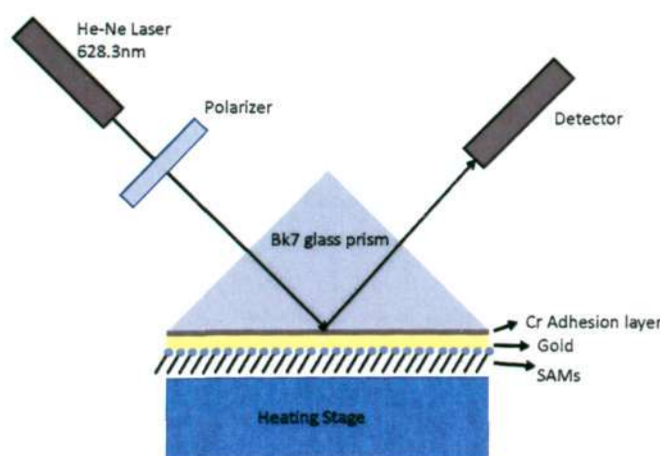

Figure 5-5 Schematic of the Kretschmann SPR Setup

ATTENTION: The Singapore Copyright Act applies to the use of this document. Nanyang Technological University Library

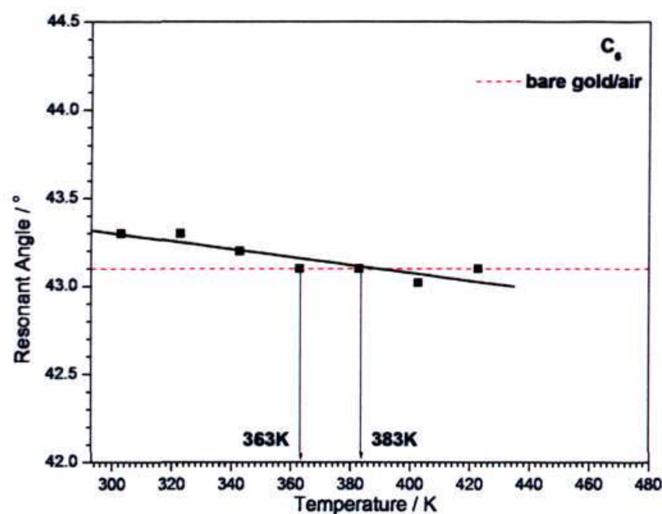

Figure 5-6 Net shifts in resonant angle of C_6 as a function of temperature

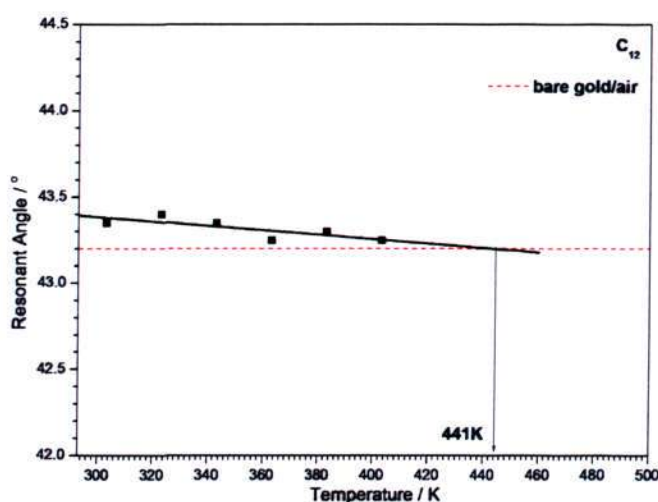

Figure 5-7 Net shifts in resonant angle of C_{12} as a function of temperature

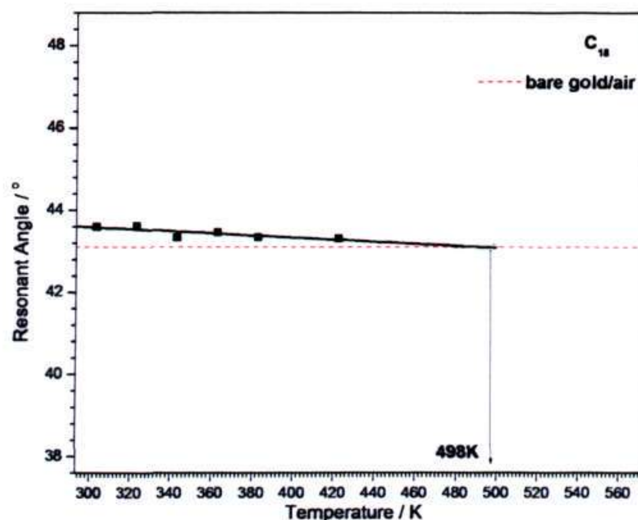

Figure 5-8 Net shifts in resonant angle of C_{18} as a function of temperature

ATTENTION: The Singapore Copyright Act applies to the use of this document. Nanyang Technological University Library

5.4.2 Surface analysis using X-ray Photoelectron Spectroscopy (XPS)

An ex-situ surface analysis using XPS was carried out to investigate the possible structural changes to the alkanethiols under ambient heating. As a reference, the Au 4f peak at 84eV is used for computing the peak area ratios of all these elements with Au 4f for all 3 types of samples.

While there is a general consensus that heating disrupts the structural ordering in the layers by causing untilting of the chains and introducing gauche defects into the layers through two phase transitions, the extent of disorder due to untilting depends on the chain length of the alkanethiols. Hence at different chain lengths, the initial layer thickness would be altered with different degree of tilt in the layers [109]. This XPS study aims to provide supporting evidence to validate the prediction on thermal stability of alkanethiols shown in SPRS measurements by verifying the presence of thiolate species near the respective desorption temperatures predicted by SPRS. Our results present the following observations: (1) upon heating, regardless of the chain length, all three alkanethiols exhibit structural response through untilting, hydrocarbon decomposition and/or loss of sulfur; (2) the extent of disordering through untilting and thermal decomposition increases with decreasing chain length.

The core spectra of the C1s and S2p for alkanethiols heated at various temperatures are plotted in Figure 5-9. These temperatures were chosen according to the range of desorption temperatures predicted by the SPRS results. An obvious broadening of C1s core peak can be seen in short chain alkanethiol (C_6) even at room temperature, unlike the longer chain alkanethiols. The broadening of the peak is often attributed to the X-ray irradiation of hydrocarbon chains which can lead to desorption of the hydrocarbon fragments [101, 102]. The susceptibility of such layer to x-ray irradiation is related to its chain length dependence[110]. Furthermore, we observed a slight peak shift in C1s after C_6 is heated above 323K while a similar shift for the

ATTENTION: The Singapore Copyright Act applies to the use of this document. Nanyang Technological University Library

longer chain thiols occurs only beyond 363K. Such peak shift corresponds to changes in surface coverage of densely packed chains that can be altered by loss in orientation order [111]. A single sharp characteristic C1s core peak at 285.1eV is attributed to the alkyl chain of the alkanethiols deposited by solution method[90, 106]. A peak shift to a lower binding energy (284.4eV) as observed can be hypothesized to be a result of the formation of striped phase due to untilting (or equivalently, a reduction in the layer thickness)[103, 111] as well as loss of surface coverage under heating[115, 120, 121]. This drop in layer thickness is also reflected in left shift of the resonant angle of Au/C_6 as temperature increases to 363K.

As mentioned earlier, SPRS observation predicts complete decomposition of C_6 at 363K. However, presence of thiolate was detected (in Figure 5-9b), indicating that the thiolate has not been decomposed completely. We attributed this to the sensitivity limits of our SPRS set up (40nm thick gold layer was used instead of a 50nm thick gold film[112]). This can be further explained by the saturation of untilting and defect formations for short chain alkanethiols (< C_8) at temperatures below 360K [105]. Further increase in temperature was reported to cause insignificant structural changes up until complete desorption [105]. Assuming C_6 is in a complete lying-down phase as temperature reaches 363K, the final layer thickness could possibly be well below 0.1nm; such minute changes in structural order or tilt is beyond the angular resolution of our SPRS . This may explain the discrepancy seen in the prediction of desorption temperature for C_6 by SPRS and XPS. In contrast, long chain alkanethiol continues disordering beyond 363K till desorption which corresponds to the continual reduction in the resonant angle with temperature in Figure 5-7 and 5-8. Broadening of the S2p peak and shift of peak to a higher binding energy (163.4eV) for C_{12} and C_{18} at 443K and 503K respectively depict the loss in the thiolate species.

ATTENTION: The Singapore Copyright Act applies to the use of this document. Nanyang Technological University Library

To compare the thermal stability among the different chain length, the percentage net loss in the amount of carbon and sulfur present after the samples were heated to 363K were computed by calculating the peak area ratio of C1s/Au4f and S2p/Au4f before and after heating, as shown in Figure 5-10. The greatest loss in both components was observed for the shortest alkanethiol, in agreement with our earlier SPRS observation. Longer chain length alkanethiols are more thermally stable than the short ones due to its stronger intermolecular interaction[90].

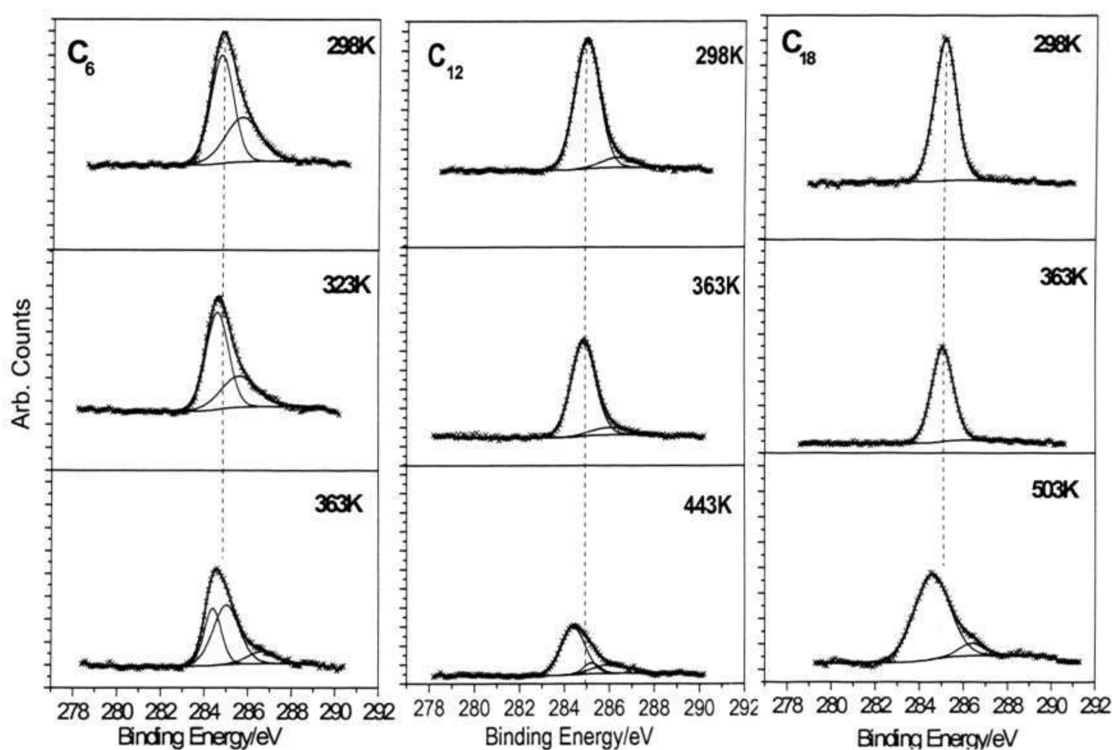

(a)

ATTENTION: The Singapore Copyright Act applies to the use of this document. Nanyang Technological University Library

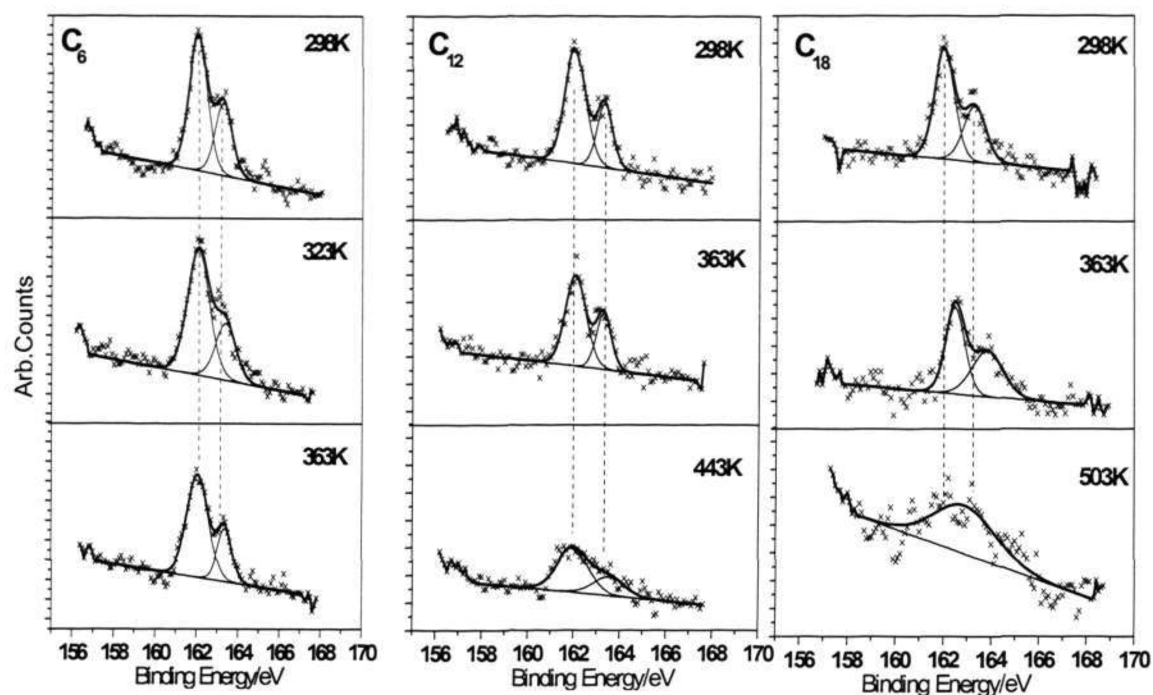

(b)

Figure 5-9 Core spectra of: (a) C1s and (b) S2p recorded at different heating temperatures for alkanethiols - C_6 at 298K, 323K & 363K, C_{12} at 298K, 363K & 443K and C_{18} at 298K, 363K & 503K.

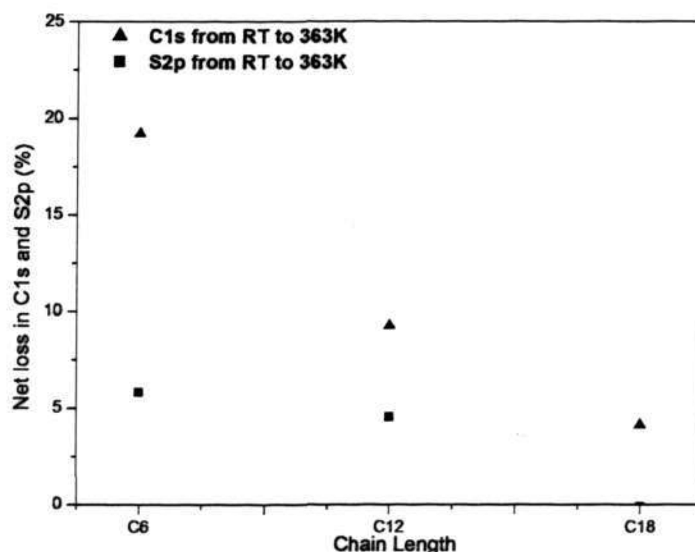

Figure 5-10 %Net loss in carbon and sulphur calculated from the peak area ratio against gold reference for C_6, C_{12} and C_{18}.

ATTENTION: The Singapore Copyright Act applies to the use of this document. Nanyang Technological University Library

5.5 Stability against Environmental Conditions

5.5.1 Introduction

One of the major industries supported by 3-D integration technology is MEMS which stands for microelectromechanical systems [113]. These are functional miniaturized systems that comprise sensing, processing and actuating functions which include electrical, mechanical, optical, fluidic and/or biological functions. The basic approach to MEMS device fabrication involves the stacking of structural metallic and sacrificial polymer layers which will undergo the usual processes including lithography, thin film deposition, etching, machining and wafer-level bonding. Often thermomechanical stresses were induced within the devices by repeated high temperature and high pressure bonding process. This leads to performance degradation and eventually, low product yield. Hence providing mildest bonding conditions which require superior cleanliness would be the viable solution. This is particularly important in BioMEMS and BioNEMS, for example micro/nanofluidic devices that can contain integrated channels, chambers or pumps on chip for drug discovery, DNA synthesis and genetic analysis, clinical diagnostics – immunology, microbiology and oncology, environmental, military and agricultural industries. As mentioned earlier, wafer-level bonding is one of the key fabrication steps and the process is also highly sensitive to the process parameters. As the scaling of the device continues, chemical contamination or slight particulate present at the bonding interface could be detrimental and this is the key culprit for the demanding bonding process parameters [95, 124]. Gold is one of the most common microfabrication material used in MEMS drug delivery devices due to its superior biocompatibility and reduced biofouling [114]. Despite its inertness to oxidation, high surface reactivity of gold to ambient organo-contaminants poses limits to the storage life and reliability of these medical devices. It is thus believed that surface passivation of gold through depositing a functional coating (self-assembled

ATTENTION: The Singapore Copyright Act applies to the use of this document. Nanyang Technological University Library

monolayers- SAMs)[89, 115] which is also bio-compatible, would be a practicable route to improving shelf-life while allowing milder bonding conditions.

Consequently, to improve shelf-life, the knowledge of the stability of this functional coating under various environmental conditions becomes important. Often it has been taken for granted that alkanethiols are stable under ambient conditions until recent study on the long term stability of SAMs reveals a limit in its shelf-life under biological conditions [127, 128]. Various studies employing techniques like laser desorption Fourier transform mass spectrometry [116], IR spectroscopy[117] UV/Ozonolysis [118], X-ray irradiation[119], static secondary ion mass spectrometry (SSIMS)[120] demonstrated both structural and chemical characterization of the degradation of alkanethiols under UV/ozone, electron bombardment and air oxidation. Here, we report the use of ex-situ time-of-flight secondary ions mass spectrometry (TOF-SIMS) and contact angle measurements to study the thermal and environment stability of alkanethiols on gold at different chain lengths. To our knowledge, no TOF-SIMs studies of alkanethiols at different chain length under ex-situ heating and ambient conditions have been considered so far.

5.5.2 Experimental Procedures

Thermal Heating

Alkanethiols – $CH_3(CH_2)_XSH$ (1-hexanethiol [C_6], 1-dodecanethiol [C_{12}], 1-octadecanethiol [C_{18}]) purchased from Sigma Aldrich were used without any purification. For thermal heating test under different environmental conditions, the samples were placed on a hotplate in chemical laboratory environment and nitrogen-purged glove box respectively and heated for two minutes at a temperature of 90°C and 150°C sequentially.

ATTENTION: The Singapore Copyright Act applies to the use of this document. Nanyang Technological University Library

Exposure Test

Freshly coated samples were placed inside plastic Petri dish in a nitrogen-purged glove box, controlled at a relative humidity of 18-20% for a period of 2 and 7 days. For comparison, another batch of freshly coated samples was placed in a chemical laboratory where the relative humidity is about 70%. Extra effort was made to cover the containers with aluminum foil to avoid the effect of UV/ light degradation on the freshly coated samples while keeping the containers ajar.

Contact Angle Measurements

The wetting behaviour of alkanethiols was investigated using contact angle measurement. A sessile drop of NanoPure water was dropped on the coated samples and the angle at the interface between the water droplet and coated substrate was recorded. A total of 4 readings were taken for each experimental parameter – temperature, number of days of exposure in air and N_2 environment, heating duration respectively. The average readings were plotted in the figures shown in Section 5.7.3 – 5.7.4.

Time-of-Flight Secondary Ions Mass Spectrometry (TOF-SIMS)

While contact angle measurements provide a simple and fast method of characterizing the film quality, it does not offer any quantitative chemical/structural analysis of the changes occurring in the film under the various process conditions. Hence ex-situ TOF-SIMS spectra were collected for alkanethiols at various chain lengths to provide insights in the changes in chemical compositions and molecular structure under thermal and environmental variation. TOF-SIMS experiment was performed using a CAMECA IONTOF-SIMS IV system which was operated in the dual beam interlaced mode. The experiment employed high energy Ga+ beam (25 keV, 2.5 pA at 10 kHz) was applied to analyze an area of 100×100 μm2. The base pressure of the TOF-SIMS chamber was 1×10^{-9} torr.

ATTENTION: The Singapore Copyright Act applies to the use of this document. Nanyang Technological University Library

5.5.3 Air Stability

a. Chain Length Influence

One of the fastest characterization tools for molecular structure of an underlying substrate is the use of contact angle measurements since its wetting properties vary drastically according to the functionality of end/head groups as well as its packing density on the substrate. The understanding of a densely packed structure of freshly deposited alkanethiols formed whereby the methyl end groups organized at a tilt angle of 30° away from the surface normal, is generally accepted as the high coverage layer formed on gold substrate. Non polar methyl tail groups form a hydrophobic surface, thus leading to the beading of water on coated gold surface, giving a contact angle of about 110 ± 5° for good quality structure. The average contact angle of alkanethiols at different chain length was plotted in Figure 5-11 in response to three main experimental conditions: - heating temperature, days of exposure and environment. In both air and nitrogen environment, it is obvious that the wetting property degrades as the chain length gets smaller. This is expected since many reported the orientation variation of the SAMs with chain length. Such orientation changes would translate into a change in the wetting properties of the surface. At shorter chain length, it is assumed that there is more disordering in the absorbates. Due to stronger van der Waals interchain interactions in longer alkanethiols, more structurally stable alkanethiols were expected. This gives rise to a denser molecular layer with less gauche defects or equivalently, higher hydrophobicity.

ATTENTION: The Singapore Copyright Act applies to the use of this document. Nanyang Technological University Library

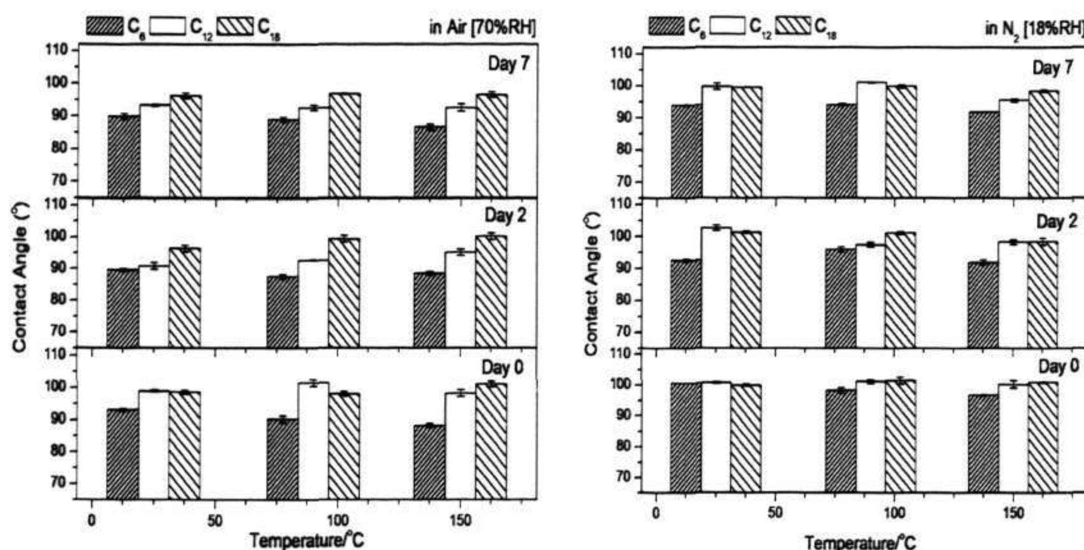

Figure 5-11 Wetting of alkanethiols (n = 5, 11, 17) absorbed on gold by water after heating at 90°C, 150°C and exposure in air (left) and nitrogen-purged (right) environment for 2 and 7 days.

Besides that, alkanethiols at all chain lengths have shown greater stability in an inert atmosphere as compared to air. Slightly poorer wettability in these organic layers was observed after exposure to air instead of nitrogen-purged environment. This further confirmed other reports which have shown that these layers oxidized into sulfinates and sulfonates over prolonged exposure in air [117, 120-124]. These species form very weak bonds with the underlying substrate that could be easily removed by simply rinsing with aqueous solvents. With structural defects that could possibly disrupt the orderness of the layer and the oxidized thiolate root causing the tilting of the chains away from its initial position[117], oxidized alkanethiols result in degradation in the wettability of the monolayer. Our TOF-SIMS findings, shown in Figure 5-12, support the above analysis where traces of sulfonates [SO_3^- (m/z = 79.9, $CH_3(CH_2)_5SO_3^-$ (m/z = 165) and $CH_3(CH_2)_{11}SO_3^-$ (m/z = 249.2)] were found for samples prepared in air for both hexanethiol and dodecanethiol. While there are very slight traces of SO_3^- present in hexanethiol prepared in inert conditions, no other oxidized species were detected.

ATTENTION: The Singapore Copyright Act applies to the use of this document. Nanyang Technological University Library

Longer chain alkanethiols have again proven more resistant to air-oxidation since no oxidized species were detected for octadecanethiol.

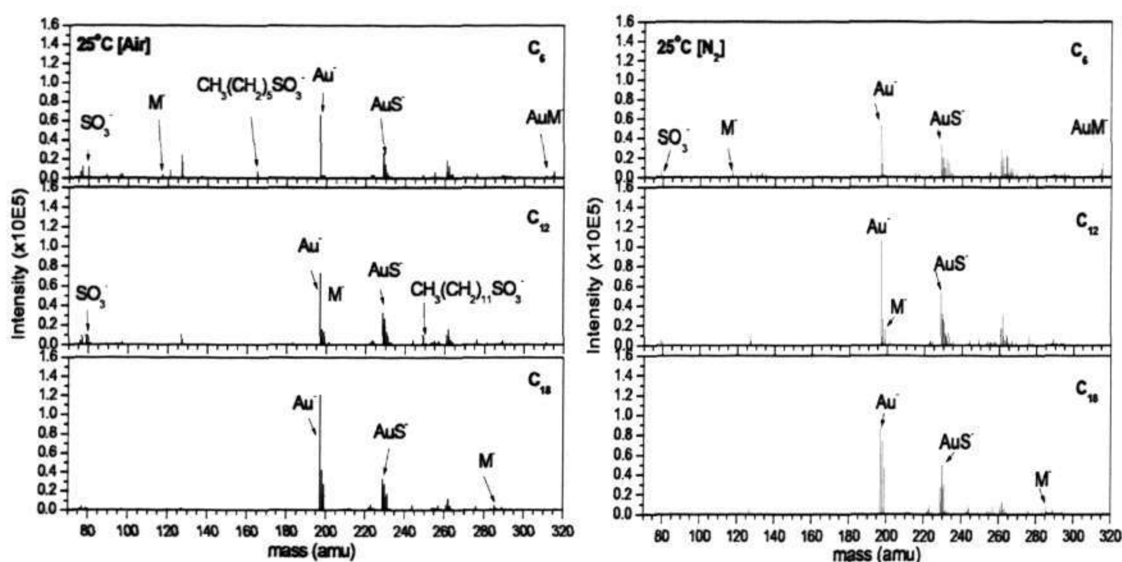

Figure 5-12 Negative TOF-SIMs spectra of freshly prepared alkanethiols (n = 5, 11, 17) in air (left) and nitrogen-purged environment (right)

b. Length of exposure

Over extended period of exposure in air for about 7 days, slight degradation was observed for all alkanethiols with lowest average contact angle of 90° for shortest chain at n = 5. While degradation was also observed for hexanethiol in nitrogen environment, both dodecanethiol and octadecanethiol remain fairly stable with no changes to their hydrophobicity. Previous reports indicated differences in the extent of stability of alkanethiols in air. One reported significant signs of oxidation even only after six hours of air exposure for dodecanethiol while complete loss of the thiolate was observed after 24hr exposure for dodecanethiol and after 1 week for octadecanethiol [121]. Another report [117] monitored changes in the orientation of the chain and found the tilting away of C_{12} and C_{18} from the surface normal saturates only after 100 and 80 days in air, respectively. Figure 5-13 is re-plotted as a function of length of exposure for better

ATTENTION: The Singapore Copyright Act applies to the use of this document. Nanyang Technological University Library

clarity. Such differences may be due to experimental differences (for example, ozone concentration, and humidity) at different locations.

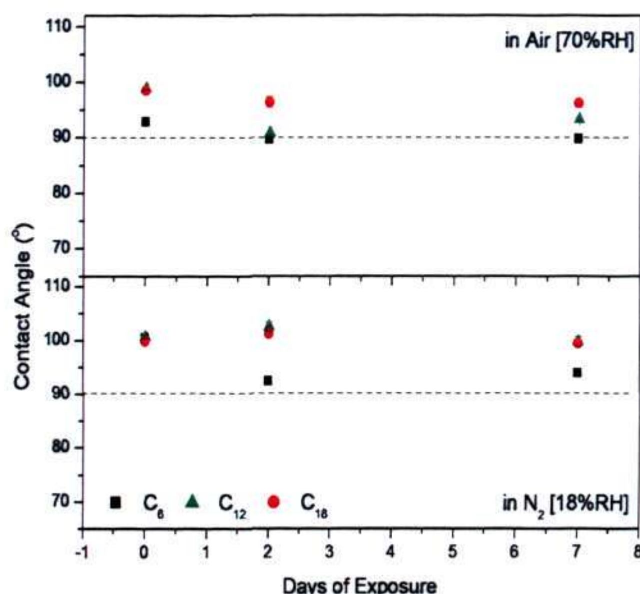

Figure 5-13 wetting angle of alkanethiols as a function of days of exposure in both air and nitrogen-purged environment

5.5.4 Thermal Stability

a. Chain length dependence

It is apparent that SAMs are more thermally stable when the environment is inert, as shown in Figure 5-14. We also observe that the short chain alkanethiol (x = 5) are less stable as heating temperature increases. Relative amount of sulphur against gold as a reference (assume that the presence of sulpur is brought about by the presence of thiol molecules and dictates the coverage of the layer on the gold surface) is lower than that of the samples tested in nitrogen environment. The slight drop in the amount of S with temperature as compared to the rest of the elemental contaminants suggests that some loss of the organic layer has occurred. This is further supported by the higher net loss in the amount of gold-thiolate cluster ions and thiolate absorbates detected for samples heated in air, shown in Figure 5-17.

ATTENTION: The Singapore Copyright Act applies to the use of this document. Nanyang Technological University Library

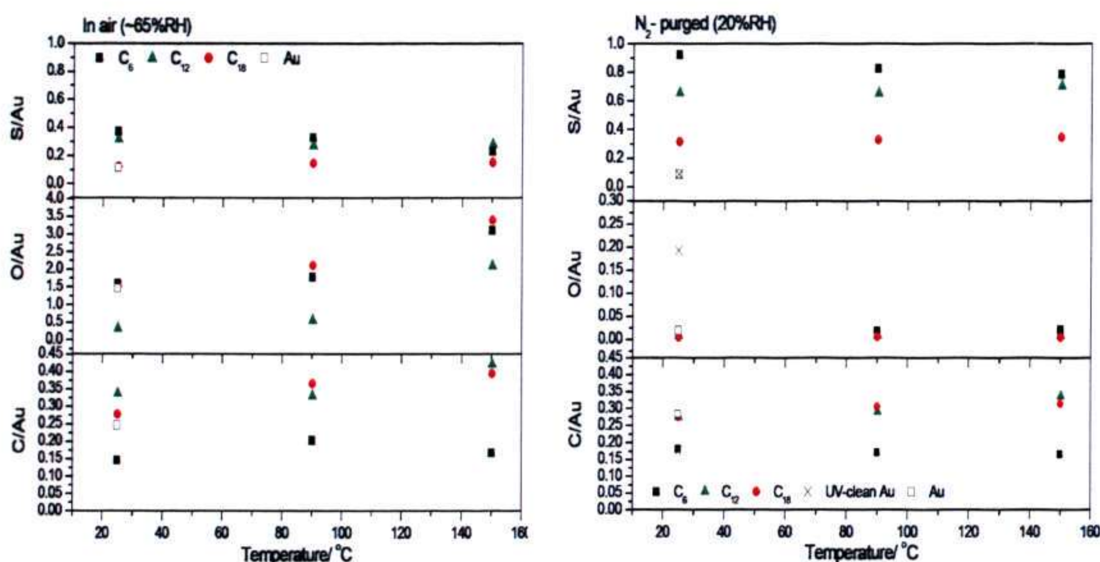

Figure 5-14 Relative intensity ratio of the elements against gold as temperature increases in air (left) and nitrogen-purged environment (right)

The existence of molecular cluster ions such as $[M_x]^-$ where, x = 5, 11 or 17 and M = $CH_3\ (CH_2)_xS^-$ is detected, as plotted in Figure 5-15 and 5-16. Cluster ions such as AuS^- are also detected in all spectra due to the breaking of C-S bond of the molecules as the surface layer absorbs energy from collisions[119]. The presence of sulfur containing clusters is evidence of the formation of a monolayer of the thiolate on the gold surface. At room temperature in air, a small amount of oxidized species such as sulfonates (SO_3- and $CH_3\ (CH_2)_5SO_3^-$ and $CH_3\ [(CH_2)_{11}SO_3^-]$ was detected despite being freshly prepared and no heating is done. This can be explained by the effect of air oxidation in the previous section since the exposure of these samples prior to loading is inevitable. As temperature increases, the relative intensities of AuS^- and M_x^- cluster ions drops, dictating the loss of the thiolate layer with higher temperature. In fact, for short alkanethiol (x = 5), almost complete loss of M_5 cluster ions is observed beyond 90°C while traces of M_{11} and M_{17} can still be detected beyond 150°C. This is true since C_{12} and C_{18} were found to desorb only at higher temperature of about 127°C and 227°C[103]. This can be further supported by Figure 5-17 where the net loss of the relative intensities for these cluster ions against Au^- reference was plotted as a function

ATTENTION: The Singapore Copyright Act applies to the use of this document. Nanyang Technological University Library

of heating temperature. It exhibits a direct relationship between net loss and temperature where greater loss is obtained with increasing temperature. It is believed that at higher temperature, some of the thiolate could have been oxidized and lost since these species are weakly bounded to the gold substrate. Compared to its longer counterparts, less structurally dense short alkanethiols enable easier penetration of oxygen through the organo-layer into the gold-thiolate interface. Higher amount of structural defects and larger extent of oxidation of short alkanethiols explains why the layer suffers the biggest loss in its sulfur-containing species.

However, its thermal stability can be enhanced when the samples are stored in an inert environment. With a significant reduction of oxygen in the atmosphere, no CH_3 $(CH_2)_5SO_3^-$ and CH_3 $(CH_2)_{11}SO_3^-$ cluster ions can be detected at all temperatures expected for some slight traces of SO_3^- ions observed. Longest alkanethiol at x = 17 contains no oxidized species even at temperature of 150°C.

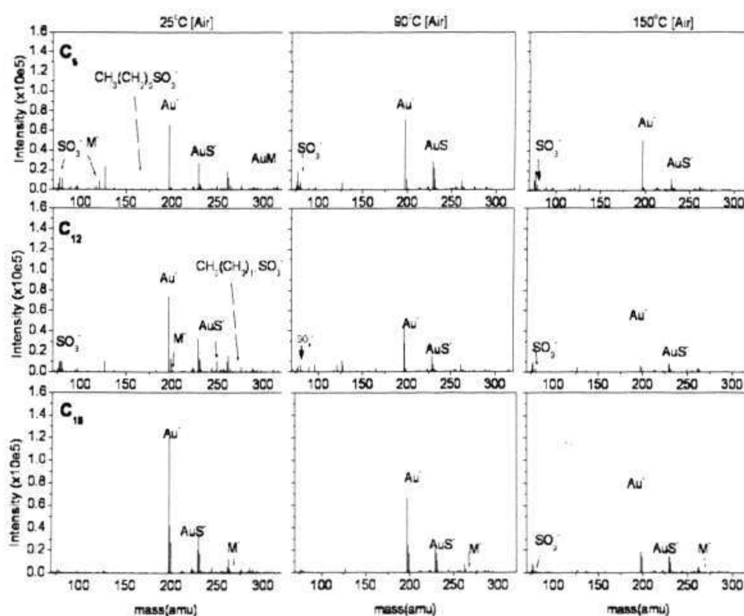

Figure 5-15 Negative TOF-SIMs spectra of alkanethiols [CH3 (CH2)x-SH] where x = 5, 11, 17 on gold at heating temperatures of 25°C , 90°C and 150°C, respectively in air.

ATTENTION: The Singapore Copyright Act applies to the use of this document. Nanyang Technological University Library

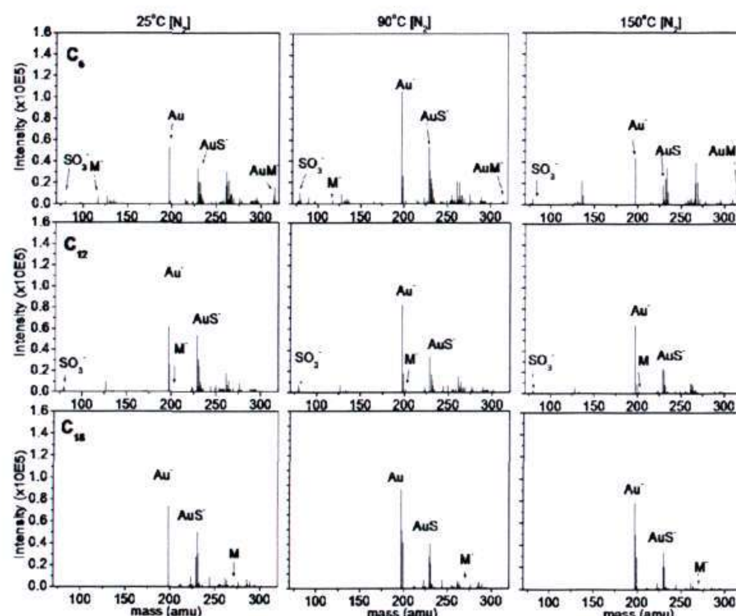

Figure 5-16 Negative TOF-SIMs spectra of alkanethiols [CH3 (CH2)x-SH] where x = 5, 11, 17 on gold at heating temperatures of 25°C , 90°C and 150°C respectively in nitrogen-purged environment.

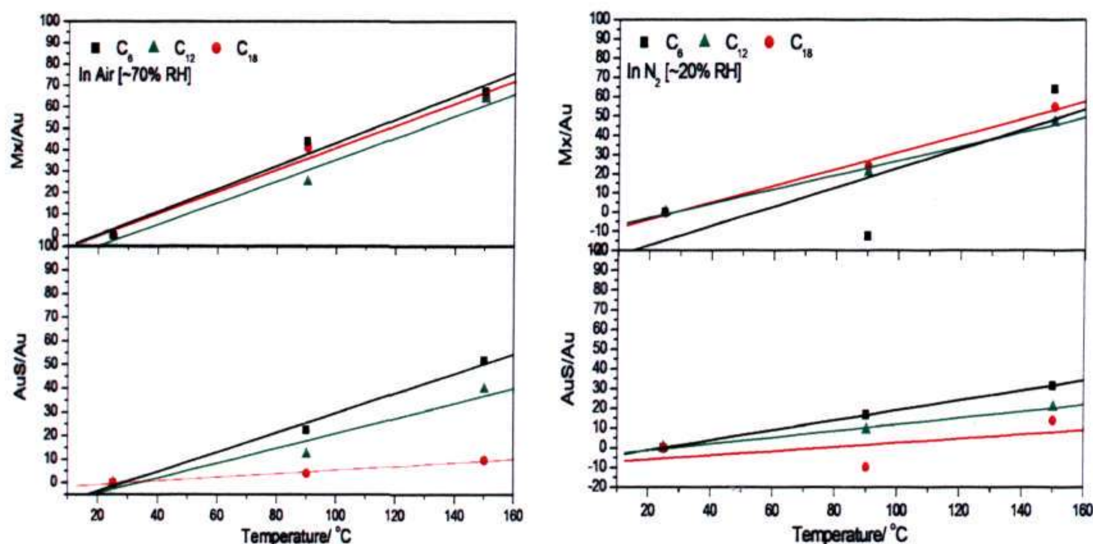

Figure 5-17 Net loss (%) of cluster ions against gold as temperature increases in (left) air and (right) nitrogen-purged environment

b. Heating Duration

Stability under different heating duration is investigated by subjecting the coated samples under 150°C for duration of 2, 30 and 60 minutes. The wetting capabilities of the alkanethiols were evaluated, exhibiting increasing amount of

ATTENTION: The Singapore Copyright Act applies to the use of this document. Nanyang Technological University Library

degradation in the following sequence (C_6 > C_{12} > C_{18}) when the alkanethiols were heated in air, shown in Figure 5-18. Again, hexanethiol showed the least stability with a greatest net loss percentage of the thiolate absorbates and gold-sulphur cluster ions in Figure 5-19. While so, it is noted n Figure 5-19 that the average net loss of M_x^- clusters remains relatively constant for both C_6 and C_{12} while slight increase in that of C_{18} was observed. It is predicted that since the heating process was done at 150°C (above desorption temperature for C_6 and C_{12}), almost all the thiolate species could have desorbed, thus resulting in the saturation in the loss of the species. The sudden drop in metal-sulfur clusters (i.e. lesser net loss) for C_{12} at longer heating process is unexplainable at this stage. Some reported the effect of thermal annealing on alkanethiols in helping to eliminate defects in the monolayer but prolonged annealing can cause structural transformation and partial desorption[125]. Therefore sufficiently long thermal annealing could have occurred, thus making C_{12} more structurally stable, leading to lesser metal-sulfur ion clusters lost. The uncertainty in the true mechanism behind thermal heating on the alkanethiols certainly poses a limit to the understanding of how temperature could have helped or degraded SAMs.

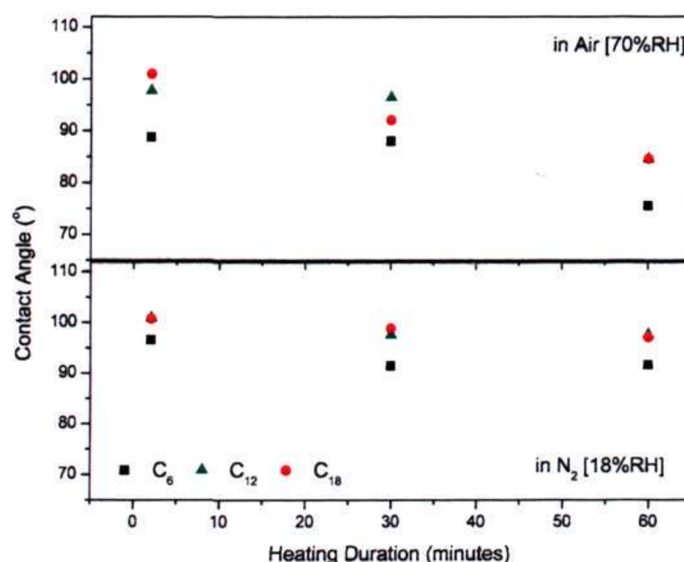

Figure 5-18 Effect of the duration of heating (2, 30 & 60 minutes, respectively) at 150° C on wetting properties of alkanethiols under different environmental conditions

ATTENTION: The Singapore Copyright Act applies to the use of this document. Nanyang Technological University Library

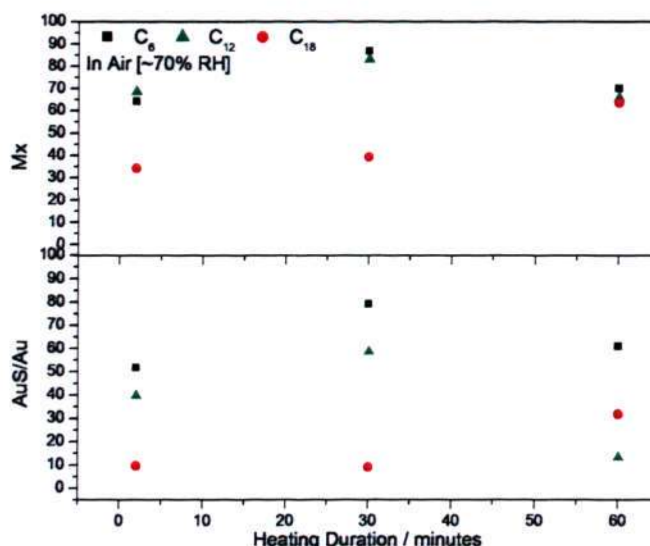

Figure 5-19 Net loss (%) of cluster ions in alkanethiols after heated over 2, 30 and 60 minutes in air at 150°C

5.6 Chapter Summary

In this chapter, we have provided experimental evidence to support the working hypothesis behind the success of self-assembled monolayers (SAMs)-assisted direct gold thermocompression. To initiate a single site for bonding between two gold surfaces, the single site must be free from any foreign atoms. This brings about the key understanding that the minimization of surface contaminations as well as an effective removal of any contaminants on the metal surfaces is vital for bonding to take place.

These are the main findings evaluated:

- SAMs replaces the ambient contaminants and passivates the gold surfaces from further contamination prior to bonding.
- Longer chain alkanethiols, having superior passivation properties compared to the shorter ones, do not necessarily work well for bond enhancement. A simulated bonding action to induce mechanical deformation at the coated bonding interface reveals that the longer chain alkanethiols are more resistant to deformation, which explains why displacement of SAMs from the bonding surfaces is equally critical.

ATTENTION: The Singapore Copyright Act applies to the use of this document. Nanyang Technological University Library

- Contact angle measurements revealed poorest structural stability in the shortest alkanethiol [hexanethiol], under thermal heating and exposure to air over prolonged period of time.
- TOF-SIMs results supported the changes observed by exhibiting greatest loss of the thiolate and gold-sulfur cluster ions and also the presence of sulfonates as temperature increases. This is believed to be due to the poorer structural integrity and a higher defect density in the monolayers, thus providing a easier route for the penetration of oxidative species such as oxygen. Finally longer alkanethiols such as octadecanethiol are found due to the close-packed structure with higher interchain forces of attraction, making them structurally more stable.

ATTENTION: The Singapore Copyright Act applies to the use of this document. Nanyang Technological University Library

Chapter 6 SELF-ASSEMBLED MONOLAYERS FOR LOW TEMPERATURE COPPER BONDING

6.1 Introduction

With many studies [19, 20, 28, 126-130] examining the influence of surface morphologies and bonding conditions on direct copper bonding over a range of sufficiently high bonding temperature and pressure, it is commonly understood that higher temperature aids strength enhancement. The adhesion criteria for successful copper-copper bonding for 3D chip bonding depend very much on the design and its specific application. To the author's knowledge, there's no a unified critieria in the industry. It has been reported though in journal paper, the adhesion energy is about $3J/m^2$ for good copper-copper wafer bonding [131]. For subsequent processes and handling such as underfilling in stacked packages, it has been mentioned that the copper joints should be around 20g/bump. For comparison, our joint strength is above 30g/bump when bonded at 60°C [Source: UTAC].

In this chapter, we explore the likelihood of bonding Cu from room temperature up to 300°C, given a sufficient amount of bonding pressure. We found an unexpected behaviour where an increase in bonding temperature beyond 80°C till 140°C does not improve bond strength. We attempt to explain this drop in bond strength with

ATTENTION: The Singapore Copyright Act applies to the use of this document. Nanyang Technological University Library

temperature by a self-limiting role of temperature. Similarly, we demonstrate that such degradation in strength can be avoided by applying a monolayer of organic molecules, in this case an alkanethiol onto the copper surfaces prior to bonding.

This chapter reports successful bonding between two copper surfaces under ambient condition at a bonding temperature below 180°C, yielding typical joint shear strength of 70MPa. We further correlate the ability of alkanethiols as a barrier layer on copper surfaces against surface oxidation to its assistance in enhancing bondability between copper surfaces at temperatures up to 180°C.

6.2 Experiments

6.2.1 Sample Preparation

Proper cleaning of the substrates and the glasswares are required for good deposition of the SAMs layer. Sputtered Cu wafers consist of these layers: SiO_2 on Si wafer, followed by 50nm Ti layer, 100nm TiW and finally 1μm Cu layer in sequence, were used. The copper bumps at bump height and diameter of 18 μm and 92 μm respectively, were fabricated by electroplating process The copper bumps were treated with hydrochloric acid (1:10 H_2O: HCl) for 30 seconds, followed by rinsing in deaerated absolute ethanol about 5 seconds before immersing into 1mM ethanolic thiol solution. Kept over 2hrs in a N_2-purged glove box at a relative humidity of 18%, a layer of undecanethiol [CH_3 $(CH_2)_{10}SH$] was deposited on the copper surfaces at room temperature. A second dipping process into a freshly prepared thiol solution was carried out to remove any residual oxidized species that could be present on the coated surfaces [74]. The samples were removed and rinsed with copious amount of absolute ethanol, followed by drying using nitrogen gas.

ATTENTION: The Singapore Copyright Act applies to the use of this document. Nanyang Technological University Library

6.2.2 Bonding Experiments

The thermocompression bonding process was done using Panasert FCB-M Flip Chip Bonder. The bonding procedure begins with the substrate sitting on a heated stage. When the stage is heated to a specified temperature, the chip is picked by the bonding tool with vacuum and is brought into contact with the substrate. After the bonding force has reached a certain level, the pick up tool is heated to a predetermined temperature and maintained for some time to complete the process. To evaluate the bonding pressure to be applied after a pressure dependence experiment at room temperature was conducted, as shown Figure 6-1. The applied pressure was evaluated at 3.28GPa so that appreciable joint strength can be measured at low bonding temperature. Again, a maximum is observed beyond an optimum bonding pressure. The explanation behind this can be attributed to the following: further pressure applied causes already-strain hardened copper asperities to reach its breaking strength. The amount of cold work on the influence of copper's yield strength, ductility and tensile strength can be referred in Appendix A2. Hence, instead of bond forming, copper bonds are destroyed, thus resulting in a drop in its strength. The chip temperature is varied from the range of 60 °C and 180 °C and the stage temperature is varied accordingly to maintain a constant bonding interface temperature. The samples are left on the heated stage long enough to eliminate any effects of temperature transients. An SEM (scanning electron microscopy) micrograph of a typical bonded joint formed is taken, as shown in Figure 6-1. Bonding quality was evaluated by die shear test, which was performed at a rate of 0.5 mm/s. The joint strength was expressed as the average shear strength in MPa.

ATTENTION: The Singapore Copyright Act applies to the use of this document. Nanyang Technological University Library

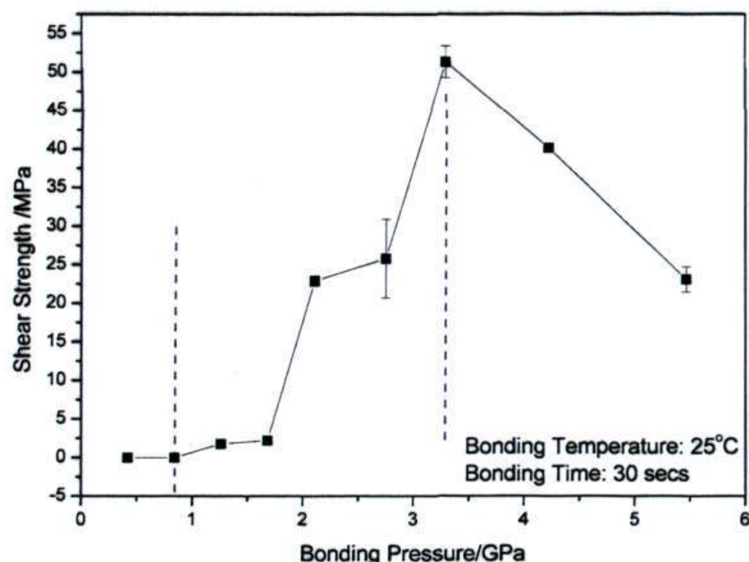

Figure 6-1 Pressure dependence of copper joints bonded at 25°C for 30secs

6.2.3 Surface Characterization using X-ray Photoelectron Spectroscopy (XPS)

Both survey spectrum and high resolution peak acquisition of coated and uncoated copper surfaces were obtained using monochromatic Al Kα radiation (1486.7 eV photons, 10^{-10} mbar background pressure) by VG ESCALAB 220i-XL instrument that is equipped with a concentric hemispherical analyzer and a magnetic immersion lens. High resolution spectra of C1s and O1s for elemental quantification were recorded with pass energy of 20 eV at 0.1 eV step width. As a reference, the Cu 2p peak is used for computing the peak area ratios of all elements for all samples.

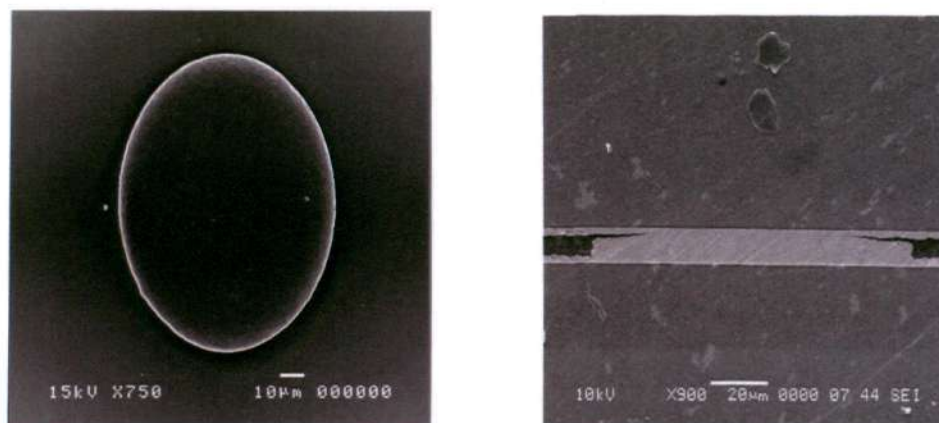

Figure 6-2 SEM micrographs on (left) Top view of electroplated Cu bump; (right) Cross-sectioned bonded Cu Joints at 25°C, 3.28GPa

ATTENTION: The Singapore Copyright Act applies to the use of this document. Nanyang Technological University Library

6.3 Effect of temperature on bond shear strength

Generally bond strength improves as bonding temperature increases [132]. When bonding temperature increases to about 300°C, the mechanical properties change too. Generally copper becomes more ductile with higher temperature while yield strength, tensile strength and young's modulus decreases, shown in Appendix A2. These promote more plastic deformation at the bonding interface, thus resulting in greater amount of bonded region. We have demonstrated successful direct copper bonding at temperature as low as room temperature and bonding pressure of 3.28GPa. To check whether such a high bonding pressure would damage the underlying substrate, a cross-section examination of the bonded joint was carried out. No cracking of the underlying silicon substrate was observed. The absence of a visible bonding interface also indicates that bonding has taken place.. Of course, further observations have to be taken when such a high amount of pressure is applied on a real test device. A stacked integrated chip consists of layers of porous low-k dielectrics within the metallization layers. Due to its porous structure, the layers have low mechanical stability which might be an issue when bonding pressure is too high. While the effect of surface roughness on bonding is not covered in this paper, it is important to bring into attention that the initial surface roughness of the copper samples may also play a vital role in determining bond quality[130, 133]. Based on the mechanism proposed by Chen [130], voids at the bonding interface after bonding may be present since surface roughness (root mean square –rms) of the electroplated bumps (~15nm) and sputtered copper layer (~4nm) differ. Since no microscopic voids were observed in our experiments, it is believed that at 3.28GPa, surface conformity is maintained with much flattened surface asperities.

Our temperature dependence study reveals two transitions in the bond strength at low temperature (T < ~80°C) and high temperature value (T > 140°C) respectively,

ATTENTION: The Singapore Copyright Act applies to the use of this document. Nanyang Technological University Library

shown in Figure 6-2. This is anomalous in the literature of bonding research, since it has been indisputably reported by many that mechanical joint integrity improves with bonding temperature. As temperature rises from room temperature, bond strength increases slightly. However, between 80°C and 140°C, the bond shear strength of the copper joints drops unexpectedly. This will be discussed in the next section. With further increase in temperature beyond this point, the upward trend in bond strength continues.

Since strong bond formation is a function of interfacial mechanical deformation leading to mechanical removal of oxide and finally the interfacial atomic diffusion, all of which are temperature-dependent, the joint strengthens with higher temperature for a given bonding time due to: (1)Larger amount of interatomic diffusion induced by thermal input and (2) Softening of copper leading to higher amount of material deformation at the interface [134]. Higher interfacial stress is induced thus resulting in greater ease of oxide removal.

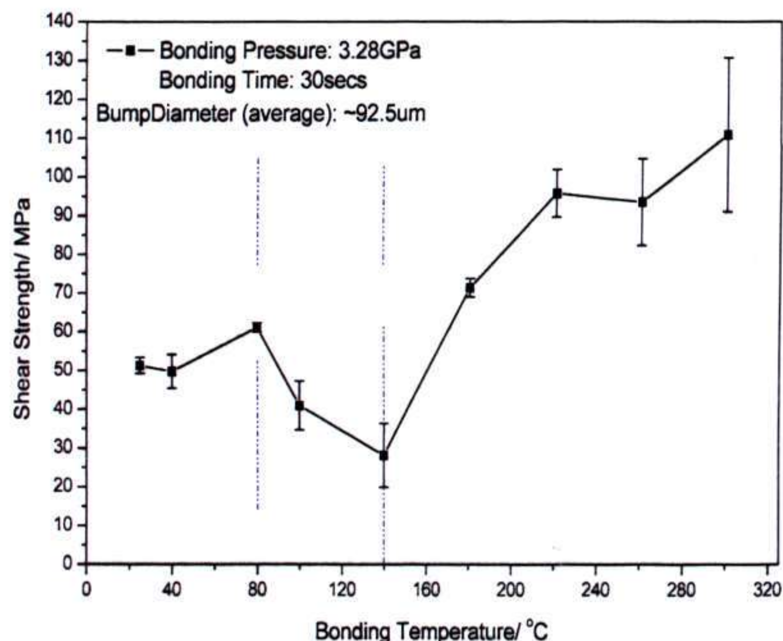

Figure 6-3 Temperature dependence of uncoated copper from 25°C to 300 °C at 3.28GPa for 30 seconds

ATTENTION: The Singapore Copyright Act applies to the use of this document. Nanyang Technological University Library

6.4 Self-Limiting Temperature Effect

The drastic drop in bond strength as temperature rises within this unique range is conceived as temperature behaving as a self-limiting parameter which is further explained as follows:

1. The oxidation of copper is highly temperature dependent such that oxidation takes place even at room temperature. Oxidation of freshly cleaned copper before bonding is inevitable. This is true since bonding is carried out under ambient laboratory conditions – in the presence of air, humidity and organic contaminants. The short time delay incurred when the bonder takes time to heat and cool prior to each test exposes the freshly prepared samples to surface oxidation. Recent study reports the formation of multilayers of complex copper oxides at different temperature range [24]. Primarily this oxide layer grows thicker with temperature and time [24, 135] and it is believed that the oxides formed at low temperature especially are both chemically and mechanically unstable. Reports on compositional changes in the oxide layer with temperature suggests the possibility of different mechanical behaviour of oxides. Interestingly, it had been demonstrated that a change from Cu_2O to Cu_3O_2 exists within 80°C and 140°C [24, 136].

2. On the other hand, temperature is also commonly known to promote interatomic diffusion across the bonding interface, thus forming strong bonds. The competition between two phenomena, namely interdiffusion of copper atoms and mechanical displacement of oxide, determines the success of forming a strong joint. Hence the two counteracting consequences of raising bonding temperature could be one of the possible reasons for the drop in joint strength seen.

Since there's no known data on how such oxides of copper can influence the deformation process at the bonding interface, we propose that the thin denser oxide layer on copper surface formed within this lower temperature window may be

ATTENTION: The Singapore Copyright Act applies to the use of this document. Nanyang Technological University Library

mechanically more stable compared to the thicker porous layer beyond 140°C. While there is a possibility of a thicker oxide being grown at higher temperature, we believe that the thicker oxide layer is more brittle, which facilitates easier removal of oxide layer, thus enabling the extrusion of copper atoms through the broken oxide layer.

6.5 Bond Enhancement Using Self-Assembled Monolayers (SAMs)

In Figure 6-3, SAMs – coated copper surfaces were found to improve bonding strength under equivalent bonding conditions (at a bonding temperature range of 60°C – 140°C) as compared to freshly clean copper, suggesting that much lower bonding temperature and pressure is possible for copper-copper bonding using self-assembled monolayers under ambient laboratory conditions. As discussed, the key consideration in enabling room temperature copper bonding is the need to resolve the issue of surface oxidation – either by passivating copper surfaces or providing means of oxide removal prior to bonding. There are various reports on the effectiveness of SAMs in corrosion passivation, oxidation prevention, diffusion barrier of copper surfaces etc [25, 26, 30, 32-34, 132, 137]. We speculate that the primary contribution by SAMs in lowering bonding temperature and pressure is its ability to passivate copper surfaces very well prior to bonding. While air exposure is unavoidable since bonding is carried out in ambient, bond strength of coated copper samples remains high from 80°C to 140°C. This deviates from what was observed in uncoated copper samples, suggesting that closely packed SAMs layer could protect copper surfaces even as bonding temperature increases to 140°C.

ATTENTION: The Singapore Copyright Act applies to the use of this document. Nanyang Technological University Library

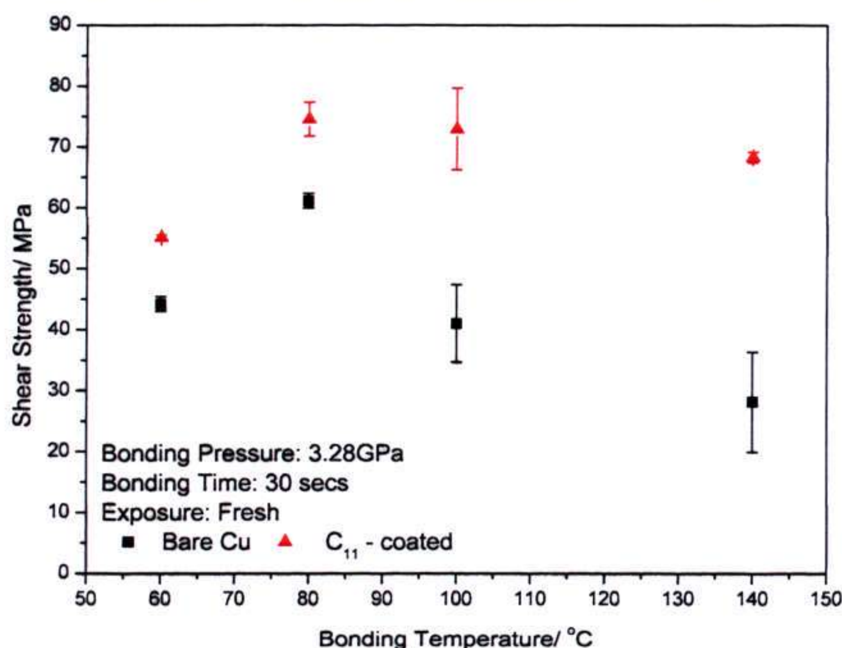

Figure 6-4 Comparison of shear strength in coated copper against uncoated copper from 60°C to 140°C

In the following sections, we validate the efficiency of the SAMs layer in passivating the copper surface during the time lag between sample preparation and actual bonding process. We also discuss the thermal stability of the alkanethiols at the respective bonding temperatures and thus evaluate the ability of alkanethiols in protecting copper oxidation above room temperature. As mentioned, surface passivation is one of the contributing factors in enhancing the metal bonding. Here we have shown that undecanethiol is capable of keeping the copper surface clean as compared to uncoated copper surface as the latter oxidizes more rapidly when heated. It is anticipated that once a SAM layer ceases to passivate copper surfaces as well as it does at lower temperature, copper bond enhancement by SAMs may reach a limit. Our preliminary bonding results and surface chemical analysis support this statement, as shown in Figure 6-4. A significant drop in the net gain in bond strength is observed at 180°C. This can be attributed to the observation of the alkanethiol layer getting dirtier [increase in carbon and oxygen content shown in Figure 6.7] than before as heating

ATTENTION: The Singapore Copyright Act applies to the use of this document. Nanyang Technological University Library

disrupts the initial close packed structure and thus, reduces its passivation efficiency against oxygen penetration.

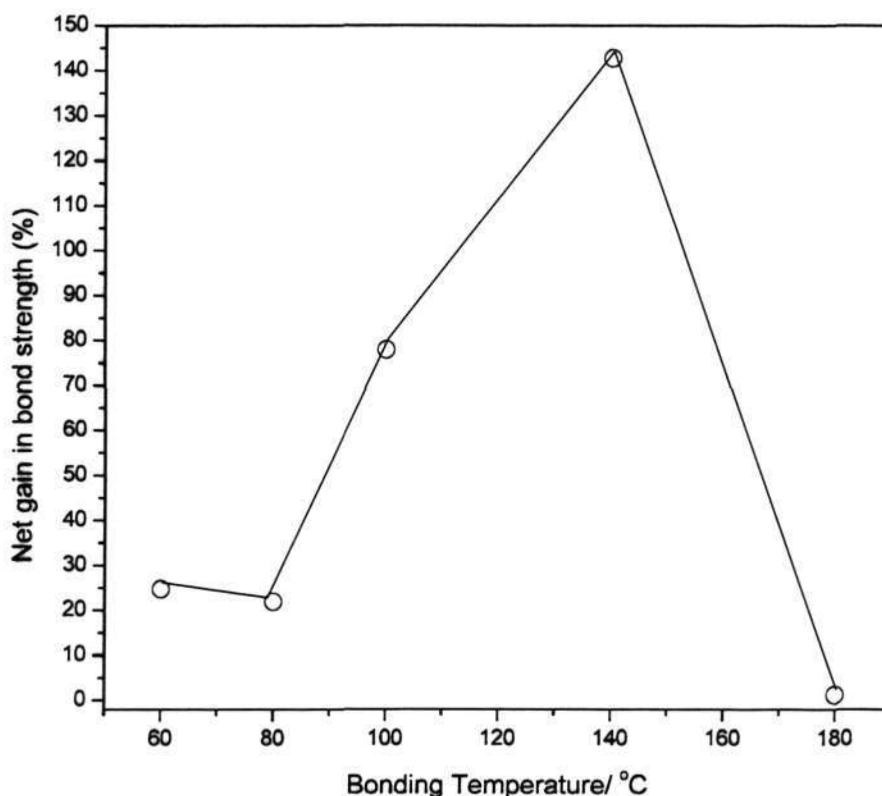

Figure 6-5 Net gain in bond strength by undecanethiol as a function of bonding temperature

6.6 Surface Characterization

6.6.1 Reduction of copper oxide

Alkanethiols on copper are known to be structurally ill-defined and entail significant complexity in preparing reproducibly high quality monolayer and characterizing their structure on copper surfaces [138]. Due to rapid oxidation of copper in air, the deposition of alkanethiols on sputtered copper substrates was done in a nitrogen-purged glove box with controlled relative humidity of 18%. Despite this precaution, presence of oxide on freshly cleaned copper surface is still observed under XPS wide spectra scan, as recorded in Figure 6-5. This indicates that once exposed in

ATTENTION: The Singapore Copyright Act applies to the use of this document. Nanyang Technological University Library

air, rapid oxidation of copper surfaces is inevitable. In contrast, freshly SAMs-coated copper surface shows an absence of oxygen on the copper surface. The presence of alkanethiol on copper surface is verified as the coated surface exhibits hydrophobicity, typically due to lower energy methyl surface.

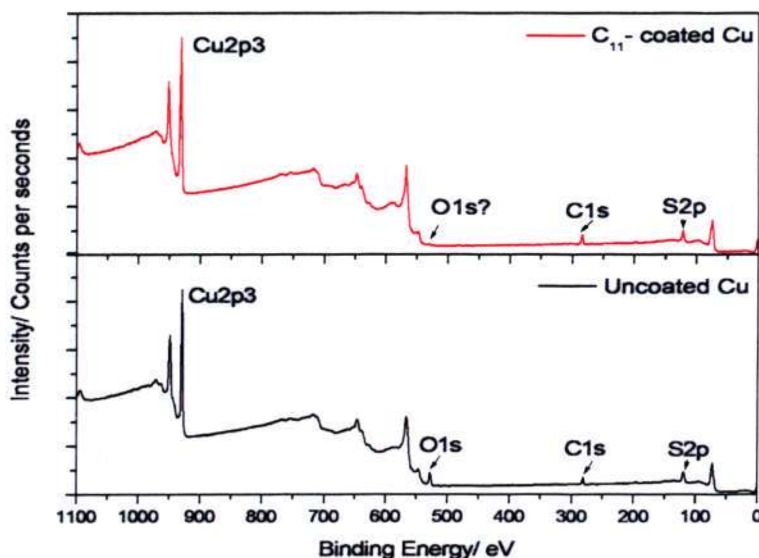

Figure 6-6 XPS survey spectrum of a coated Cu surface (top) and an uncoated Cu (bottom)

6.6.2 Thermal Stability

Both coated and uncoated sputtered wafers (about 5mm by 5mm square) were heated over a hotplate in a chemical laboratory at a range of temperature (80°C - 180°C) for two minutes to simulate the estimated exposure time before two bonding metal surfaces were brought into contact by the bonding head. XPS surface scans for C1s and O1s after the samples underwent heating were plotted as a function of temperature in Figure 6-6. It revealed consistently higher amount of carbonaceous contaminants and oxide species on bare copper surfaces as compared to C_{11}-coated samples with temperature. Since successful metal-metal bonding is a function of three key variables – efficiency of surface passivation, thermal and mechanical activation, the ability of protecting heated copper surfaces from oxidation explains why bond enhancement

ATTENTION: The Singapore Copyright Act applies to the use of this document. Nanyang Technological University Library

occurs even at temperature at 180°C. However alkanethiols on copper has finite thermal shelf-life. We observed slow built-up of oxide species on the coated surface as temperature increases to 180°C which could be the reason for the reduction of bond improvement seen in Figure 6-4. This is further supported as we compare the carbon to sulfur (C/S) ratio of the undecanethiol layer on copper with its theoretical C/S ratio at 11/1 which gives an indication of the surface coverage of alkanethiols on copper. For undecanethiol, it revealed 10.7/1 even at temperature of 80°C. When temperature increases to 180°C, the C/S ratio drops to about 9/1, suggesting some desorption (S/Cu ratio drops by 16%) have occurred. This provides available exposed Cu sites to oxygen penetration, which explains why oxide species resembling $Cu(OH)_2$ at binding energy of 530.9 ± 0.2 [23] was detected., in Figure 6-7. As reported, complete desorption of alkanethiols (n = 10) from clean copper surfaces occurs only at above 250°C (10mins) [139].

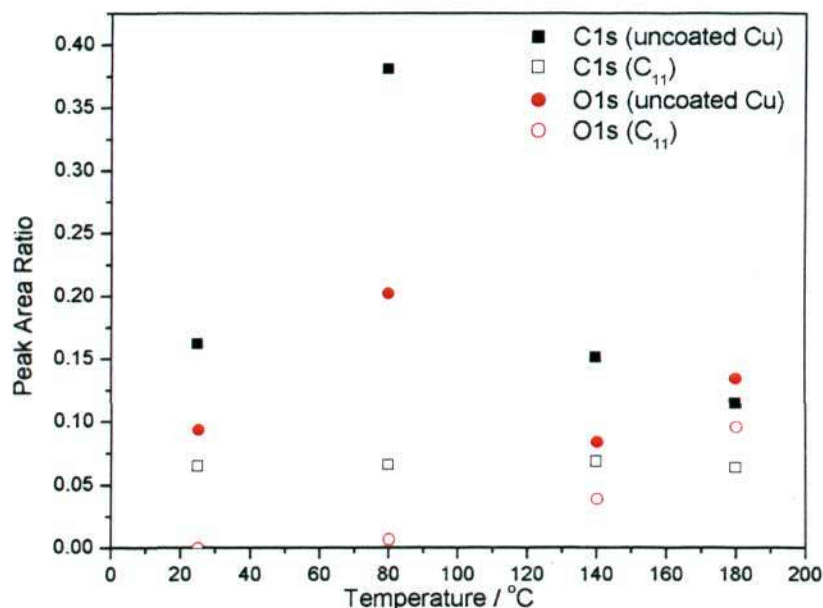

Figure 6-7 Peak Area Ratio against Cu 2p as a function of temperature for both coated and uncoated samples

ATTENTION: The Singapore Copyright Act applies to the use of this document. Nanyang Technological University Library

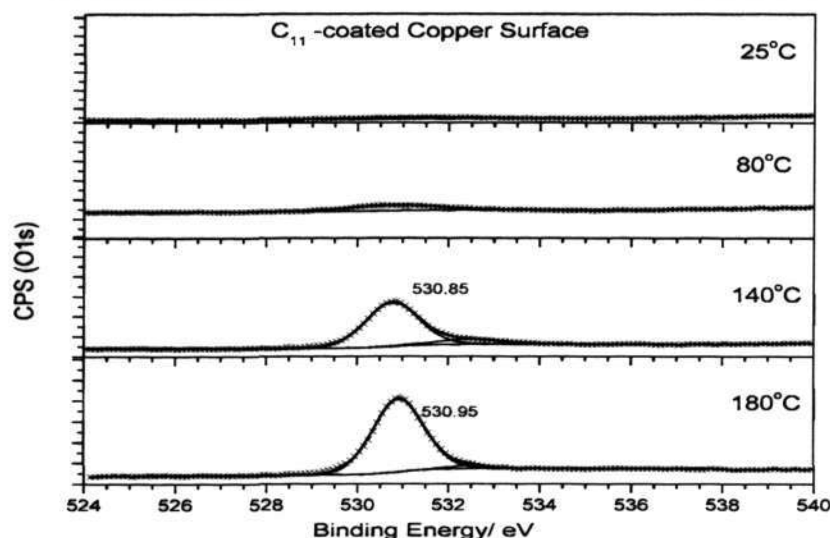

Figure 6-8 Core spectra of O1s of undecanethiol on copper at temperatures (top) 25 °C, 80°C, 140°C and 180°C (bottom).

6.7 Chapter Summary

A typical copper-copper thermocompression bonding process is carried out in an ultrahigh vacuum (UHV) or inert environment at a bonding temperature >300°C. The ultraclean environment serves a single purpose – to maintain oxide-free copper surfaces, allowing intimate physical contact between copper atoms. Yet often, a time lag between sample preparation and bonding leads to an inevitable formation of surface oxide which necessitates more stressful bonding conditions for successful bonding. Prevention of oxidation of copper surface during this time lag is therefore necessary. This is made possible by coating the copper surface with 1-undecanethiol prior to bonding. The densely packed monolayer serves to passivate the copper surface against oxidation under ambient conditions. The ultrathin organic monolayer structure, as compared to a bulk oxide layer, could be easily displaced during the mechanical deformation at the bonding interface which accompanies thermocompression. This method could be an effective simple bonding solution for three-dimensional integrated chips.

ATTENTION: The Singapore Copyright Act applies to the use of this document. Nanyang Technological University Library

Chapter 7 CONCLUSION AND FUTURE WORK

The first part of the thesis aims to extend current understanding of how direct metal joints form under the influence of both temperature and pressure through process optimization and characterization, simple finite element modeling and fracture analysis. Such understanding is important in the midst of industries' exploration for solutions to discover reliable bonding options for 3D IC integration. Further on, this thesis also present a novel bonding solution to harsh bonding conditions needed in current direct metal bonding process through the incorporation of an ultrathin layer of molecules onto the metallic bonding surfaces. This chapter summarizes the key findings and major contributions as discussed below:

7.1 Investigated the effects of Temperature and Pressure in Gold Thermocompression Bonding

7.1.1 Temperature Influence: Barrier Layer /Oxide Theory

- A critical temperature is found for direct gold bonding and it can be explained by the barrier film theory whereby the critical value depicts the temperature at which barrier film is completely displaced such that bonding between two gold surfaces takes place.

ATTENTION: The Singapore Copyright Act applies to the use of this document. Nanyang Technological University Library

- The critical temperature required is reduced in the presence of higher interfacial shear. This means that, under similar bonding conditions, the threshold temperature is lower for harder substrate than for softer substrate.

7.1.2 Pressure Influence: Optimum Pressure

- Pressure dependence is demonstrated by an optimum strength profile recorded at a constant bonding temperature and time. Below a critical value, no bonding takes place. Finite element modeling based on the critical interfacial stress distribution supports the experimental observations that at any interfacial stress below the critical value, the region can be depicted as the unbonded region. Fracture analysis revealed a ring structure, representing two distinct regions depicting the state of bonding. As pressure increases, a transition in failure modes from interfacial [non-bonding state] to interfacial/cohesive [bonded state] failure is seen. This can be further validated by mathematical expressions representing the type of dominant fracture strength.

- Bonding begins from the periphery of microbumps – both gold stud and plated bumps. This observation is attributed to the presence of higher interfacial shear stress distribution at the peripheral region which resulted in greater amount of interfacial deformation as compared to the central region. The simulated results are supported by the ring structure found in both gold stud and plated bumps.

- A hypothesis in the bonding mechanism concludes that at any particular critical pressure value which provides a critical interfacial shear stress value to deform and displace the barrier film, the existence of critical temperature is required to sufficiently activate the exposed surface for bonding to take place through the

ATTENTION: The Singapore Copyright Act applies to the use of this document. Nanyang Technological University Library

removal of an ultrathin deformed barrier layer on the surface. Further increase in bond strength scales with bonding temperature due to thermally-induced interdiffusion of atoms across the bonding interface. When sufficiently high amount of pressure is applied [above $P_{min.r}$] at constant bonding temperature, further increase in pressure continues to improve bond strength but the amount of bonded area does not scale correspondingly. The observations suggest that beyond $P_{min.r}$, bond strengthening occurs due to the increase in the amount of locally bonded sites rather than the microscopic expansion of bonded area.

7.2 Demonstrated low temperature gold Thermocompression bonding by self-assembled monolayers

Through the assistance of self-assembled monolayer, it has been successfully demonstrated that the bonding temperature required for reliable bond integrity for both gold stud and plated gold microbumps can be significantly reduced to 40°C. The working hypothesis behind this phenomenon has been systematically investigated and we verified that the enhanced mechanical integrity at such low temperature can be attributed to three key contributions: [1] the effectiveness of SAMs layer in passivating the exposed bonding surface up till actual bonding, [2] the ease of thermal activating SAMs-coated surface for bonding and [3] the ease of mechanical displacement The mechanical strength of the joints formed behaves similarly with those predicted by the hypothesis on classical bonding theory.

7.3 Achieved Low Temperature Direct Copper Thermocompression Bonding in Ambient

Inspired by the success exhibited in SAMs-enhanced gold Thermocompression bonding, we subjected the copper samples to similar treatment prior to bonding process.

ATTENTION: The Singapore Copyright Act applies to the use of this document. Nanyang Technological University Library

We observed obvious enhancement of bond integrity in such samples as compared to uncoated copper samples at bonding temperature as low as 60°C in ambient. Such phenomenon is demonstrated for the first time. The densely packed monolayer passivates the copper surface against oxidation effectively. The enhancement in bond strength also suggests that the greater ease of removal of such an organic monolayer compared to a bulk oxide layer is an important consideration during mechanical deformation at the interface in order to enable low temperature thermocompression bonding.

A few recommendations for future work will be proposed in the following section.

1. Time Dependence in Metal Thermocompression Bonding

Successful bond formation depends on the amount of bonding temperature, pressure and time applied. Much attention had been given to studies on the effect of bonding temperature and pressure on bonding mechanism which are believed to be the main process variables in Thermocompression bonding. It has been reported that bonds of sufficient strength can be formed at temperature lower than optimum values with compensating increase in bonding pressure or vice versa. Improved bond strength can be obtained at higher bonding temperature and pressure. Contrasting reports were found regarding the effect of post annealing processes. It was found that post annealing at temperature lower or above bonding temperature induce strengthening effect [38] while another study reported bond strength only improves after thermal annealing at high temperature but not low temperature [21]. Bond quality had been reported to improve with time under the absence of external load while in the presence of high external load, it becomes temperature independent with time [42]. Therefore the true mechanism

ATTENTION: The Singapore Copyright Act applies to the use of this document. Nanyang Technological University Library

governing the effect of bonding time remains controversial. It is unclear to distinguish the phenomenon behind bond strengthening with bonding time at (1) Different bonding temperatures and (2) with or without external pressure applied. Therefore a study on the bonding time is necessary to determine the optimum bonding time as well as a better understanding on the correlation between the three main process variables. The time dependence study could help to unravel the origin behind this phenomenon. A theory governing thermocompression bonding can also be developed as a result.

2. Low temperature bonding processes using self-assembled monolayers for multi-level applications

Having shown significant enhancement in both gold-gold and copper-copper thermocompression bonding at die-to-die level, it would be very interesting to extend this to the die-to-wafer as well as wafer-to-wafer level applications. In the case of bonding both noble and oxidative metals such as copper, one of the key issues for low temperature process is to eliminate contaminants/oxides as well as suppress further oxidation during time lag between subsequent process steps. While we have demonstrated that SAMs on copper have been able to fulfill these requirements at die level and passivation properties of SAMs on copper have been widely investigated, it remains poorly understood for its capability on wafer-scale bonding. Previous studies [137] demonstrated larger amount of effective wire bonds formed on coated copper bond pads on 8 inch Cu/SiO_2 Back-End-of-Line (BEOL) wafers as compared to uncoated wafers, ball shear strength assessment and high temperature storage test for stability of ball shear strength over 1500hrs of aging at 150°C. Yet none has been demonstrated on wafer-to-wafer bonding. The main technical challenge involves bonding similar materials such as gold and copper at low temperature, with strong joint integrity and reliability as scaling up of process fabrication for various IC technologies

ATTENTION: The Singapore Copyright Act applies to the use of this document. Nanyang Technological University Library

[for e.g. wafer level bonding for MEMS, MOEMS, NMENs wafer-level packages, 3D stacked chips, silicon-on-insulators (SOI)] occurs. Therefore to do so, a thorough study on factors governing SAMs-assisted bonding [for example, substrate surface morphology and roughness, substrate cleanliness, surface growth structure of SAMs, thermal and mechanical stability etc] is necessary to determine how similar improvement can be translated when the bonding surface area has increased by factors of ten in magnitude. Lab-based coating and cleaning techniques has to be revised for realization of this method for industrial applications.

3. Joint Electron Devices Engineering Council (JEDEC) tests for commercialization of SAMs-enhanced devices

Besides taking into account of the structural properties of the bonded joints, the electrical properties have to be assessed to ensure long term reliable metal interconnects formed for three-dimensional integrated circuits. It is unknown whether the presence of clusters or fragments of organic monolayers that could possibly be trapped within the small percentage of voids present near the bonding interface, would reduce overall device performance such as electrical resistivity electrical resistivity as well as reliability issues such as fatigue and time-dependent creep failure during thermal cycling, high temperature storage and thermal humidity tests.

Fatigue occurs when structures are subjected to cyclic stresses. When this happens, these structures usually fail at a stress level that is much lower than its yield strength. Fatigue failure is governed by three key steps, namely: (1) crack initiates at stress-concentrated sites; (2) crack propagates during each stress cycle and (3) material fails finally when the crack reaches a critical size. No materials are idealized solids. All materials contain imperfection and defects. For instance, it is very common to detect the presence of voids in electroplated copper and gold-based structures such as metallic

ATTENTION: The Singapore Copyright Act applies to the use of this document. Nanyang Technological University Library

microbumps for interconnects such as copper dual damascene interconnect for electronic devices [140, 141], films for metallization and through-silicon vias for three-dimensional integrated chips [142]. These voids are detrimental to the fracture strength of the materials because they serve as sites of stress concentration when external stress is applied. This is also illustrated in Figure 7-1 which summarizes the possible failure mechanisms that contribute to the copper bump failure [143]. It is apparent that presence of voids resulting from processes and the stresses resulting from thermal cycling, shock, high temperature process and electromigration are the few key major causes of failure.

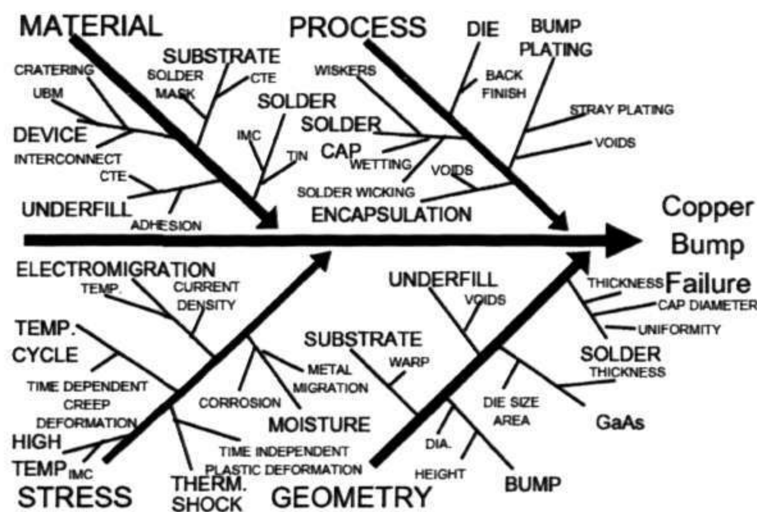

Figure 7-1 A combination of causes leading to copper bump failure: Materials, processes, aging stresses and geometry [Source: Roesch et. al. (2004)].

At the stress amplification sites which are usually present on surfaces or bonding interfaces, fatigue life can be affected significantly since most cracks originate from these sites. Hence, when fatigue crack propagates through void-filled materials or structures, crack propagation will be much more rapid as compared to a void-less structure since the material the crack needs to traverse is less. Presence of voids, in turn reduces fatigue life of materials. In the case of thermal cycling test [JEDEC Standard: JESD22-A104C] where samples are soaked at recommended test conditions such as

ATTENTION: The Singapore Copyright Act applies to the use of this document. Nanyang Technological University Library

cycling rate, maximum and minimum temperatures and number of thermal cycles per hour, thermal fatigue is normally induced. Another effect of such temperature cycling process is time-dependent creep deformation. Creep occurs when the temperature is high enough such that the structure deform plastically at a stress level lower than the yield stress. This process is time-dependent and hence structures undergoing creep deform differently as a function of time. Creep is one of the dominant failure mechanisms in metals. When metals deform at different temperatures, the dominant fracture mechanism depends on the rate of deformation [144].

The necessity to look at the influence of voids or defects such as cracks and the failure mechanisms in direct metal joint reliability studies can be explained in the following:

We found that higher amount of bonding pressure in the range of GPa is necessary to bond SAMs-assisted copper directly in order to achieve reasonably high bond strength at bonding temperatures as low as room temperature. In our recent findings, bonding between direct copper at 25°C occurs at a bonding pressure of 50MPa [Figure 7-2], which is much lower than the bonding pressure required in the previous result [Figure 7-3/Figure 6-4]. While the amount of bonding pressure needed to bond copper at low temperatures differs in magnitude depending on other contributing parameters such as material properties such as hardness, and yield strength, bump geometry/profile and surface morphology etc, high bonding pressure (i.e. high stress level) is deemed undesirable since issues such as cracking in the underlying metallization, silicon cratering or even catastrophic material failure would degrade device performance. Cracks present, as discussed earlier on, serves as stress amplification sites which will accelerate fatigue and creep failure during reliability tests. Therefore when stress levels are rather high, it was reported that failure occurs by transgranular creep fracture or ductile fracture [144]. Such failure is governed by the

ATTENTION: The Singapore Copyright Act applies to the use of this document. Nanyang Technological University Library

power law creep of material around the voids. This emphasizes the influence of voids present within the material prior to reliability tests which aim to determine the long term device usage.

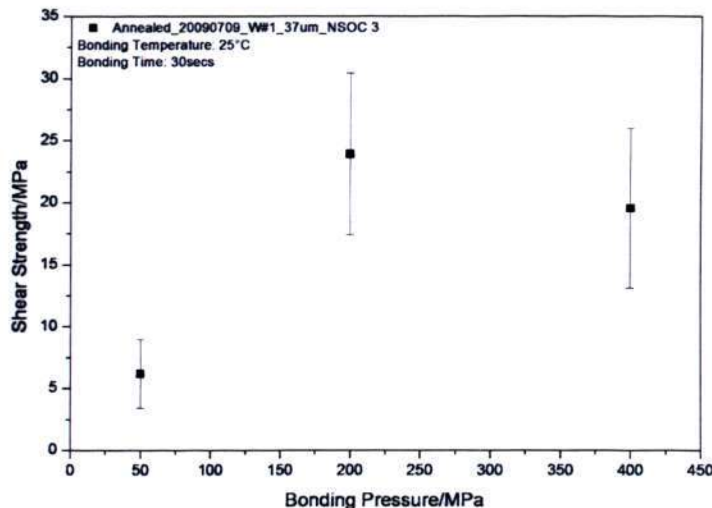

Figure 7-2 Shear strength of coated copper bonded at 25°C as a function of bonding pressure

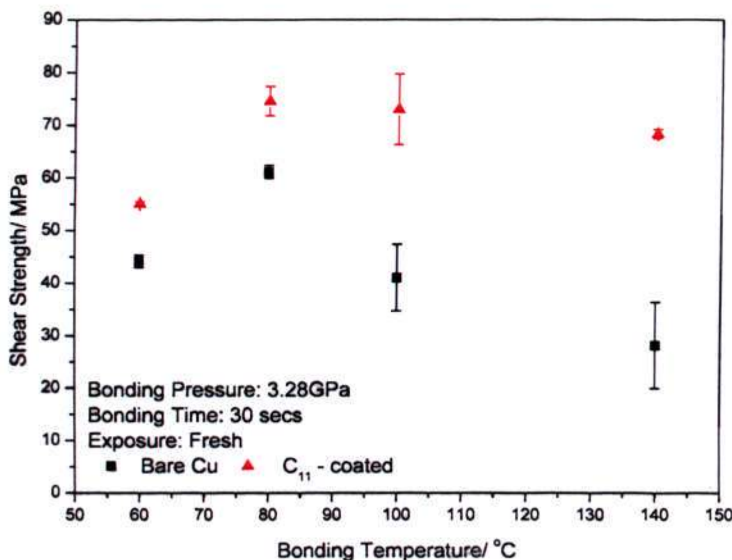

Figure 7-3 Comparison of shear strength in coated copper against uncoated copper from 60°C to 140°C

Assuming that voids are already present before deformation during bonding, ductile fracture of metals depends on the type of stress state metals are subjected to – tensile or compressive stress states. Often, failure under tensile stress states occurs

ATTENTION: The Singapore Copyright Act applies to the use of this document. Nanyang Technological University Library

through void nucleation, growth and coalescence. Voids present may change its shape to form crack-like defects. When cracks grow sufficiently large, catastrophic material fracture may happen [145-147]. However under high compressive stress induced when bonding pressure applied perpendicular to the bonding interface, material failure may occur through a different mechanism referred as shear de-cohesive fracture or stress rupture. Depending on the amount of pressure applied, voids may shrink and change to a stationary shape[148]. In either stress state, the correlation of applied bonding pressure and the evolution of voids present at the bonding interface especially is significant in determining the long term reliability of direct metal joints.

Therefore to truly demonstrate the usefulness of SAM-induced low temperature bonded interconnects for 3D integration, systematic studies on the electrical integrity due to temperature cycling and mechanical stresses brought about during different stages of process fabrication, temperature, humidity and bias (THB) test, thermal cycling test, shock and high temperature storage tests based on JEDEC standards [3, 149, 150] should be carried out. It is unknown at this point where SAMs would have gone after bonding. We proposed the following: Since the monolayer does not desorb completely prior to bonding, it is apparent that deformed monolayer would be trapped within the bonding interface. Since the true contact area is very much smaller than the nominal area [151], the unbonded region [vacant sites or voids] would serve as residing sites where SAMs would be displaced to. It is intriguing how trapped SAMs in voids would play a role in the reliability performance. To our knowledge, there is limited reliability studies of 3D stacked structures based on direct copper interconnect [152-155], not to mention for SAMs-assisted Cu interconnections. Upon in-depth investigations of the electrical and reliability performances using various 3D IC technology verification test vehicles, in particular bonding verification test structures as

ATTENTION: The Singapore Copyright Act applies to the use of this document. Nanyang Technological University Library

well as the test structures for circuit performance integrity, the readiness of incorporating SAMs process in the 3D technology will be fulfilled.

4. Passivation and adhesion enhancer layer between similar and dissimilar materials for interconnects.

Following the development of the mechanism behind low temperature thermocompression bonding for gold and copper using SAMs, there are many more other materials that can possibly benefit from this method. There are various conducting materials suitable for electrical interconnects that can be chosen from the family of metals, namely aluminum, indium, lead, silver, solder or lead-free solder such as copper-tin, copper-indium and many more. These materials such as aluminium requires relatively high bonding temperature and pressure (>400ºC) [152]. Other than metals, it will be intriguing to explore its possibility in non-metallic bonding materials such as glass or dielectric glue layer to reduce the bonding conditions needed. So far, there has not been any work done on this.

While the first idea attempts to alleviate what is believed to be the key culprit for the challenges faced in copper-copper bonding, that is, surface oxidation, it will be very interesting to exploit the versatility of functionalizing self-assembled monolayers, such that it not only serves as a oxidation inhibition layer but also an adhesion enhancer. This novel concept can be explained in the following context: a nanolayer with identical functional groups at both ends (for example, HS-R-SH where R is a short alkyl group and S is sulphur) binding two contacting yet similar metallic surfaces due to the thermodynamically favoured adsorption of sulphur on gold or copper surfaces. However this concept challenges existing techniques of sandwiching the monolayers between two surfaces which usually involves first, a solution-based deposition of the nanolayer on the one surface and then a subsequent evaporation of a thin layer of

ATTENTION: The Singapore Copyright Act applies to the use of this document. Nanyang Technological University Library

compatible material that binds with the exposed tail group. The creation of the idea was initiated when a recent article published in Nature by G. Ramanath from Rensselaer Polytechnic Institute (RPI) demonstrated a significant improvement in the adhesion between copper and silicon oxide surfaces using mercaptan-silane monolayers and further toughening between the copper-dielectric interface was observed as temperature increased beyond a temperature limit [35]. The versatility of synthesizing SAMs with suitable end groups for various types of substrates and incorporating appropriate strengthening molecular species within the chain structure respectively could thus act to satisfy specific device requirements.

ATTENTION: The Singapore Copyright Act applies to the use of this document. Nanyang Technological University Library

REFERENCES

1. R. R. Schaller, "*Moore's law: past, present and future*," Spectrum, IEEE, **34**, 52-59, (1997).
2. K. Banerjee, S. J. Souri, P. Kapur, and K. C. Saraswat, "*3-D ICs: a novel chip design for improving deep-submicrometer interconnect performance and systems-on-chip integration*," Proceedings of the IEEE, **89**, 602-633, (2001).
3. A. W. Topol, J. D. C. La Tulipe, D. J. Frank, K. Bernstein, S. E. Steen, A. Kumar, G. U. Singco, A. M. Young, K. W. Guarini, and M. Leong, "*Three-dimensional integrated circuits*," IBM Journal of Research & Development, **50**, 491, (2006).
4. Y. Akasaka, "*Three-dimensional IC trends*," Proceedings of the IEEE, **74**, 1703-1714, (1986).
5. B. Knapp, "*3-D ICs address SiPs' technical shortfalls*," in EE Times Online, 10th May, 2004.
6. K. Tanida, M. Umemoto, Y. Tomita, M. Tago, Y. Nemoto, T. Ando, and K. Takahashi, "*Ultra-high-density 3D chip stacking technology*," in Electronic Components and Technology Conference, 2003. Proceedings. 53rd, 2003, pp. 1084-1089.
7. E. T. Eisenbraun, D. Lishan, E. Ostan, and H. Auer, "*3D Integration – The Packaging Technology for Tomorrow's Performance Needs*," Albany Nanotech & Unaxis Semiconductors.
8. S. Gupta, M.Hilbert, S.Hong, and R.Patti, "*Techniques for Producing 3D ICs with High-Density Interconnects*," in VLSI Mutilevel Inteconnection Conference, 2004.
9. T. Brunschwiler and B. Michel, "*Thermal Management of Vertically Integrated Packages*," in *Handbook of 3D Integration:Technology and Applications of 3D Integrated Circuits* vol. 2, P. Garrou, C. Bower, and P. Ramm, Eds.: WILEY-VCH Verlag GmbH & Co., (2008).
10. P. Garrou and C. Bower, "*Overview of 3D Integration Process Technology*," in *Handbook of 3D Integration:Technology and Applications of 3D Integrated Circuits* vol. 1, P. Garrou, C. Bower, and P. Ramm, Eds.: WILEY-VCH Verlag GmbH & Co., (2008).
11. N.Mokhoff, "*Interconnect conference highlights silicon-optical paths*," in EE Times, 2005.
12. L. Peters, "*Wafer Bonding Enables New Technologies and Applications*," in Semiconductor International, 2003.

ATTENTION: The Singapore Copyright Act applies to the use of this document. Nanyang Technological University Library

13. J. L. Jellison., "*Effect of surface contamination on thermcompression bondability of gold*," IEEE Transactions On Parts, Hybrids, And Packaging, **11**, 206-212, (1975).
14. G. E. McGuire, J. V. Jones, and H. J. Dowell, "*The Auger analysis of contaminants that influence the thermocompression bonding of gold*," Thin Solid Films, **45**, 59-68, (1977).
15. F. P. Bowden and G. W. Rowe, "*The Adhesion of Clean Metals*," Proceedings of the Royal Society of London. Series A, Mathematical and Physical Sciences, **233**, 429-442, (1956).
16. R. F. Tylecote, "*Solid Phase Welding of Metals*." New York: St.Martin's Press, (1968).
17. K. Buchanan, "*The evolution of interconnect technology for silicon integrated circuitry.*," in The International Conference on Compound Semiconductor Manufacturing Technology (GaAsMANTECH), 2002.
18. R. Liu, C.-S. Pai, and E. Martinez, "*Interconnect technology trend for microelectronics*," Solid-State Electronics, **43**, 1003-1009, (1999).
19. K. N. Chen, C. S. Tan, A. Fan, and R. Reif, "*Morphology and bond strength of copper wafer bonding*," Electrochemical and Solid-State Letters, **7**, G14, (2004).
20. K. N. Chen, A. Fan, C. S. T. and, and R. Reif, "*Temperature and Duration Effects on Microstructure Evolution During Copper Wafer Bonding*," Journal of Electronic Materials, **32**, 1371 -1374, (2003).
21. K. N. Chen, S. M. Chang, L. C. Shen, and R. Reif, "*Investigations of strength of copper-bonded wafers with several quantitative and qualitative tests* " Journal of Electronic Materials, **35**, 1082-1086, (2006).
22. T. H. Kim, M. M. R. Howlader, T. Itoh, and T. Suga, "*Room temperature Cu-Cu direct bonding using surface activated bonding method*," Journal of Vacuum Science & Technology A: Vacuum, Surfaces, and Films, **21**, 449-453, (2003).
23. N. S. McIntyre and M. G. Cook, "*X-ray photoelectron studies on some oxides and hydroxides of cobalt, nickel, and copper*," Anal. Chem., **47**, 2208-2213, (1975).
24. D. L. Cocke, R. Schennach, M. A. Hossain, D. E. Mencer, H. McWhinney, J. R. Parga, M. Kesmez, J. A. G. Gomes, and M. Y. A. Mollah, "*The low-temperature thermal oxidation of copper, Cu3O2, and its influence on past and future studies*," Vacuum, **79**, 71-83, (2005).
25. R. M. S. Yea-Yang Su, "*Qualitative and quantitative identification of copper oxides*," Surface and Interface Analysis, **9999**, n/a, (2008).
26. R. Schennach and A. Gupper, "*Copper Oxidation Studied by In-Situ Raman Spectroscopy*," in Materials Research Society Symposium Proceedings, San Francisco, CA, USA, 2003, p. E3.2.1.
27. K. I. Johnson and J. D. V. Keller, "*Effect of Contamination on the Adhesion of Metallic Couples in Ultra-High Vacuum*," Journal of Applied Physics, **38**, 1896-1904, (1967).
28. K. N. Chen, A. Fan, C. S. Tan, and R. Reif, "*Bonding Parameters of Blanket Copper Wafer Bonding*," Journal of Electronic Materials, **35**, 230, (2006).
29. P. Banda, H. H. M., C. Whelan, L. W., C. J. Vath, III, and E. Beyne, "*Direct Au and Cu wire bonding on Cu/low-k BEOL*," in Electronics Packaging Technology Conference, 4th. 344-349, 2002, pp. 344-349.
30. H. M. Ho, W. Lam, S. Stoukatch, P. Ratchev, C. J. Vath, and E. Beyne, "*Direct gold and copper wires bonding on copper*," Microelectronics Reliability, **43**, 913-923, (2003).

ATTENTION: The Singapore Copyright Act applies to the use of this document. Nanyang Technological University Library

31. C. M. Whelan, M. Kinsella, L. Carbonell, H. M. H., and K. Maex, "*Corrosion inhibition by self-assembled monolayers for enhanced wire bonding on Cu surfaces*," Microelectronic Engineering, **70**, 551-557, (2003).
32. C. M. Whelan, M. Kinsella, M. H. H., and K. Maex, "*Corrosion Inhibition by Thiol-Derived SAMs for Enhanced Wire Bonding on Cu Surfaces*," Journal of The Electrochemical Society, **151**, B33-B38, (2004).
33. C. Whelan, M. Kinsella, H. M. &, and K. Mae, "*In-Situ Cleaning and Passivation of Oxidized Cu Surfaces by Alkanethiols and Its Application to Wire Bonding*," Journal of Electronic Materials, **33**, 1005-1012, (2004).
34. C. Liu and D. A. Hutt, "*Fluxless Soldering of Copper Substrates Using Self-Assembled Monolayers for Preservation*," Components and Packaging Technologies, IEEE Transactions on, **29**, 512-521, (2006).
35. D. D. Gandhi, M. Lane, Y. Zhou, A. P. Singh, S. Nayak, U. Tisch, M. Eizenberg, and G. Ramanath, "*Annealing-induced interfacial toughening using a molecular nanolayer*," Nature, **447**, 299-302, (2007).
36. M. C. McKinnon and R. F. Hoeckelman, "*Mechanical and electrical properties of thermocompression bonds*," Proceedings of the IEEE, **51**, 519-519, (1963).
37. O. L. Anderson, H. Christensen, and P. Andreatch, "*Technique for Connecting Electrical Leads to Semiconductors*," Journal of Applied Physics, **28**, 923-923, (1957).
38. A. T. English and J. L. Hokanson, "*Studies of Bonding Mechanisms and Failure Modes in Thermocompression Bonds of Gold Plated Leads to Ti-Au Metallized Substrates*," in Reliability Physics Symposium, 1971. 9th Annual, 1971, pp. 178-186.
39. K. C. Joshi, "*The Formation of Ultrasonic Bonds between Metals*," Welding Journal, **50**, 840-848, (1971).
40. P. H. Holloway and D. W. Bushmire, "*Detection by Auger Electron Spectroscopy and Removal by Ozonization of Photoresist Residues*," in Reliability Physics Symposium, 1974. 12th Annual, 1974, pp. 180-186.
41. H.Ramsey, "*Metallurgical Behavior of Gold Wire in Thermal Compression Bonding*," Solid State Technology, 43-47, (1973).
42. J. Jellison, "*Kinetics of Thermocompression Bonding to Organic Contaminated Gold Surfaces*," Parts, Hybrids, and Packaging, IEEE Transactions on, **13**, 132-137, (1977).
43. R. Cuthrell and D. Tipping, "*The Bonding Characteristics of Gold in Ultrahigh Vacuum*," Parts, Hybrids, and Packaging, IEEE Transactions on, **10**, 4-10, (1974).
44. N.Ahmed and J.J.Svitak, "*Characterization of Gold-Gold Thermcompression Bonding*," Solid State Technology, 25-32, (1975).
45. Y. Takahashi, S. Shibamoto, and K. Inoue, "*Numerical analysis of the interfacial contact process in wire thermocompression bonding*," Components, Packaging, and Manufacturing Technology, Part A, IEEE Transactions on [see also Components, Hybrids, and Manufacturing Technology, IEEE Transactions on], **19**, 213-223, (1996).
46. N. Bay, "*Cold Pressure Welding--a Theoretical Model for the Bond Strength* " The Joining of Metals: Practice and Performance, **2**, 47-62, (1981).
47. L. Condra, J. Svitak, and A. Pense, "*The High Temperature Deformation Properties of Gold and Thermocompression Bonding*," Parts, Hybrids, and Packaging, IEEE Transactions on, **11**, 290-296, (1975).
48. G. G. Zhang and C. C. Wong, "*Review of Direct Metal Bonding for Microelectronic Interconnections*," 2004.

ATTENTION: The Singapore Copyright Act applies to the use of this document. Nanyang Technological University Library

49. C. S. Tan, R. Reif, N. D. Theodore, and S. Pozder, "*Observation of interfacial void formation in bonded copper layers*," Applied Physics Letters, **87**, 201909, (2005).
50. H. Piao and N. S. McIntyre, "*Adventitious carbon growth on aluminium and gold-aluminium alloy surfaces*," Surface and Interface Analysis, **33**, 591-594, (2002).
51. C. f. M. A. a. Packaging, "*Review of Failure Modes and Mechanisms in Solder Joints Subjected to Thermal Cycling*," in MIET REPORT 2004.
52. S. Choe, W. W. So, and C. C. Lee, "*Low temperature fluxless bonding technique using In-Sn composite*," in Electronic Components and Technology Conference, 2000. 2000 Proceedings. 50th, 2000, pp. 114-118.
53. V. V. Zenin, V. N. Belyaev, Y. E. Segal, and A. A. Kolbenkov, "*Lead-Free Solders in IC Manufacture: A Review*," Russian Microelectronics, **32**, 247-256, (2003).
54. A. Klumpp, "*Bonding with Intermetallic Compounds*," in *Handbook of 3D Integration:Technology and Applications of 3D Integrated Circuits* P. Garrou, C. Bower, and P. Ramm, Eds.: WILEY-VCH Verlag GmbH & Co., (2008).
55. P. D. Moor, W. Ruythooren, P. Soussan, B. Swinnen, K. Baert, C. V. Hoof, and E. Beyne, "*Recent Advances in 3D Integration at IMEC*," in Mater. Res. Soc. Symp. Proc., 2007, pp. 0970-Y01-02.
56. C. Taek Ryong, L. Yang, N. Hosoda, H. Takagi, and T. Suga, "*Wafer direct bonding of compound semiconductors and silicon at room temperature by the surface activated bonding method*," Applied Surface Science, **117-118**, 808-812, (1997).
57. P. Enquist, "*High Density Bond Interconnect (DBI) Technology for Three Dimensional Integrated Circuit Applications*," Mater. Res. Soc. Symp. Proc., **970**, 0970-Y01 - 04, (2007).
58. Q. Y Tong, G. G. Fountain, and P. M. Enquist, "*Method for Low Temperature Bonding and Bonded Structure*," in United States Patent. vol. US 6902987: Ziptronix, Inc., 2005.
59. J.-P. Joly, "*Overview of Bonding Technologies for 3D Integration*," in *Handbook of 3D Integration:Technology and Applications of 3D Integrated Circuits* vol. 1, P. Garrou, C. Bower, and P. Ramm, Eds.: WILEY-VCH Verlag GmbH & Co., (2008).
60. F. Niklaus, "*Adhesive Wafer Bonding for Microelectronic and Microelectromechanical Systems*," Stockholm: Royal Institute of Technology, 2002.
61. T. S. Cale, J. Q. Lu, and R. J. Gutmann, "*Three-Dimensional Integration in Microelectronics: Motivaton, Processing and Thermomechanical Modeling*," Chem. Eng. Comm, **195**, 847 - 888, (2008).
62. S.Tomiyama and Y. Fukui, "*Gold Bonding Wire for Semiconductor Applications*," Gold Bull, **15**, 43, (1982).
63. G. Omar, M. R. Muhamad, and A. Daud, "*Effect of annealing and alloying to the microstructural property of gold bond wire in wire bond interconnect*," in Semiconductor Electronics, 2002. Proceedings. ICSE 2002. IEEE International Conference on, 2002, pp. 480-484.
64. S. J. Hu, G. E. Lim, T. L. Lim, and K. P. Foong, "*Study of temperature parameter on the thermosonic gold wire bonding of high-speed CMOS*," Components, Hybrids, and Manufacturing Technology, IEEE Transactions on [see also IEEE Trans. on Components, Packaging, and Manufacturing Technology, Part A, B, C], **14**, 855-858, (1991).

ATTENTION: The Singapore Copyright Act applies to the use of this document. Nanyang Technological University Library

65. W. D. Callister, "*Materials Science and Engineering: An Introduction*," 5th ed. United States of America: John Wiley & Sons, Inc., (2000).
66. D. Tabor, "*The Hardness of Metals*." London: Oxford University Press, (1951).
67. T. S. McLauren and Y.-C. Lee, "*Modeling and Evaluation Criterion for Thermocompression Flip-Chip Bonding*," IEEE Transactions on Advanced Packaging, **23**, 652-661, (2000).
68. T.S.Ellington, "*Lead Frame Bonding*," Solid State Technology, **16**, 59-62, (1973).
69. G. Harman and J. Albers, "*The Ultrasonic Welding Mechanism as Applied to Aluminum-and Gold-Wire Bonding in Microelectronics*," Parts, Hybrids, and Packaging, IEEE Transactions on, **13**, 406-412, (1977).
70. J. A. Greenwood and J. B. P. Williamson, "*Contact of Nominally Flat Surfaces*," Proceedings of the Royal Society of London. Series A, Mathematical and Physical Sciences, **295**, 300-319, (1966).
71. B. Bhushan, J. N. Israelachvili, and U. Landman, "*Nanotribology: friction, wear and lubrication at the atomic scale*," Nature, **374**, 607-616, (1995).
72. M. T. McDermott, J. B. D. Green, and M. D. Porter, "*Scanning Force Microscopic Exploration of the Lubrication Capabilities of n-Alkanethiolate Monolayers Chemisorbed at Gold: Structural Basis of Microscopic Friction and Wear*," Langmuir, **13**, 2504-2510, (1997).
73. J. C. Love, L. A. Estroff, J. K. Kriebel, R. G. Nuzzo, and G. M. Whitesides, "*Self-Assembled Monolayers of Thiolates on Metals as a Form of Nanotechnology*," Chem. Rev., **105**, 1103-1170, (2005).
74. P. E. Laibinis and G. M. Whitesides, "*Self-assembled monolayers of n-alkanethiolates on copper are barrier films that protect the metal against oxidation by air*," J. Am. Chem. Soc., **114**, 9022-9028, (1992).
75. A. Ulman, "*An Introduction to Ultrathin Organic Films From Langmuir-Blodgett to Self-Assembly*." New York Academic Press (1991).
76. Colin D. Bain, E. Barry Troughton, J. E. Yu Tai Tao, George M. Whitesides, and R. G. Nuzzo, "*Formation of monolayer films by the spontaneous assembly of organic thiols from solution onto gold*," J. Am. Chem. Soc., **111**, 321-335, (1989).
77. F. Choplin, S. Navarre, J. Bousbaa, P. Babin, B. Bennetau, J. L. Bruneel, and B. Desbat, "*Structural characterization of self-assembled monolayers by unenhanced Raman spectroscopy*," Journal of Raman Spectroscopy, **34**, 902-906, (2003).
78. P. L. Stiles, J. A. Dieringer, N. C. Shah, and R. P. Van Duyne, "*Surface-Enhanced Raman Spectroscopy*," Annual Review of Analytical Chemistry, **1**, 601-626, (2008).
79. M. M. Sung, K. Sung, C. G. Kim, S. S. Lee, and Y. Kim, "*Self-Assembled Monolayers of Alkanethiols on Oxidized Copper Surfaces*," The Journal of Physical Chemistry B, **104**, 2273-2277, (2000).
80. M. M. Sung, W. J. Yun, S. S. Lee, and Y. Kim, "*Thermal decomposition of octanethiolate self-assembled monolayers on Cu(111) in UHV*," Bulletin of Korean Chemical Society, **24**, 610, (2003).
81. R. W. Carpick and M. Salmeron, "*Scratching the Surface: Fundamental Investigations of Tribology with Atomic Force Microscopy*," Chemical Reviews, **97**, 1163-1194, (1997).
82. F. P. Zamborini and R. M. Crooks, "*Corrosion Passivation of Gold by Alkanethiol Self-Assembled Monolayers: Effect of Chain Length and End Group*," Langmuir, **14**, 3279-3286, (1998).

ATTENTION: The Singapore Copyright Act applies to the use of this document. Nanyang Technological University Library

83. Takao Ishida, Naoki Nishida, Satoshi Tsuneda, Masahiko Hara, H. Sasabe, and W. Knoll, "*Alkyl Chain Length Effect on Growth Kinetics of n-Alkanethiol Self-Assembled Monolayers on Gold Studied by X-Ray Photoelectron Spectroscopy* " Japanese Journal of Applied Physics, **35**, L1710-L1713, (1996).
84. K. V. Wolf, D. A. Cole, and S. L. Bernasek, "*High-Resolution TOF-SIMS Study of Varying Chain Length Self-Assembled Monolayer Surfaces*," Analytical Chemistry, **74**, 5009-5016, (2002).
85. F. Schreiber, "*Structure and growth of self-assembling monolayers*," Progress in Surface Science, **65**, 151-257, (2000).
86. G. G. Zhang, X. F. Ang, Z. Chen, C. C. Wong, and J. Wei, "*Critical temperatures in thermocompression gold stud bonding*," Journal of Applied Physics, **102**, 063519, (2007).
87. E. K. David, "*Oxidation of gold by ultraviolet light and ozone at 25 [degree]C*," 1995, pp. 1247-1253.
88. L. H. Dubois and R. G. Nuzzo, "*Synthesis, Structure, and Properties of Model Organic Surfaces*," Annual Review of Physical Chemistry, **43**, 437-463, (1992).
89. X. F. Ang, F. Y. Li, W. L. Tan, Z. Chen, C. C. Wong, and J. Wei, "*Self-assembled monolayers for reduced temperature direct metal thermocompression bonding*," Applied Physics Letters, **91**, 061913, (2007).
90. C. D. Bain and G. M. Whitesides, "*Formation of Monolayers by Coadsorption of Thiols on Gold: Variation in the Length of Alkyl Chain*," Journal of American Chemical Society, **111**, 7164-7175, (1989).
91. R. G. Nuzzo, B. R. Zegarski, and L. H. Dubois, "*Fundamental studies of the chemisorption of organosulfur compounds on gold(111). Implications for molecular self-assembly on gold surfaces*," Journal of American Chemical Society, **109**, 733-740, (1987).
92. Ralph G. Nuzzo and D. L. Allara, "*Adsorption of bifunctional organic disulfides on gold surfaces*," Journal of American Chemical Society, **105**, 4481-4483, (1983).
93. K. A. Peterlinz and R. Georgiadis, "*In Situ Kinetics of Self-Assembly by Surface Plasmon Resonance Spectroscopy*," Langmuir, **12**, 4731-4740, (1996).
94. Taina Laiho and J. A. Leiro, "*ToF-SIMS study of 1-dodecanethiol adsorption on Au, Ag, Cu and Pt surfaces*," Surface and Interface Analysis, **40**, 51-59, (2008).
95. M. S. D. L. H. F. A. S. Sohn, "*ToF-SIMS investigations of the degeneration processes of self-assembled monolayers of alkanethiols on gold*," Surface and Interface Analysis, **36**, 1222-1226, (2004).
96. T. Laiho and J. A. Leiro, "*Influence of initial oxygen on the formation of thiol layers*," Applied Surface Science, **252**, 6304-6312, (2006).
97. H. L. L. Watton, A. G. Fitzgerald, and P. A. Moir, "*Composition of thin surface layers obtained by X-ray photoelectron spectroscopy*," Surface and Interface Analysis, **17**, 320-324, (1991).
98. S. Tennyson, "*The hydrophilic nature of a clean gold surface*," Journal of Colloid and Interface Science, **75**, 51-55, (1980).
99. P. R. Norton, R. L. Tapping, and J. W. Goodale, "*High resolution photoemission study of the physisorption and chemisorption of CO on copper and gold*," Surface Science, **72**, 33-44, (1978).
100. T. M. Willey, A. L. Vance, T. van Buuren, C. Bostedt, L. J. Terminello, and C. S. Fadley, "*Rapid degradation of alkanethiol-based self-assembled monolayers on gold in ambient laboratory conditions*," Surface Science, **576**, 188-196, (2005).

ATTENTION: The Singapore Copyright Act applies to the use of this document. Nanyang Technological University Library

101. T. Laiho, J. A. Leiro, and J. Lukkari, "*XPS study of irradiation damage and different metal-sulfur bonds in dodecanethiol monolayers on gold and platinum surfaces*," Applied Surface Science, **212-213**, 525-529, (2003).
102. K. Heister, M. Zharnikov, M. Grunze, L. S. O. Johansson, and A. Ulman, "*Characterization of X-ray Induced Damage in Alkanethiolate Monolayers by High-Resolution Photoelectron Spectroscopy*," Langmuir, **17**, 8-11, (2001).
103. N. Nishida, M.Hara, H.Sasabe, and W. Knoll, "*Thermal Desorption Spectroscopy of Alkanethiol Self-Assembled Monolayer on Au(111)* " Japanese Journal of Applied Physics, **35**, 5866-5872, (1996).
104. Q. Guo, X. Sun, and R. E. Palmer, "*Structural dynamics induced by self-assembled monolayers on Au(111)*," Physical Review B (Condensed Matter and Materials Physics), **71**, 035406, (2005).
105. N. Prathima, M. Harini, N. Rai, R. H. Chandrashekara, K. G. Ayappa, S. Sampath, and S. K. Biswas, "*Thermal Study of Accumulation of Conformational Disorders in the Self-Assembled Monolayers of C8 and C18 Alkanethiols on the Au(111) Surface*," Langmuir, **21**, 2364-2374, (2005).
106. Y. W. Yang and L. J. Fan, "*High-Resolution XPS Study of Decanethiol on Au(111): Single Sulfur-Gold Bonding Interaction*," Langmuir, **18**, 1157-1164, (2002).
107. R. Ristau, R. Tiruvalam, P. L.Clasen, E. P. Gorskowski, M. P. Harmer, and C. J. Kiely, "*Electron microscopy studies of the thermal stability of gold nanoparticle arrays*," Gold Bulletin, **42**, 133, (2009).
108. S. Ekgasit, A. Tangcharoenbumrungsuk, F. Yu, A. Baba, and W. Knoll, "*Resonance shifts in SPR curves of nonabsorbing, weakly absorbing, and strongly absorbing dielectrics*," Sensors and Actuators B: Chemical, **105**, 532-541, (2005).
109. B. Rai, SathishP, C. P. Malhotra, Pradip, and K. G. Ayappa, "*Molecular Dynamic Simulations of Self-Assembled Alkylthiolate Monolayers on an Au(111) Surface*," Langmuir, **20**, 3138-3144, (2004).
110. M. Zharnikov, S. Frey, K. Heister, and M. Grunze, "*Modification of Alkanethiolate Monolayers by Low Energy Electron Irradiation: Dependence on the Substrate Material and on the Length and Isotopic Composition of the Alkyl Chains*," Langmuir, **16**, 2697-2705, (2000).
111. T. Ishida, M. Hara, I. Kojima, S. Tsuneda, N. Nishida, H. Sasabe, and W. Knoll, "*High Resolution X-ray Photoelectron Spectroscopy Measurements of Octadecanethiol Self-Assembled Monolayers on Au(111)*," Langmuir, **14**, 2092-2096, (1998).
112. D. G. Hanken, C. E.Jordan, B. L. Frey, and R. M. Corn, "*Surface Plasmon Resonance Measurements of Ultrathin organic Films at Electrode Surface*," in *Electroanalytical Chemistry: A Series of Advances*. vol. 20, A. J. Bard and I. Rubinstein, Eds. New York: CRC Press, (1998).
113. G. Alison, C. James, and X. Bai, "*Wafer bonding for 3D integration of MEMS/CMOS*," 2006, p. 611100.
114. G. Voskerician, M. S. Shive, R. S. Shawgo, H. v. Recum, J. M. Anderson, M. J. Cima, and R. Langer, "*Biocompatibility and biofouling of MEMS drug delivery devices*," Biomaterials, **24**, 1959-1967, (2003).
115. X. F. Ang, F. Y. Li, W. L. Tan, Z. Chen, C. C. Wong, and J. Wei, "*Low Temperature Direct Metal Bonding by Self Assembled Monolayers*," in Materials Research Society Symposium Proceedings. vol. 990 San Francisco, US, 2007, pp. 0990-B10-03.
116. J. R. Scott, L. S. Baker, W. R. Everett, C. L. Wilkins, and I. Fritsch, "*Laser Desorption Fourier Transform Mass Spectrometry Exchange Studies of Air-*

ATTENTION: The Singapore Copyright Act applies to the use of this document. Nanyang Technological University Library

Oxidized Alkanethiol Self-Assembled Monolayers on Gold," Analytical Chemistry, **69**, 2636-2639, (1997).

117. A. Horn, B., D. A. Russel, L. J. Shorthouse, and T. R. E. Simpson, "*Aging of alkanethiol self-assembled monolayer*," Journal of the Chemical Society, Faraday Transactions, **92**, 4759-4762, (1996).
118. Y. Zhang, R. H. Terrill, and P. W. Bohn, "*Ultraviolet Photochemistry and ex Situ Ozonolysis of Alkanethiol Self-Assembled Monolayers on Gold*," Chemistry of Materials, **11**, 2191-2198, (1999).
119. S. P. Chenakin, B. Heinz, and H. Morgner, "*Sputtering of hexadecanethiol monolayers self-assembled onto Ag(111)*," Surface Science, **397**, 84-100, (1998).
120. M. J. Tarlov and J. G. Newman, "*Static secondary ion mass spectrometry of self-assembled alkanethiol monolayers on gold*," Langmuir, **8**, 1398-1405, (1992).
121. M. H. Schoenfisch and J. E. Pemberton, "*Air Stability of Alkanethiol Self-Assembled Monolayers on Silver and Gold Surfaces*," Journal of American Chemical Society, **120**, 4502-4513, (1998).
122. M. T. Lee, C. C. Hsueh, M. S. Freund, and G. S. Ferguson, "*Air Oxidation of Self-Assembled Monolayers on Polycrystalline Gold: The Role of the Gold Substrate*," Langmuir, **14**, 6419-6423, (1998).
123. E. Cooper and G. J. Leggett, "*Static Secondary Ion Mass Spectrometry Studies of Self-Assembled Monolayers: Influence of Adsorbate Chain Length and Terminal Functional Group on Rates of Photooxidation of Alkanethiols on Gold*," Langmuir, **14**, 4795-4801, (1998).
124. J. R. Scott, L. S. Baker, W. R. Everett, C. L. Wilkins, and I. Fritsch, "*Laser Desorption Fourier Transform Mass Spectrometry Exchange Studies of Air-Oxidized Alkanethiol Self-Assembled Monolayers on Gold*," Anal. Chem., **69**, 2636-2639, (1997).
125. X. Xiao, B. Wang, C. Zhang, Z. Yang, and M. M. T. Loy, "*Thermal annealing effect of alkanethiol monolayers on Au(1 1 1) in air*," Surface Science, **472**, 41-50, (2001).
126. C.S. Tan, K.N. Chen, A. Fan, and R. Reif, "*The Effect of Forming Gas Anneal on the Oxygen Content in Bonded Copper Layer*," Journal of Electronic Materials, **34**, 1598, (2005).
127. K. N. Chen, C. S. Tan, A. Fan, and R. Reif, "*Morphology and Bond Strength of Copper Wafer Bonding*," Electrochemical and Solid-State Letters, **7**, G14-G16, (2004).
128. A. Fan, A. Rahman, and R. Reif, "*Copper Wafer Bonding*," Electrochemical and Solid-State Letters, **2**, 534-536, (1999).
129. K. N. Chen, A. Fan, and R. Reif, "*Microstructure Examination of Copper Wafer Bonding*," Journal of Electronic Materials, **30**, 331, (2001).
130. K. N. Chen, A. Fan, and R. Reif, "*Interfacial Morphologies and Possible Mechanisms of Copper Wafer Bonding*," Journal of Materials Science, **37**, 3441, (2002).
131. C. S. Tan, "*Recent progress in copper-based wafer bonding for 3-D ICs application*," in Electronic Materials and Packaging, EMAP International Conference Taipei, 2008, pp. 45-48.
132. K. N. Chen, "*Copper Wafer Bonding In Three-Dimensional Integration*," in Electrical Engineering and Computer Science. vol. Doctor of Philosophy Boston, MA: Massachusetts Institute of Technology, 2005.
133. K. N. Chen, C. S. Tan, A. Fan, and R. Reif, "*Copper bonded layers analysis and effects of copper surface conditions on bonding quality for three-dimensional integration* " Journal of Electronic Materials, **34**, 1464 - 1467, (2005).

ATTENTION: The Singapore Copyright Act applies to the use of this document. Nanyang Technological University Library

134. T. H. Youssef and R. A. Essawi, "*Effect of Working Temperature on Young's Modulus of Electrolytic Copper*," Czechoslovak Journal of Physics, **29**, 1266, (1979).
135. H. Derin and K. Kantarli, "*Optical Characterization of thin thermal oxide films on copper by ellipsometry*," App. Phys. A, **75**, 391, (2002).
136. H. Wieder and A. W. Czanderna, "*Optical Properties of Copper Oxide Films*," Journal of Applied Physics, **37**, 184-187, (1966).
137. P. Banda, H. H. M., C. Whelan, L. W., C. J. Vath, III, and E. Beyne, "*Direct Au and Cu wire bonding on Cu/low-k BEOL*," in Electronics Packaging Technology Conference, 4th. , 2002, pp. 344-349.
138. P. E. Laibinis, G. M. Whitesides, D. L. Allara, Y. T. Tao, A. N. Parikh, and R. G. Nuzzo, "*Comparison of the structures and wetting properties of self-assembled monolayers of n-alkanethiols on the coinage metal surfaces, copper, silver, and gold*," Journal of American Chemical Society, **113**, 7152-7167, (1991).
139. L. Carbonell, C. M. Whelan, M. Kinsella, and K. Maex, "*A thermal stability study of alkane and aromatic thiolate self-assembled monolayers on copper surfaces*," Superlattices and Microstructures, **36**, 149-160, (2004).
140. T. C. Wang, Y. L. Wang, T. E. Hsieh, S. C. Chang, and Y. L. Cheng, "*Copper voids improvement for the copper dual damascene interconnection process*," Journal of Physics and Chemistry of Solids, **69**, 566-571.
141. P. C. Andricacos, C. Uzoh, J. O. Dukovic, J. Horkans, and H. Deligianni, "*Damascene copper electroplating for chip interconnections*," IBM Journal of Research and Development, **42**, 567, (1998).
142. C. Song, Z. Wang, and L. Liu, "*Bottom-up copper electroplating using transfer wafers for fabrication of high aspect-ratio through-silicon-vias*," Microelectronic Engineering, **In Press, Corrected Proof**.
143. W. J. Roesch and S. Jittinorasett, "*Cycling copper flip chip interconnects*," Microelectronics and Reliability, **44**, 1047-1054, (2004).
144. M. F. Ashby, C. Gandhi, and D. M. R. Taplin, "*Overview No. 3 Fracture-mechanism maps and their construction for f.c.c. metals and alloys*," Acta Metallurgica, **27**, 699-729, (1979).
145. B. Sun, Z. Suo, and A. G. Evans, "*Emergence of cracks by mass transport in elastic crystals stressed at high temperatures*," Journal of the Mechanics and Physics of Solids, **42**, 1653-1677, (1994).
146. H. Wang and Z. Li, "*Diffusive shrinkage of a void within a grian of a stressed polycrystal*," Journal of the Mechanics and Physics of Solids, **51**, 961-976, (2003).
147. H. Wang and Z. Li, "*Stability and shrinkage of a cavity in stressed grain*," Journal of Applied Physics, **95**, 6025-6031, (2004).
148. H. Wang and Z. Li, "*The shrinkage of grain-boundary voids under pressure*," Metallurgical and Materials Transactions A, **34**, 1493-1500, (2003).
149. K. Takahashi, M. Hoshino, H. Yonemura, M. Tomisaka, M. Sunohara, M. Tanioka, T. Sato, K. Kojima, and H. Terao, "*Development of advanced 3D chip stacking technology with ultra-fine interconnection*," in Electronic Components and Technology Conference 2001, 2001, pp. 541-546.
150. Y. Seung Wook, D. Witarsa, S. Yak, L. Long, V. Ganesh, A. G. K. Viswanath, C. Tai Chong, K. O. Navas, and V. Kripesh, "*Reliability Studies of a Through Via Silicon Stacked Module for 3D Microsystem Packaging*," in Electronic Components and Technology Conference, 2006. Proceedings. 56th, 2006, pp. 1449-1453.

ATTENTION: The Singapore Copyright Act applies to the use of this document. Nanyang Technological University Library

151. H. L. Leong, C. L. Gan, C. V. Thompson, K. L. Pey, and H. Y. Li, "*Application of contact theory to metal-metal bonding of silicon wafers*," Journal of Applied Physics, **102**, 103510, (2007).
152. S. K. Kang, "*Thermocompression bonding of aluminum bumps in TAB applications*," in Electronic Components & Technology Conference, 1998. 48th IEEE, 1998, pp. 1305-1310.
153. N. Tanaka, T. Sato, Y. Yamaji, T. Morifuji, M. Umemoto, and K. Takahashi, "*Mechanical effects of copper through-vias in a 3D die-stacked module*," in Electronic Components and Technology Conference, 2002. Proceedings. 52nd, 2002, pp. 473-479.
154. K.-N. Chen, S. H. Lee, P. S. Andry, C. K. Tsang, A. W. Topol, Y.-M. Lin, J.-Q. Lu, A. M. Young, M. Ieong, and W. Haensch, "*Structure, Design and Process Control for Cu Bonded Interconnects in 3D Integrated Circuits*," in Electron Devices Meeting, 2006. IEDM '06. International, 2006, pp. 1-4.
155. Y. Yang, H. Bender, K. Arstila, B. Swinnen, B. Verlinden, and I. D. Wolf, "*Detection of failure sites by focused ion beam and nano-probing in the interconnect of three-dimensional stacked circuit structures*," Microelectronics Reliability, **48**, 1517-1520, (2008).
156. H. F. Boyer, "*Atlas of Stress-Strain Curves*." Metals Park, Ohio: ASM International (1987).

ATTENTION: The Singapore Copyright Act applies to the use of this document. Nanyang Technological University Library

APPENDIX A1: LIST OF AUTHOR'S PUBLICATIONS

Patent

[1] J. Wei, **X. F. Ang**, C. C. Wong, Z. Chen, "Room Temperature Direct Metal-Metal Bonding", PCT Application No. PCT/SG2008/000448, International Filing Date: 27 November 2008

Journal

[1] **X. F. Ang**, G. G. Zhang, J. Wei, Z. Chen, and C. C. Wong, "Temperature and pressure dependence in thermocompression gold stud bonding", *Thin Solid Films*, Vol. 504 (1-2), p. 379 (2006).

[2] L.C. Chin, **X. F. Ang**, J. Wei, Z. Chen, and C. C. Wong, "Enhancing direct metal bonding with self-assembled monolayers", *Thin Solid Films*, Vol. 504 (1-2), p. 367 (2006).

[3] G. G. Zhang, **X. F. Ang**, Z. Chen and C. C. Wong, "Critical Temperatures in Thermocompression Gold Stud Bonding", *Journal of Applied Physics*, Vol.102, p. 063519 (2007)

[4] **X. F. Ang**, F. Y. Li, W. L. Tan, Z. Chen and C. C. Wong, "Self-assembled Monolayers for Reduced Temperature Direct Metal Thermocompression Bonding", *Applied Physics Letters*, Vol. 91, 061913 (2007); also in *Virtual Journal of Nanoscale Science & Technology*, Vol. 16, Iss. 8, (2007)

[5] **X. F. Ang**, Z. Chen, C. C. Wong and J. Wei, "Effect of Chain Length in Low Temperature Gold-Gold Bonding by Self-Assembled Monolayers", *Applied Physics Letters*, Vol. 92, 131913 (2008); also in *Virtual Journal of Nanoscale Science & Technology*, Vol. 17, Iss. 16 (2008)

ATTENTION: The Singapore Copyright Act applies to the use of this document. Nanyang Technological University Library

[6] **X. F. Ang**, F. Y. Li, J. Wei, W. L. Tan, and C. C. Wong, "A Thermal and Passivation Study of Self-Assembled Monolayers on Thin Gold Films", *Thin Solid Films,* Vol. 516, p. 5721 (2008)

[7] Q. Yan, **X. F. Ang,** C. C. Wong and Y. - M. Chiang, "Ordered Macroporous gold Thin Film with Encaptured Polymer Spheres", *Applied Physics A,* vol. 94, pp. 271-274 (2008)

[8] J. Li, **X. F. Ang**, K. H. Lee, F. Romanato, C. C. Wong, "In-situ monitoring of Thermal Heating of Alkanethiols at Different Chain Lengths using Surface Plasmon Resonance Spectroscopy (SPRS)", Presented at Thin Films 2008. (Accepted by *Journal of Nanoscience & Nanotechnology*)

Conference

[1] **X. F. Ang**, L.C. Chin, J. Wei, Z. Chen and C. C. Wong, Self-assembled monolayers for enhanced Au-Au thermocompression bonding, *3rd International Conference on Materials for Advanced Technologies (ICMAT2005) and IUMRS-9th International Conference on Advanced Materials (ICAM2005)*, 3-8 July 2005, Singapore.

[2] **X. F. Ang**, G. G. Zhang, J. Wei, Z. Chen and C. C. Wong, Temperature and Pressure Dependence in Thermocompression Gold Stud Bonding, *3rd International Conference on Materials for Advanced Technologies (ICMAT2005) and IUMRS-9th International Conference on Advanced Materials (ICAM2005)*, 3-8 July 2005, Singapore.

[3] **X. F. Ang**, G. G. Zhang, J. Wei, Z. Chen and C. C. Wong, Effects of Bonding Temperature and Pressure on Thermocompression Gold Bonding, *Proceedings of ASME IMECE2005*, IMECE2005-79454, 5-11 Nov. 2005, USA.

[4] **X. F. Ang**, G. G. Zhang, B. K. Tan, J. Wei, Z. Chen and C. C. Wong, Direct Metal to Metal Bonding for Microsystems Interconnections and Integration, *Proceedings of 2005 Electronics Packaging Technology Conference*, 390-393 (2005), 7-9 December 2005, Singapore.

[5] **X. F. Ang**, H.Y. Gan, J. Wei, Z. Chen and C.C. Wong, Pressure dependence in peripheral bonding in gold-gold thermocompression, *2006 Electronics Packaging Technology Conference*, 6-8 December 2006, Singapore.

[6] **X. F. Ang**, F. Y. Li, W. L. Tan, J. Wei, Z. Chen, C.C. Wong, Investigation on the Thermal Stability of Self-Assembled Monolayers on Gold Using Surface Plasmon Resonance Spectroscopy, *The 5th International Conference on Materials Processing for Properties and Performance (MP3)*, 11-15 December 2006, Singapore.

ATTENTION: The Singapore Copyright Act applies to the use of this document. Nanyang Technological University Library

[7] **X. F. Ang**, F.Y. Li, J. Wei, W. L. Tan, C.C. Wong, A Thermal and Passivation Study of Self-Assembled Monolayers on Thin Gold Films, *Thin Films 2006*, 11- 15 December 2006, Singapore.

[8] **X. F. Ang**, F.Y. Li, J. Wei, W. L. Tan, Z. Chen, C.C. Wong, J. In Low Temperature Direct Metal Bonding by Self Assembled Monolayers, *Materials Research Society Symposium Proceedings*, 9-13 April 2007, San Francisco, CA, USA, pp 0990-B10-03.

[9] **X. F. Ang**, J. Wei, Z. Chen and C. C. Wong, Surface passivation of gold using alkanethiols of different molecular chain length, *5th International Symposium on Nanomanufacturing Singapore*, 23-25 January 2008, Singapore.

[10] **X. F. Ang**, J. Li, J. Wei, Z. Chen and C. C. Wong, Stability of Self-Assembled Monolayers on Gold for MEMS/NMEMS Applications, *Proceedings of the ASME International Mechanical Engineering Congress and Exposition, IMECE 2008*, 31 Oct-06 Nov 2008, Boston, Massachusetts, USA.

[11] **X. F. Ang**, A. T. Lin, J. Wei, Z. Chen and C. C. Wong, Low Temperature Copper-Copper Thermocompression Bonding, *10th Electronics Packaging Technology Conference*, 9-12 December 2008, Singapore.

[12] **X. F. Ang**, J. Wei, Z. Chen, C.C. Wong, In Ambient Copper-Copper Thermocompression Bonding using Self Assembled Monolayers, *Materials Research Society Symposium Fall Meeting*, 1–5 December 2008, Boston, USA.

[13] J. Li, **X. F. Ang**, K.H. Lee, F. Romanato, C. C. Wong, In-situ monitoring of Thermal Heating of Alkanethiols at Different Chain Lengths using Surface Plasmon Resonance Spectroscopy (SPRS), *Thin Films 2008*, 13-16 July, 2008, Singapore.

ATTENTION: The Singapore Copyright Act applies to the use of this document. Nanyang Technological University Library

APPENDIX A2: Estimation of True Bonded Area and Stress-Strain Curves

Table A2-1 Calculation of yield stress using nanoindentation data.

Bonding P/Pa	Hardness- H (Pa)	Yield stress -Y (Pa)[1]	Shear Force (N)	A_{Tshear} [2] (m^2)	$A_{Tshear}/A_{measured}$
4.21E+08	901850000	300616666.7	9.75E-01	3.24E-09	1.46E-01

[1] H=3Y
[2] A_{Tshear} = Shear Force/Y

Hardness: Average value over seven indentation points using Berkovich indenter
Yield Stress: Using Tabor's Rule, hardness is approximately three times the yield/flow stress of gold
Shear Force: Measured through shear test of the gold ring left on substrate

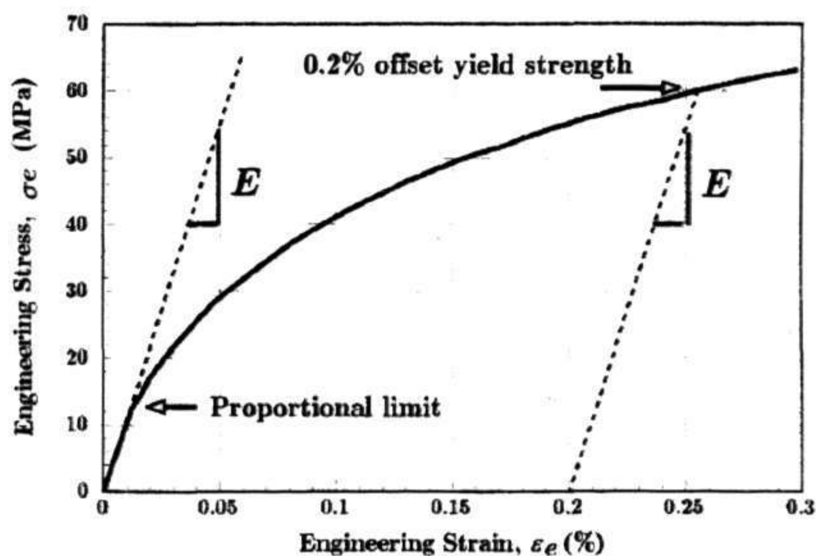

Figure A2-1 Stress-strain curve of polycrystalline copper at low strain range. Such behaviour is typical of that of many ductile metals. [156]

ATTENTION: The Singapore Copyright Act applies to the use of this document. Nanyang Technological University Library

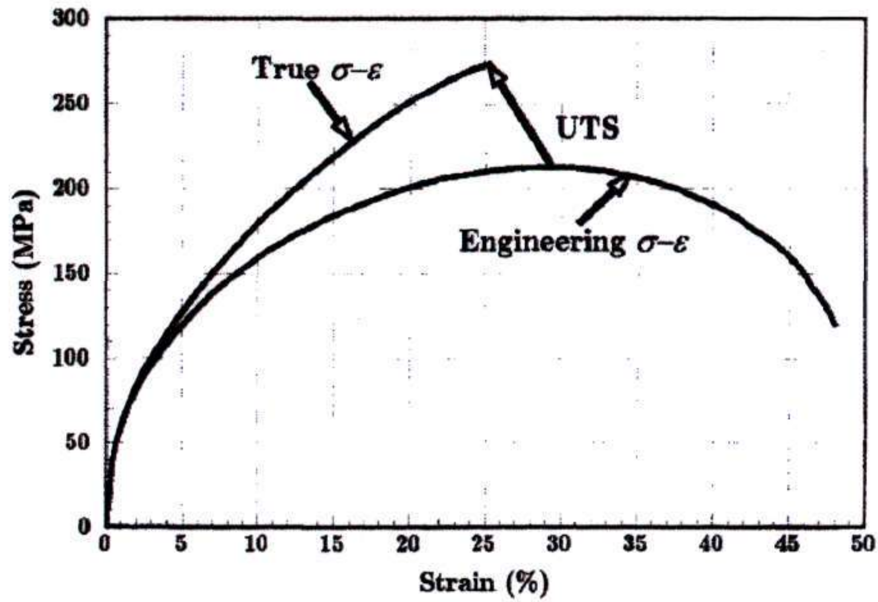

Figure A2-2 True stress-strain curve versus engineering stress-strain curve of copper. [156]

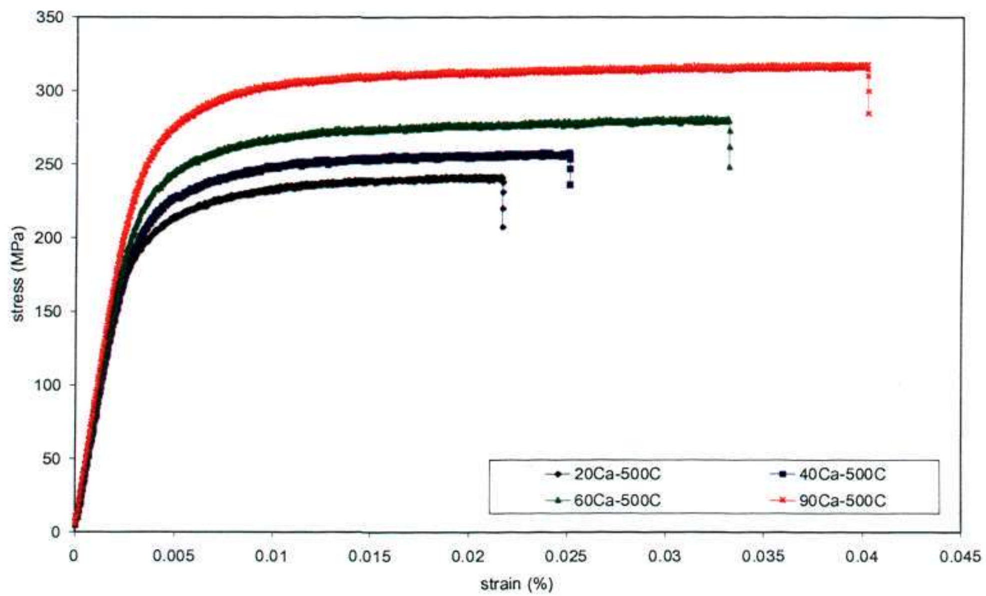

Figure A2-3 Stress-strain curve of calcium-doped gold wire annealed at 500°C [By courtesy of Heraeus Materials– Unpublished work]

ATTENTION: The Singapore Copyright Act applies to the use of this document. Nanyang Technological University Library

Table A2-2 Influence of temperature on tensile strength of gold wire, cold-worked 49%.

Annealing Temp/°C	Non-annealed	250	300	500	900
Tensile strength/MPa	235	220	140	140	140

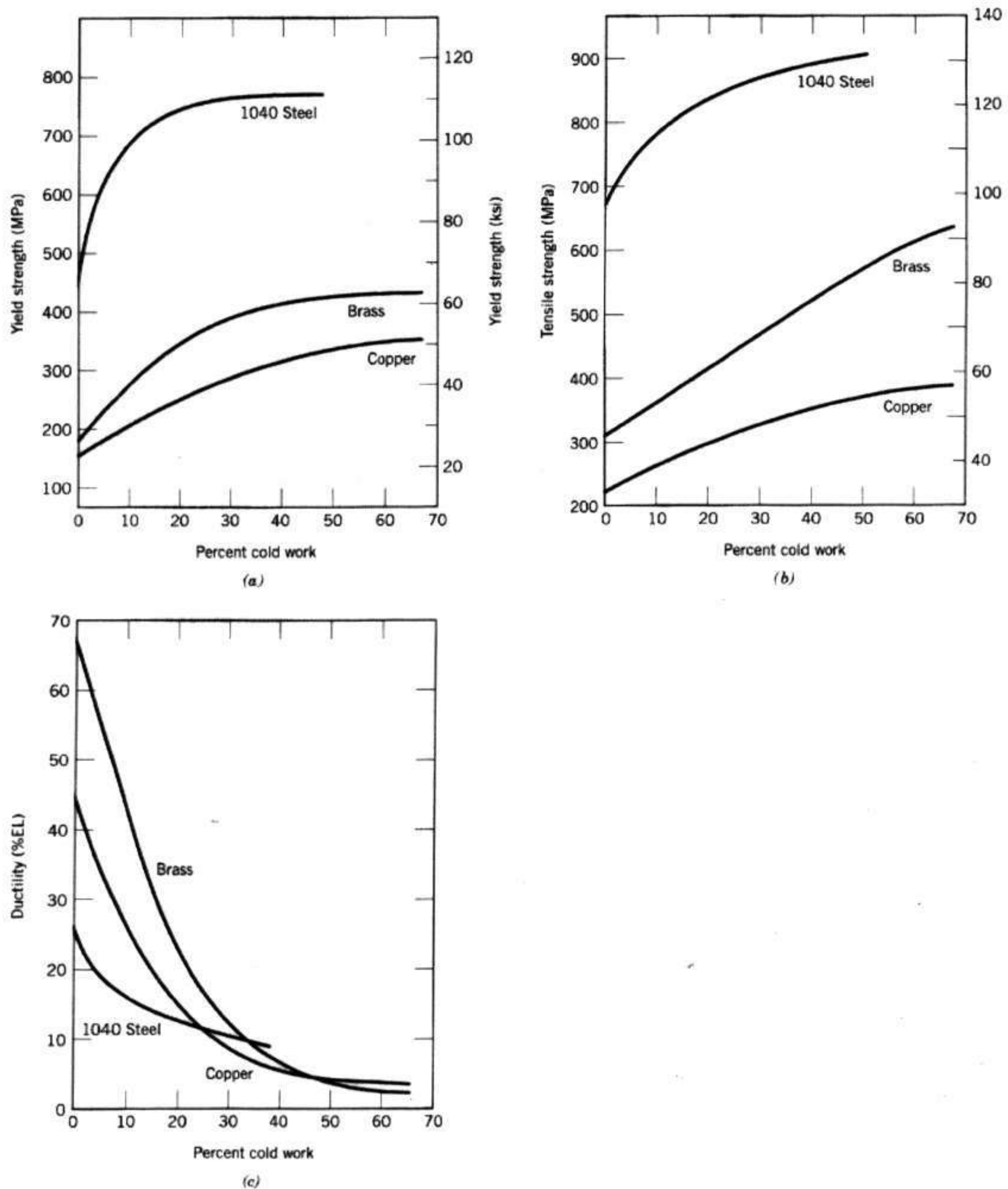

Figure A2-4 Behaviour of yield strength, tensile strength and ductility of metal with percent cold work [Metals Handbook]